Republic of Iraq

Ministry of Higher Education

And Scientific Research

University of Babylon

Faculty of Materials Engineering

Department of Metallurgical Engineering

Effect of Graphite and Thermo- mechanical Treatment on Physical, Mechanical and Machining Properties of Cu-10%Sn Alloy.

A Dissertation

Submitted to the Council of the Faculty of Materials Engineering/ University of Babylon in Partial Fulfillment of the Requirements for the Master of Degree in Materials Engineering / Metallurgical Engineering

By

Rasha Hussien Ali Abid

(B.Sc. In Materials Engineering)

(2006-2007)

Supervised by

Prof. Haydar Al-Ethari (Ph.D.)

Asst. Prof. Talib A. Jasim

2022 A.D **1443 A.H**

وزارة التعليم العالي والبحث العلمي
جامعـــــــــــة بابـــــــــــل
كليـــــــــة هنـــــــــــــدسة المواد
قسم هنـــــــــــــدسة المعادن

تأثير الكرافيت والمعاملة الحرارية -الميكانيكية على الخواص الفيزياوية والميكانيكية والتشغيلية لسبيكة نحاس-10%قصدير

رسالة

مقدمة إلى قسم المعادن في كلية هندسة المواد / جامعة بابل وهي جزء من متطلبات نيل درجة الماجستير في علوم

هندسة المواد/هندسة معادن .

من قبل

رشا حسين علي عبد

(بكالوريوس هندسة مواد)

(2007-٢٠06)

بإشراف

أ.د. حيدر عبد الحسن حسين العذاري

أ.م. طالب عبد الامير جاسم

1443/هـ **2022 / م**


بسم الله الرحمن الرحيم
الله لا إله إلا هو الحي القيوم لا تأخذه
سنة ولا نوم له ما في السموات وما في
الأرض من ذا الذي يشفع عنده
إلا بإذنه يعلم ما بين أيديهم وما خلفهم
ولا يحيطون بشيء من علمه إلا بما شاء
وسع كرسيه السموات والأرض ولا
يؤوده حفظهما وهو العلي العظيم

Supervisors Certificate

We certify that this thesis entitled "***Effect of Graphite and Thermo- mechanical Treatment on Physical, Mechanical and Machining Properties of Cu-10Sn Alloy.***" Has been done by

(**Rasha Hussein Ali**)

under our supervision at the Department of Metallurgical Engineering/ Faculty of Materials Engineering /University of Babylon in partial fulfillment of the requirements for the degree of Master of Science in Materials Engineering.

Signature:

Name: : Prof. Dr. Haydar Al-Ethari

(supervisor)

Date: / / 2022

Signature:

Name Asst. Prof. Talib A. Jasim

(supervisor)

Date: / / 2022

Examining Committee Certification

We certify that we had read this thesis entitled "***Effect of Graphite and Thermo-mechanical Treatment on Physical, Mechanical and Machining Properties of Cu-10Sn Alloy***" and as an examining committee, we have examined the student (***Rasha Hussien Ali Bairmani***) in its contents and that is related to it, and in our opinion, it meets the requirements to have the master degree in Materials Engineering/ Department of Metallurgical Engineering

Signature:

Prof. Dr. Saad Hameed AlShafaie

(Chairman)

Date: / / 2022

Signature:

Asst. Prof. Dr. Amar Jaabbar Albaji

(Member)

Date: / / 2022

Signature:

Asst. Prof. Dr. Basem Mohysen Mohammed

(Member)

Date: / / 2022

Signature:

Prof. Dr. Haydar Al-Ethari

(Supervisor)

Date: / / 2022

Signature:

Asst. Prof. Talib A. Jasim

(Supervisor)

Date: / / 2022

Signature

Prof. Dr. Saad Hameed AlShafaie

Head of Metallurgical Engineering Department

Date: / / 2022

Signature

Prof. Dr. Imad Ali Disher

Dean of Materials Engineering College

Date: / / 2022

Dedication

To my father and mother

To my husband and my lovely Sons

To my brothers and sister

To my friends

With my love and respect

Rasha

2022

Acknowledgments

First of all, profusely all thanks be for **ALLAH** God of all creations who enable me to achieve this work.

I would like to express my gratitude to my supervisor, **Dr. Haydar Al-Ethari, and Assist. Prof. Talib A. Jasim** for guidance, advice and enthusiastic encouragement throughout this investigation which I hope will develop the reality of our country to the best in the near future.

I am very grateful to my distinguished family especially my dear father who supported me and my late mother, my distant star, whose shadow has always been my companion on the darkest nights, May God have mercy on you, and to my husband, brothers and my sister "Best friend" for their assistance, encouragement and support during the period of preparing this work.

Rasha

2022

الخلاصة:

يركز العمل على تحضير مادة مركبة أساسها نحاس وقصدير لمحامل انزلاقية (محامل تشحيم ذاتي). حيث غطت الدراسة تصنيع عينات من (نحاس- 10% قصدير) مع إضافة أطوار تشحيم على شكل مسحوق جرافيت. تم تحضير المواد المركبة عن طريق الصب بالتحريك. ولتحسين قابلية البلل لجزيئات الجرافيت، تم طلاء جزيئات الجرافيت بالنحاس عن طريق الترسيب الكهربائي قبل إضافتها إلى السائل المنصهر. تم صب العينات باستخدام (0، 1، 3 و 5٪ بالوزن) من الجرافيت المطلي. تم اجراء العصر الساخن عند 600 درجة مئوية وبتسليط احمال مختلفة 445و555و665 ميكا باسكال للعينات المصبوبة. أظهرت النتائج تجانس البنية المجهرية على طول السبيكة بالكامل مع ميل منخفض نسبيًا لفصل جميع المركبات المنتجة. تميزت المركبات الناتجة بانخفاض معامل الاحتكاك وزيادة مقاومة البلى وتقليل حجم الحبيبات ، مما أدى إلى تحسين الصلادة وقابلية التشغيل بالنسبة للعينة التي تحتوي على 5٪ بالوزن من الجرافيت المطلي تحت الضغط الساخن عند 665 ميكا باسكال حيث تشير النتائج لهذه العينة إلى تحسن في الصلابة بنسبة 93٪ وتقليل حجم الحبيبات بنسبة 61٪وزيادة الكثافة بنسبة 2٪ وانخفاض المسامية بنسبة 28٪ وزيادة مقاومة البلى بنسبة 51٪ وانخفاض بنسبة 33٪ في معامل الاحتكاك. اظهر الاسلوب السابق لعمليه تحضير العينات المسبوكة إلى أن الجرافيت المطلي والعصر الساخن قد حسنا من قابلية تشغيل المادة المركبة. اظهرت العينة التي تحتوي على 5%بالوزن كرافيت مطلي افضل النتائج تحت الظروف التشغيلية المستخدمة حيث تم تقليل العمر الافتراضي للأداة المستخدمة بنسبة 8٪ وخشونة سطح العينة المشغولة بنسبة 47٪. تشير هذه النتائج إلى إمكانية تصنيع المواد المركبة مع جزيئات طور التشحيم (الجرافيت) عن طريق الصب بالتحريك بجودة جيدة ، خاصة من حيث الخواص الميكانيكية والفيزياوية ، وتأكيد إمكانية تطبيق المواد المركبة من النحاس الخالي من الرصاص من نوع نحاس- جرافيت للأجزاء المنزلقة التي تعمل في ظروف زيادة الاحتكاك والبلى مثل المحمل والجلبة.

ABSTRACT:

The work focuses on the preparation of **CuSn** based composite material for slide bearings (self lubricating bearings) .The study covered **Cu10%Sn** with addition of lubricating phases in a form of graphite particles. Composite materials were prepered by stir casting . To improve the wettability of the graphite particles these particles were coated by copper by electroless deposition before adding to the molten melt. The samples were cast with (**0, 1, 3** and **5wt %**) of coated graphite. Hot forming at **600ºC** by squeezing pressure of **445, 555, 665MPa** was performed for specimens of the cast samples. Qualitative metallographic assessment showed uniformity of microstructure over the entire length of the ingot at relatively low tendency to segregation of all produced composites. The resulting composites are characterized by reduction in coefficient of friction and increase in the wear resistance, reduction in the grain size, which led to improvement of the hardness and the machinability. For the specimen having **5wt.%** of coeted graphite and hot formed by **665MPa**, the results indicate **93%** improving in the hardness, reduction in grain size **61%,** increase in density by **2%** and decreasing in porosity by **28%** , **51 %** increase in wear resistance and **33%** reduction in the coefficient of friction. The preformed machining program indicate that the coated graphite and the hot forming improved the machinability of the composite. . For the specimen having **5wt.%** of coated graphite and hot formed by **665MPa,** the results indicate the tool life of the used tool was decreased by **8%** and the roughness of the machined specimen was reduced by **47%**. This results indicate the possibility of manufacturing with good quality, especially in terms of mechanical and physical properties, the composite materials with particles of lubricating phase (graphite) by stir casting and confirm the possibility of application of the examined composite materials of lead-free copper-graphite type for sliding elements operating in conditions of increased friction and wear such as bearing and bushing.

The Table of Contents

Table of Figures

List of Tables

Table of Latin Symbols

symbols	Description	Unit
α	Alpha Phase	-
Ra	Arithmetic Mean Value of Surface Roughness	Mm
β	Beta Phase	-
δ	Delta Phase	-
ρ	Density	g/cm^3
d	Depth of cut	mm
ε	Epsilon Phace	-
f	Feed rate	Mm/sec
γ	Gamma Phase	-
VB	Maximum Flank wear tool	Mm
σSV	The Surface Energy of The Solid	$J\,m^{-2}$
T	Temperature	$^{\circ}C$
t	Time	sec
σLV	The Surface Energy of The Liquid	$J\,m^{-2}$
σSL	The Solid/Liquid Interface Energy	$J\,m^{-2}$
RZ	Ten - point mean roughness	Mm
rpm	Spindle speed	n

List of Subscripts & Superscripts

Symbol	Meaning	Units
BHN	Brinell hardness number	Kg/mm^2
D	density	g/cm^3
P	Porosity	%
R.W	Rate of Wear	g/m
W	Weight	g
W_d	dry weight of the samples	g
W_{sat}	saturated weight	g
W_s	suspended weight	g
W_w	wet weight	g

Chapter One
Introduction

1.1 Self-lubricating Materials:

Self-lubricating materials are materials having the property of lubrication when it is in used. Such materials are needed in bearing and bushing applications. The self -lubricating function of these materials works by means of lubrication inside the sliding of its layers. The lubricating materials may be liquid or solid. The oil inside pores in the sliding layers serves to lubricate the outer surface of the protective bearings. The materials that are often used as solid lubricants are graphite, lead, polytetrafluoroethylene (PTFE, teflon, tarflen, fluon), molybdenum disulphide, tungsten disulphide, glassy carbon, sulphur compounds including hexagonal zinc sulphide and boron nitrides(h-NB) [1]. There are many self lubricating metal matrix such as copper, aluminum, manganese and nickel etc.

Bronze is a copper-based alloy. There are many types of this alloy such as, manganese bronze, tin bronze, aluminum bronze, leaded bronze and silicon bronze. Tin bronze are used for various engineering applications such as bearing and bushing application [2]. Tin bronze alloy is one of the most famous alloys that used as self lubricating material. In general tin bronze is known for their good corrosion resistance, wear resistance, good strength and good toughness [3]. Bronze consisting of (Cu10%Sn) is in common used as the base material for a bearing component. Lead is a common ingredient for use as an industrial additive [1]. It has important applications as a solid lubricant, and lead bronze is a useful material for sliding bearings, but lead is harmful to human health, especially the workers. For this reason, various regulations are in place to protect people. As a result, many industries have developed new materials as an alternative to lead. One of theses alternative is the graphite [4].

1.2. Application of self lubrication alloy:

1.2.1. Self lubricating Bearing:

In general bearing materials, copper-based alloys are the great source for bearing and bushing. Tin bronze, aluminum bronze, silicon bronze and leaded bronze are used for various engineering applications [5]. For all types of moving machinery and equipment, the bearings are important parts and successful machine operation may depend on the performance of the bearing surfaces. In order to improve bearing performance, it is necessary to produce a good design and also to choose the right set of materials for the particular design. A good bearing design includes three basic elements: understanding of the service environment, design of appropriate lubrication and selection of the best bearing materials for the job. The bearing material must be suitable for service environment and operating conditions. Bronze bearings provide a wide range of properties that simplify the material selection process and ensure that these selected alloys will provide optimum bearing performance [6].

In general, the characteristics of self-lubricants are: Low friction coefficient, good wear resistance, good toughness and high compressive strength, low shear strength at the bearing at the interface with the shaft; high resistance to abrasion and reasonable cost**.** Bronze alloys have low friction coefficients against steel. Efforts are usually made to keep bearings and their lubricants clean. A good loading material should be able to compensate for this by including these dirt particles in its structure to keep them away from the steel shaft [6].

1.2.2. Self lubricating Bushing:

It is one of the types of bearings used in various industries under the name of liner, to reduce the friction and wear between two surfaces sliding against each other. The difference between bearings versus bushings is that the bushings are a type of bearings. While the term carries a general term for something that allows movement between two components, bushings are specific pieces of equipment. Bushings, unlike roller bearings, are designed as a single part [7]. Machinery and equipment with rotary or sliding poles need bushings to improve overall efficiency and reduce vibration, noise and wear. Bronze bushings are more popular nowadays as they can effectively resist impact, abrasion and corrosion. These bushings can also be used at high temperatures without being damaged. There are two types of bronze bushings in the industry [8].

These two types are cast bronze bushings and oil impregnated bronze bushings.The bronze bushings are cast by continuous casting or centrifugal casting, with fine granular structure and strong mechanical properties and then machined to the final bushing. Cast bronze bushings are known to be much stronger, more durable and more resistant to compressive forces. These features make cast bronze bushings recommended for heavy duty applications require additional lubrication. Oil impregnated bronze bushings are manufactured by powder metallurgy technique. For oil-impregnated bronze bushings, the final porosity is about 25%. It is impregnated with a vacuum at the end to force the oil into the bonded porosity. Given these processes, oil impregnated bronze bushings can be beneficial due to reduced scrap loss. As for the draw backs, oil-impregnated bronze bushings are not good for applications that might interact with their impregnated oil. These bushings also have limitations regarding their mechanical properties [9].

1.3. The Target of the present study:

Due to the current industrial development, the aim of this research is to produce self-lubricant copper base alloy for bearings and bushings by casting method at a lower cost. Tin bronze is the most common material used in these applications, because it has good mechanical properties, good corrosion resistance and wear resistance. Graphite was added as solid lubricating particles instead of lead, which has a toxic effect on humans despite having high lubricating properties. The work also presents a study to the effects of graphite content and hot pressing on the microstructure and some characteristics, such as grain size, density, porosity, hardness, wear resistance, friction coefficient and the machinability of the (Cu-10Sn) alloy with graphite reinforcement. The alloy (90Cu-10 Sn) known as tin bronze (C91600), used as the master alloy in this work.

CHAPTER TWO

Theoretical Part and Literature Review

2.1. Introduction

This chapter will focus on the common materials used in bearing bushing application, manufacturing methods, and effects of reinforcing the tin bronze alloy by adding graphite particles on its applications in this field. The emphasis will be on the phase diagram of Cu-Sn alloy, reinforcing by graphite, required mechanical and machining properties for the bearing and bushing applications. Some recent studies on Cu-Sn alloy will be discussed in this chapter.

2.2. Metals and Alloy for Bearing Application:

The bearing is a partial mechanical element that supports the position of the shaft. Endurance efficiency affects the successful operation of systems or mechanisms. Therefore, bearing materials must make these systems operate successfully, bear working condition and meet performance expectations. Many metals used for bearing applications, such as aluminum, copper, gold, silver, indium, iron, tin and Lead. Bearing materials can be metallic or non-metallic. Metallic bearings are made from; tin and lead based, bronzes (copper based), aluminum based, porous metals, and coated metals. Non-metallic bearings are made of polymers, ceramics, and composites. Bearings can also be classified based on their geometry, half-round sleeves called bearings and full round sleeves are called bushes [10]. Bearing materials are required mechanical and tribological properties, such as, low friction, high wear resistance, compatibility etc. [11, 12].

2.2.1. Copper and Its Alloys:

Effective use of self lubricant materials is of critical importance due to the strong demand for miniaturization the coefficient of friction and enhancement of the wear resistance [13]. Copper (Cu) and its alloys are the most widely used materials for bearing and bushing because its excellent thermal properties, good strength and toughness, good machinability and weldability, excellent resistance to corrosion and fatigue, and generally non-magnetic properties [14].

Copper is a soft, flexible metal with good machinability, which makes it ideal for architectural applications such as roofs, wall cladding, gutters and downspouts. Additions of elements to copper strengthen it and form copper alloys such as brass and bronze like phosphor bronzes and aluminum bronze. Some copper alloys overpowered aluminum alloys in terms of tensile properties and approached those of stainless steel. In general, the strength of copper alloys is proportional to the quantity and quality of alloying elements added to pure copper, for example (silver, tin, nickel, etc.). Its strength increased in proportion to the amount of cold work [15].

Cast copper alloys have a broad range of application. They are used in different industrial components, and used in electronic components and state-of-the-art marine and nuclear equipment. Their favorable properties are often available in useful combinations. This is very important when, as is usually the case, a product must satisfy several requirements simultaneously [15].

Common copper forms can be categorized into: Copper-pure; Copper Bronze alloy and brass alloy. Each of these alloys have complex thermal equilibrium diagram, they have a similar solubility. Solid state pass by intermediate phases: the solid solution formed the alpha (α) phase whose atoms are arranged with a crystal type FCC network, which is characterized

by high ductility and elasticity. The (β) phase have atoms are arranged with a crystal type BCC network and is characterized by high strength and low ductility. It will produce two phases, like (α) and (γ). The (γ) Phase transform to α and δ during ordinary rates of cooling. The (δ) Phase transform to (α + ε) occur by the slow rate of cooling and low temperature. The (δ) (Cu31Sn8)-phase is hard and brittle and therefore decreases the strength and ductility of the alloy, to control the oddity by addition element in alloying or by heat treatments to prevent occur this phases and obtaining a suitable structure will produce desired mechanical properties. These alloying elements introduce secondary phase particle that interact with dislocation motion. This phases are produced the brittle ε (Cu3Sn) phase in slow cooling rate because the slow rate of copper diffusion in liquid tin below 350 °C [16].

2.2.2. Copper –Tin alloy:

Copper -Tin alloy is called tin bronzes. They characterize with good plasticity, strength and good impact resistance, they show good corrosion resistance in water vapors and sea water [17]. Tin (Sn) content in low-tin bronzes is (< 5% Sn), while in high-tin bronzes it is (> 5% Sn). The β phase being the solid solution on basic, it is subjected to eutectoid decomposition into α and γ phases. The γ phase, in turn, by one of the reactions possible at lower temperature values is transformed into δ, or ε phases [18]. The high-tin bronzes found their application for example in production of bearing. The bronze composed of Cu to Sn in proportion about (9:1)%, used in the bearing bronze is known as the corrosion resistant material. Bearing bronzes, besides the mentioned basic components, the presence of metals such as Zn, Pb, Sb, Ag, Fe and Ni was found [19]. Tin bronze with 10 to 12 wt. % Sn has a high strength and high

wear resistance. So, it's used for self-lubricating bearings and bushings. This alloy has a density of (8.775 g/cm^3). Tin bronze alloy with a higher Sn content are very brittle due to the intermetallic phases present in its structure. The Cu-10 wt.% Sn alloy shows excellent mechanical properties with a high strength and high ductility as well as high corrosion resistance in salt water. These properties enable application in navigation and machinery industries, such as in marine parts and high-precision bearings. The Cu-Sn alloys with Sn less than 5 wt.%, have a good plastic working property and it is widely used as electrical connectors [20].

2.2.3. Copper-Tin Phase Diagram:

In copper - tin system the relationship between the equilibrium diagram and the actual microstructure produced for a given alloy is rather more complex than the brass, the rate of diffusion of copper and tin into each other is much lower than it is with copper and zinc [21]. This is indicated by the wide range of composition at any temperature, between the liquidus and the solidus as shown in figure (2.1).

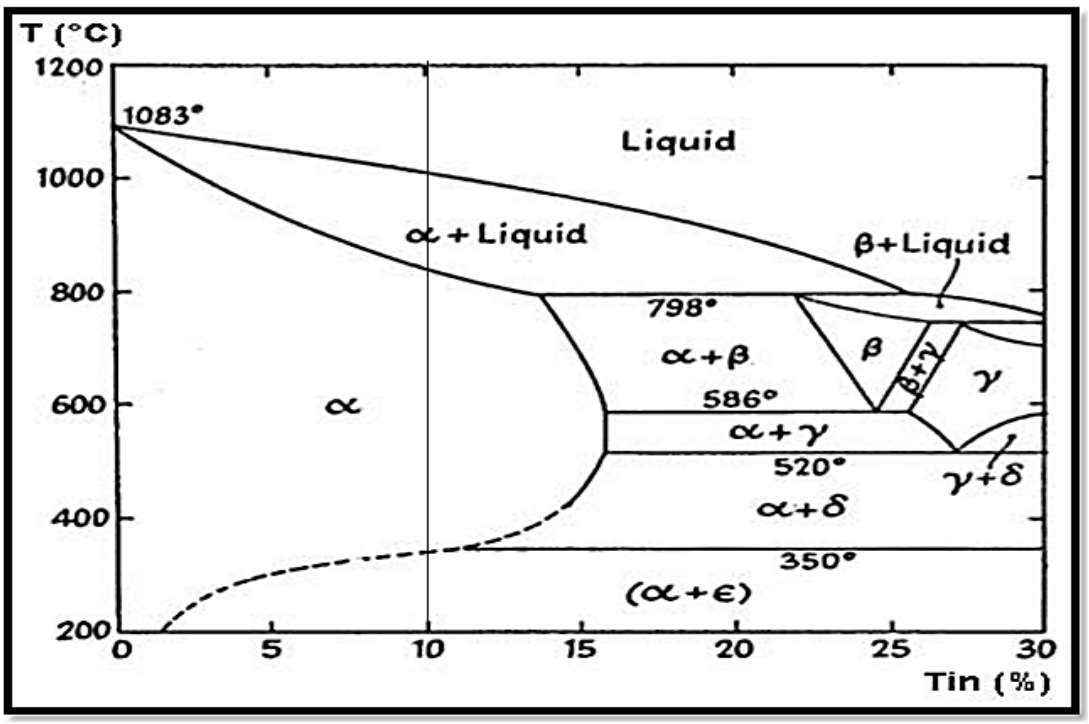

Figure (2.1): Thermal Equilibrium Diagram of Copper-Tin Alloy [22].

Moreover, structural changes below approximately 400 °C take place in copper-tin alloys with extreme sluggishness. When tin bronze alloy cooled to room temperature under very low cooling rate, exhibit the structure indicated by the equilibrium diagram, and the most important reactions that can be appear in the thermal equilibrium diagram of this alloy the peritectic reaction (α, β) at 798°C, while the eutectoid transformations β(α + γ) at 586 °C and γ (α + δ) at 520 °C will take place as indicated by the diagram during ordinary rates of cooling. The eutectoid transformation δ (α + ε) at 350 °C would occur only under conditions of extremely slow cooling due to the slow rate of diffusion of copper and tin atoms below 350 °C [21]. The α -phase, is tough and ductile a solid solution, so that α -phase alloys can be cold-worked successfully. The ε - phase, however, is an intermetallic compound of composition equivalent to Cu3Sn. It is hard and brittle. So, it has a negative influence on the ductility and decreases the strength of alloy in case of higher Sn content (above 20 wt %) [23]. Tin bronze has a composition of 90 wt % Cu and 10 wt % Sn contains of two phases at room temperature: α-phase, which is copper govern of a very small amount of tin in solid solution, and ε-phase, which contain of approximately 37 wt.% Sn [24]. According to the Cu-Sn phase diagram, the solubility of Sn in Cu is as high as ~ 16 wt.% at high temperatures between 500°C and 650°C, but it suddenly decreases as the temperature approaches room temperature. The alloy with 10 wt.% Sn can retain the single α phase with limit formation of the hard and brittle δ (Cu41Sn11) phase during cooling at room temperature after an appropriate homogenization treatment [25].

The grain size affects on mechanical properties. Increasing of grain size can reduce mechanical properties of the alloy. It causes a weak microstructure, lower hardness, decreasing density, decreasing toughness

and easy to crack propagation compared to fine grains [26]. Density affects on the mechanical properties and microstructure of the products. It is affected by the percentage of porosity, that be forming in the cast product. Porosity is caused by shrinkage of the metal and gas trapped in the molten metal. Porosity rate affects on the mechanical and physical properties of the materials. The density is affected by size, shape, locates of porosities and the grain size. Hot pressing technique is a method by which resulted products will have low pores and a structure with a lower grain size. The recrystallized microstructures observed in archaeological copper alloys are likely to have been produced between 500°C and 700°C [27]. This means that the hot working process for this studied alloy can be performed at such temperatures.

2.3. Composite Materials:

A rapid industrial development required the preparation of materials with better properties than metals, non-metals and alloys. These materials are known as the composite materials. Such materials consist of two or more materials, having different physical and chemical properties combined together, produce a material with new properties [28].

2.3.1. Metal Matrix Composite:

In metal matrix composites (MMCs), the matrix is either metal or metal based alloy. These composites can be reinforced by ceramics as particulate, continuous or discontinuous fibers and whiskers [29]. The composite materials can be manufactured by many techniques including casting. MMCs provide high strength, lightweight and stiffness required in many systems as high speed machinery and high-speed rotating shafts [30]. Copper metal matrix composite is one of the best material for many

engineering applications where the higher temperature resistance and good microstructural stability are required, due to their high sustainability, high conductivity, high wear resistance and good corrosion resistance. The choice of reinforcement material is dependence on their mechanical properties such as hardness, wear resistance, cost advantage, availability in market and refractory nature [28].

2.3.2. Strengthing Mechanism of Particle:

The strengthening mechanism depends on the size of the particles. Large particles (diameter$\geq 100\ \mu m$) tend to restrain the movement of the matrix phase. Matrix transforms part of the applied load to the particles, which bear a fraction of this load. The large particles form incoherent interface with the matrix, a wide number of dislocations are created at the interface. This increases the dislocation density and impedes their motility, so materials become strengthened. The strengthing by particles depends on many factors. These factors are the ability of impeding the motion of dislocation. The strength of the particles; with stand and transfer the load, the grain boundary of the matrix and the good interfacial bonding of the particles with the matrix; the distribution of the particles in the matrix, the shape and the size of the particle and their volume fraction [31]. When the particles size (the diameter between 0.001 and 0.1μm), the matrix carries the main part of the load and the particles become a hurdle up on the dislocation motion [32]. The reinforcement materials such as SiC, Al_2O_3, B_4C, TiC, TiB_2 and graphite provide increased stiffness and strength to the matrix, because these particles having high elastic modulus and high strength [33].

2.4. Graphite as Reinforcement:

Graphite is known to be good solid lubricants. It has low-friction behavior because it has low resistance to shear between neighboring atomic layers .Its high wear resistance, makes it spread as enhancing particles in metal matrix composites (MMC). Graphite has excellent lubricating properties, high abrasion, and thermal resistance. Therefore it is used with metals to get unmatched functionality for many applications, in automotive and nuclear industries [34].

Graphite is an industrial mineral, have various uses, with special properties that have eased technological innovation, beginning in the 16th century with discovery of high-grade lump graphite at Borrowdale, England. Graphite was transfer into pencils sticks and had strategic importance as a refractory lining materials for moulds that produced superior, smooth and round cannonballs with greater projectile range. At present, natural graphite is a key component in high-performance refractory linings for steel manufacture, high-charge capacity anodes for lithium-ion batteries, and a source of graphene to inspire a new generation of smart materials. Graphite, like diamond, is a crystalline form of carbon [35].

Graphite and diamond are natural allotropes of carbon that arise from the way the carbon atoms are joined together and arranged to form regular structures. In diamond, each carbon atom is bound to four other carbon atoms by strong covalent bonds in a regular isometric structure that gives rise to the hardest known mineral. In graphite, carbon atoms are bonded to only three other carbon atoms to form strong, two dimensional layers, that are extremely stable, but where each layer is only weakly linked to adjacent layers by van der Waal's forces. The resulting hexagonal layered structure forms one of the softest minerals. The presence of an unpaired valence electron makes graphite an excellent electrical conductor within the plane of the layers [35].

Graphite is inert towards most chemicals and has a high melting point of ~3,550 °C, but in the presence of oxygen will begin to oxide at temperatures >300 °C the rate of thermal oxidation is slow but increases with increasing temperature. Thermal conductivity in graphite is anisotropic but is very high in the direction parallel to the plane of the layers [36]. The crystal density of graphite is 2.266g/cm^3 but the measured specific gravity is typically between 2.20–2.30 depending on purity, low values of porosity. Graphite is soft, greasy to the feel, and is flexible and sectile. It commonly forms as foliated or scaly masses but may be radiated or granular, and is opaque black with a metallic luster but can also be dull and earthy [35].

Graphite surface profile and roughness of the graphite are some of the most important parameters to determine many physical and mechanical behaviors including friction or bonding condition [37]. Graphite is an ideal second phase into copper based alloys, usually added as self-lubrication and reinforcement particles into copper matrix due the ductile nature of the graphite. But because of poor wettability, agglomerating together, none uniformly distribute in copper matrix and a high specific gravity difference between graphite and copper it is very hard to add graphite particles into copper liquid. In metal matrix composites (MMC), the enhancement of mechanical properties and machinability to the reinforcement materials, depended on homogeneous distribution and good bonding between the metal matrix and reinforcements. So these difficulties are essential to be solved specially when using stir casting process to fabricate the composite [38].

2.5-Wetability:

Graphite with self-lubrication and superior thermal and electrical conductivity is usually added to copper as an ideal second phase. Until

now, many researchers have tried to fabricate copper graphite composites (CGC) by casting or powder metallurgy [39- 41].

According to poor wettability and a high specific gravity difference between graphite and copper, it is very difficult to add graphite particles into copper molten through casting, and they can't distribute uniformly in copper matrix, instead agglomerating together [42]. The wetting is very important in some applications such as oil recovery, lubrication, liquid coating, printing, and spray quenching. The contact angles, indicates the degree of wetting. When solid and liquid interact, there will be a contact angle. The contact angle values refer some parameter—the solid surface tension, quantifies the wetting characteristics of a solid materials. Small contact angles (<<90°) correspond to high wettability, while large contact angles (>>90°) correspond to low wettability. Figure (2.2) shows the contact angle [42].

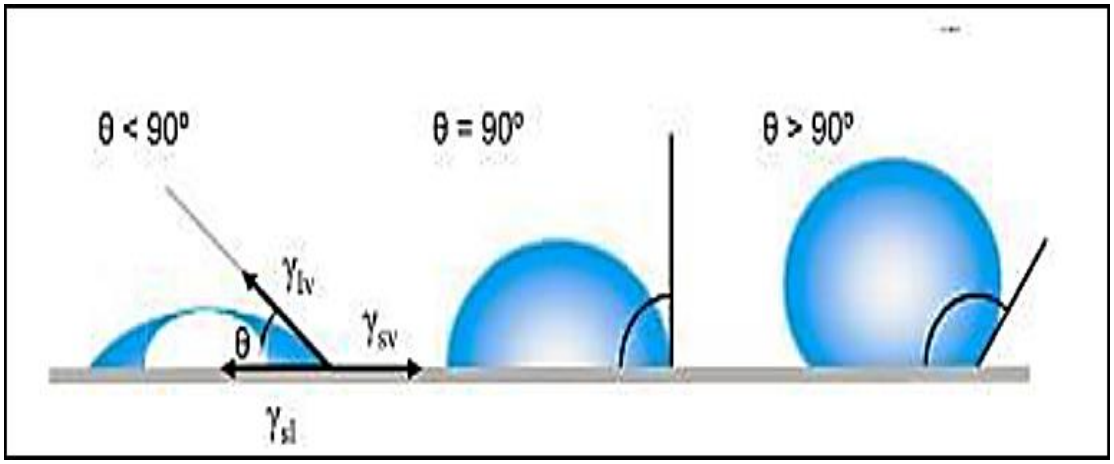

Figure (2.2): Wettability angles [42]

The intrinsic contact angle θ_y in a non-reactive solid-liquid system is given by the classical equations of Young Equation (2-1) [42].

$$\cos\theta y = \frac{\gamma sv - \gamma sl}{\gamma lv} \quad \text{..... (2-1)}$$

where is:

γ_{SV}: refer to the surface energy of the solid (J m^{-2}).

γ_{LV}: refer to the surface energy of the liquid (J m^{-2}).

γ_{SL}: the solid/liquid interface energy (J m^{-2}).

According to Equation (2-2), the intrinsic contact angle θ_y in a non-reactive liquid/solid system results from two types of competing forces: adhesion forces and solidarity forces. Adhesion forces that develop between the liquid and the solid phases, plain the amount of adhesion energy which promotes wetting. Solidarity forces of the liquid are represented by the surface energy of the liquid γ_{LV} acting in the opposite direction (the solidarity energy of the liquid is equal to ($2\gamma_{LV}$) [42].

In general, liquid metals are high surface energy liquids. Their surface energy γ_{LV} = 0.5 J m^{-2} for low melting point metals such as Pb and Sn, while γ_{LV} = 2 J m^{-2} for high melting point metals such as Fe and Mo. These values, discern the high cohesion of metals.

According to Equation (2-2), a contact angle of a few degrees or tens of degree (i.e., good wetting) of a liquid metal on a solid substrate if the adhesion energy is close to the cohesion energy of the liquid 2 γ_{LV}. This is happen or occur only if the interfacial bond is strong, i.e., chemical in nature. It is for liquid metals on solid metals regardless of the miscibility between the liquid and the solid, because in this type of system the interfacial bond is metallic. Liquid metals wet ceramics such as carbides, nitrides because a significant part of the cohesion of these materials is provided by metallic bonds.The solids that are not wetted by non-reactive liquid metals are the different forms of carbon, the ion covalent oxides and the mostly covalent ceramics with a high band gap like boron nitrite (BN). In these non-wetting systems' adhesion is provided by weak Vander Waals interactions [42]. The reinforcement particle wettability can be improved, by modification of its surface, and formation of a metallic coating [43].

2.6. Composite Casting :

Metal matrix composites (MMCS) have emerged as an important class of materials for structural, wear, thermal, transportation and electrical applications. This is due to their ability to exhibit superior strength-to-weight and strength-to-cost ratio when compared to equivalent monolithic commercial alloys [44]. Copper-tin -based particulate reinforced metal matrix composite has scattered paramount form of high performance material for use in bearing, bushes, filters and other industries because of its improved strength, high hardness, increased corrosion and wear resistance over conventional base alloy [45]. The manufacturing techniques of the metal matrix composites are classified in to three types namely [46]: Liquid state methods, semi solid methods, and powder metallurgy methods . In liquid state methods, the ceramic particulates are incorporated into a molten metallic matrix and casting of the resulting MMC is done. Stir Casting is a liquid state method of composite materials fabrication, in which a ceramic particle is mixed with a molten matrix metal by means of mechanical stirring. The liquid composite material is then cast by conventional casting methods [46].

The non-metallic “soft” phase particles, providing low friction and self-lubrication, are represented by graphite particle. In production of composites a method of melting and casting with mechanical stirring during the liquid state is to be used in the present study. Mechanical stirring can usually be applied in order to mix the particles into the melt, but when stirring stops, the particles tend to return to the surface because poor wettability of graphite in the melt means that the molten base alloy cannot wet the surface of graphite particles. Therefore, when the reinforcement (graphite) particles are added into the bronze molten, they will float on the melt surface. This is due to the surface tension, very large specific surface area and high interfacial energy of reinforcement particles, presence of

oxide films on the melt surface and presence of a gas layer on the ceramic particle surface.

There are some methods to improve the wettability of the reinforcement particles within the molten matrix alloy; for example heat-treatment of the particles before dispersion into the melt caused removal of the adsorbed gases from the particle surface. Another problem is distributing of reinforcement particles uniformly in molten matrix. When the particles were wetted in the melt, the particles will tend to sink or float due to the density differences between the reinforcement particles and the matrix alloy melt, so that the dispersion of the ceramic particles is not uniform and the particles have high tendency for agglomeration and clustering [47- 49].

2.7. Thermo-Mechanical Treatment:

High mechanical and physical properties with high performance can be achieved by refinements of the grain size. There are many processes to refine the grain size such as severe plastic deformation under hydrostatic hot pressure. Cu and its alloys are commonly used in many fields as bearings and bush sleeves, and in many other applications, therefore Cu-Sn alloys are performed to expand their applications [50]. The mechanical properties of Cu-Sn alloys improve by dynamic recrystallization at high-temperature deformation, which can control the microstructure [51].

Severe plastic deformation is an excellent way to get fine grain size and high strength for an alloy. The processes of sever plastic deformation are using simple shear [50]. The mainly hot deformation mechanisms of copper alloys are slipping and twinning. Twins boundary can try to stop the dislocations movement energy. While continuous twins boundary generate more dislocations sequentially as source of dislocations. The hot deformation can be defined by applying unidirectional isothermal load or isostatic-exsial hot press, which significantly decreased in grain size of the

alloy [51]. The major effect of refining the grain size that increasing in density and strength through severe plastic deformation.

2.8. Mechanical properties for the self lubrication bearing:

Copper alloys specially Cu-Sn alloy have a wide range of uses in the form of bearing, bushings and sliding elements . These elements ensure transmission or conversion of the drive energy in machines, plants and in internal combustion engines [52]. Figure (2.3) shows the location of bearing in typical engine block [53]. Tin bronze alloys require reliable and good lubrication, because these alloy have high hardness, they are used in high-load, low-speed systems such as bearings, gear bushings for off-road vehicles, rolling-mill bearings, and in internal combustion engines. Cast-bronze bearings give good compatibility, casting, easy machining, low cost, good structural properties and high load capacity [54].

Three critical performance parameters in bearings can be expressed. These parameters are the friction coefficient; the wear rate, which reflects material loss during the sliding; and the local bearing temperature, which is an important parameter in seizure. Among the properties required in the applications of bearings and bushings, the hardness, the wear resistance, the machinability, the high density, the low porosity, the high plastic formability and the corrosion resistance are preferable to increase the efficiency of the product and increase the mechanical workability of these parts and thus reduce the cost [53].

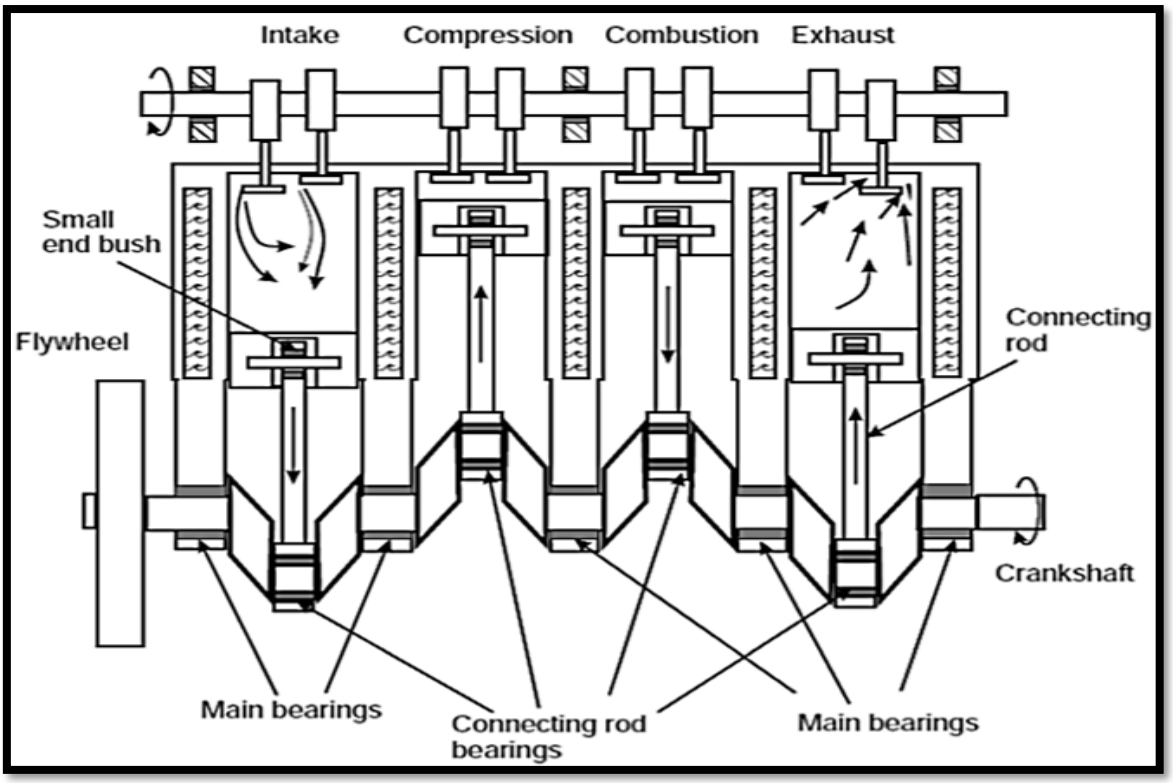

Figure (2.3): Location of bearings in typical engine block [53]

2.9. Machinability:

Machinability is the ease or difficulty for cutting, which a given material can be machined in a different machining technique. Various engineering applications used MMCs, which increasing of producing MMC, characteristics of MMCs are better from other alloy and metals; they are difficult to machine and increasing tool wear and decreases the tool life [55].

Machinability can be described by more than one explanation, and there are factors that influence it such as; tool wear, chip formation, cutting forces, cutting temperature and surface roughness. Other factors such as the condition of the work piece material, the reinforcement particles, the cutting operation, type of the machine tool and cutting tool used the cooling fluids for lubrication also affecting on machinability [56].

The composition and the microstructure of the workpiece and additives may causes machining problems or enhance in machinability [57]. Figure (2.4) shows the properties that affect the machinability of a material [58].

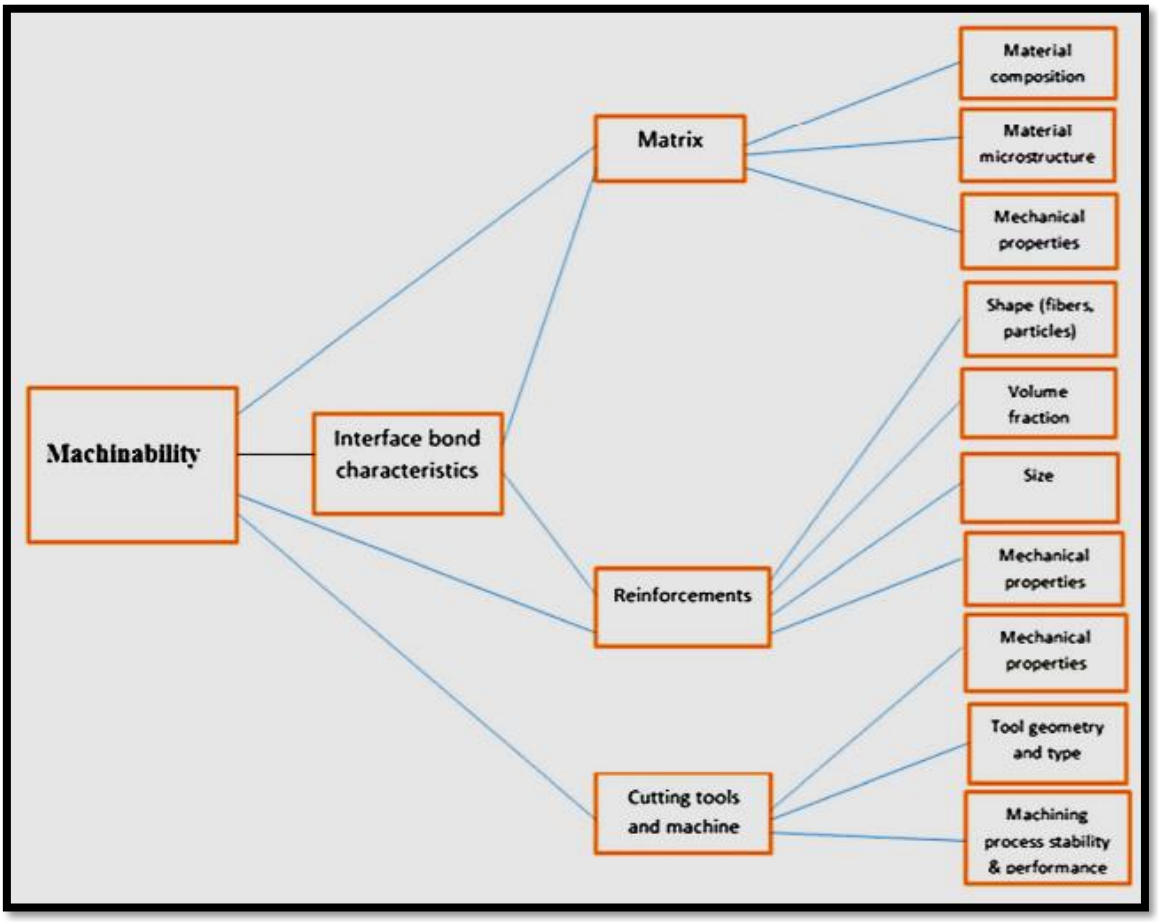

Figure (2.4): Properties that affect the machinability of a material [58]

The uniform structure, high hardness of the reinforcement phase, and abrasive properties affects on machining operation. As an excellent solid lubricant, the graphite particles dispersed in bronze matrix can play as breaking and lubricating role in the cutting process, which can reduce tool wear, increasing tool life and improve cutting force through reinforcing the mechanical properties of composite material matrix [59]. Bronze Cu-10Sn alloys after Homogenization and hot press observed that the microstructure with fine grains improved the hardness and wear resistance, which

improved the machinability [50]. The density, and porosity of the composites, increased with increasing of weight percentage of the reinforcements which may be due to the accumulation of the reinforcements having the high densities [60].

2.9.1 Surface Roughness:

One critical factor for part quality is surface roughness values [61]. Roughness is detrimental and determined for the available work piece in operation systems and determined the mechanical properties behaviors. For instance, it is well known that higher surface roughness adversely affects machined products' fatigue performance. The surface roughness influence on the behavior of materials is a complicated [62]. The decreasing surface roughness is observed to better interfacial bonding between metallic chips due to increased production parameters [63]. Temperature, surface characteristics and the reinforcement ratio are factors have effect on the surface roughness [64].

Surface roughness is important to study because it influences the fatigue strength, wear rate, coefficient of friction, and corrosion resistance of the elements machining. The most common choices in the roughness of technical surfaces are Ten - point mean roughness (R_Z) and the arithmetical mean roughness (R_a). Tool variables, work piece hardness and cutting conditions, are factors which affect the surface roughness. Tool variables include tool material, nose radius, rake angle, cutting edge geometry, tool vibration, tool point angle, etc. It is found that increasing in surface roughness increases with an increase in the feed rate and depth of cut and a decrease in cutting speed. Roughness reduced drastically up to a particular critical value of surface speed which is attributed to the reduction in size of the built up edge [65].

Finally, in metal matrix composite the parameters are affected on the surface quality of machined MMC, such as tool material, MMC materials, and typical machining parameters. The surface quality is breakdown, by higher feed rate [66].

2.9.2. Tool Wear:

Machinability affected by the mechanical and chemical relationship between the reinforcement and matrix material of the MMC. Tool type, stability of the machine, tool material, and tool geometry are the main factors that characterize the machining performance and cutting tool. Mainly description of the materials machinability is the tool life. Tool life is dependent on the type of material and also includes other factors machining aspects such as the tool material, cutting tool clamping, cutting tool geometry, and cutting parameters. There are many cutting tools types (i.e., carbide tool and High Speed Steel tool) [67].

The major factors during machining process of MMCs; Tool life and wear mechanisms, Cutting force and power required, Chip formation and behavior, Built-up edge (BUE) formation trend. The cutting process becomes more severe when cutting tool interacts with the workpiece, because the friction between the workpiece and the cutting tool and the produced heat from the plastic deformation of the workpiece material. Chip formation process begins by shearing the workpiece material in the machining process. There are two type of wear mechanism: abrasive wear and flank wear. Abrasive wear: most principal wear mechanism is recorded as abrasive wear mechanism, is occurring in the machining process of MMCs. Abrasive wear is occurs when the reinforcement particles impacting the cutting edge in machining MMCs, which these particles increase mechanical and thermal load on the cutting tool due to their

movement. The factors that affect on abrasive wear of cutting tool are in particular, the volume fraction, shape, and distribution of the reinforcement inside the MMCs [58].

Flank wear is a result of mechanical and thermal load that strains the cutting edge of the cutting tool. It is the most common wear type. Cutting forces is a major impact on the tool flank wear [67]. When particles of the workpiece material impact can be abrasive and hard, flank wear increases which increases the heat at cutting edge. The flank wear is measured by its width, which is increasing constantly during machining. Flank wear is also affected by the cutting parameters during machining MMC [58].

2.10. Literature Review:

There are several studies done to investigate the possibility of manufacturing self-lubricating composite materials by adding graphite as a reinforcement material in addition to its lubricating property.

In 2013, Dyachkova, & Feldshtein [68] used the sintered tin bronze (Cu-5Sn) as the base material to study the effect of additions of aluminum and nickel oxides. The result of the addition of the mixture of alumina and nickel oxide to tin bronze reduced the coefficient of friction and wear rate. The chipping of oxide micro-particles was observed at wear, which led to a change in the roughness of the working surfaces.

In 2013, Dhanabalakrishnan, et al, [69] developed Babbitt metal. , Babbitt with bronze particulate reinforced composite with different reinforcement compositions of bronze particles in the range of (1-5)%, using stir casting technique after melting pure Babbitt at 350c, bronze particles are introduced into the melt. Babbitt is used as the matrix of the composite, it is common material used in many bush and bearing applications, it is a better bearing to high seizure and reduces operating

costs. The results showed that the better resistance to abrasive wear at higher volume fraction of reinforcement and hardness also increased with the increase in reinforcement volume.

In 2014, Han et al, [70] used hot-pressing for 4 min at 421, 520 and 600°C to cast tin bronze alloy (75% Cu–25% Sn) to obtain a self sharpening bond for diamond honing stones. The result of the tests, showed improvement in mechanical properties such as hardness improved from 79.1 to 105.1 and from 104.2 MPa to 201.4 MPa. The hot pressing increased the density value at 421ºC and 520ºC from 104.2 MPa to 121.5 MPa from 7.4 g/cm^3 to 7.6 g/cm^3. At the hot pressing temperature was increased to 600 ºC, the microstructure consisted of α (Cu) + δ eutectoid.

In 2014, Juszczyk et al. [71] used powder metallurgy and stir casting routes to prepare copper-based composites reinforced by lubricating particles graphite, tungsten disulphide (WS_2), molybdenum disulphide (MoS_2) and glassy carbon. The composites are characterized by compact structure and the matrix adheres to the introduced lubricating particles, friction coefficient and high resistance to wear. The achieved results of these composite materials have low friction coefficient and high resistance to wear.

In 2015, Guo et al. [72] used mechanical blending of the powders to produce metal matrix composites (MMCs)reinforced with quasicrystalline particulates ,were deposited by cold spray process, by using the powder quasicrystal particles (AlCuFeB) as a reinforcement with tin bronze powder (CuSn8). Quasicrystal materials(QC), are have good mechanical, physical, and chemical properties, such as low surface energy, high hardness, low coefficient of friction and good wear and corrosion resistance because it have unique atomic structures, it is similar to brittle ceramics properties. The composite coatings hardness, wear resistance, and denser microstructures, increased with the increase of the incorporation of QC

phase, but the porosity of composite coatings decreases with increasing the content of incorporated QC phase.

In 2016, Jitendra kumar et al., [73] used stir casting to prepare copper-based composite reinforced by 5, 10 and 15wt.% of graphite particles. The particles are uniformly distributed in the matrix. The present of graphite particles causes increasing, in the wear resistance and mechanical properties of the composite when compared to that of pure copper. Also it is observed that the copper-15wt% graphite significantly improved the wear resistance of the composites, and the mechanical properties, compared to copper-10wt% graphite.

In the 2016, Wang et al., [74], in this study the addition of Ni particles in the composite material (graphite-lead free tin bronze composite layers on surface of steel sheets), linked them together. In this paper used powders of graphite and CuSn10 with addition of a nickel nitrate and poly vinyl alcohol (PVA) solution in an ammonia decomposition atmosphere. They was treated by cold rolling and second sintering, the results shown that no cracks observed at the interface between graphite and CuSn10 matrix and improved the mechanical properties due to the effect of Ni particles in graphite-CuSn10 composites , which makes them promising lead free bearing materials for heavy load engines.

In (2017), Ilayaraja, et al., [75], prepared copper based hybrid composite materials by using powder metallurgy technique with titanium dioxide (5wt.% TiO2) and 0wt.%, 2wt.% and 4wt.% of graphite. The research studied the workability of sintered composite and distribution of titanium dioxide and graphite reinforcements. This study, found that the workability increasing with increasing graphite content due to lubricating effect of graphite found equal distribution of reinforcements in the copper hybrid composite.

In 2018 Kumar, J., & Mondal, S. [76] studied copper matrix composites reinforced with graphite (5, 10, 15 wt.%) by using powder metallurgy process under 637 MPa pressure. The specimens were sintered under vacuum at 900, 950, 1000 ºC for 2 hour holding time at highest temperature. It is observed that a homogeneous distribution of graphite reinforcement particles, increasing the compression strength in composites with graphite (5, 10wt.%) and decrease of compression strength in composites with 15 wt% of graphite. The effect of reinforcement particles into copper matrix has improved the wear property for all specimens.

In 2019, Ramasamy et al., [77] In this research studied the mechanical properties of the sintered bronze with (5, 15 and 25) volume percentage of graphite as a reinforcement composites by using powder metallurgy method, a different compaction loads of (80, 120)Ton . It was observed that the porosity decreasing with decreasing in graphite volume percentage at increase of the true axial stress. Composite density and hardness increased with decreasing of volume percentage of graphite and increasing axial stress.

In 2019, Krishnan et al.,[78], the composite Cu-6Sn reinforced with 4wt.% Si, has been fabricated by using stir casting technique. It was observed that increased the hardness is due to the dispersion hardening of the reinforcement particles into matrix. The tensile strength of the composite increasing with an increase in the reinforcement addition but the ductility and the wear rate decreased in the composite as compared to the pure bronze alloy. In this study also observed that a uniform dispersion of reinforced particles is obtained by effect of the continuous stirring during casting of the molten metal**.**

In 2019, Ail et al., [79] copper matrix composite, bronze matrix (90% Cu and 10% Sn) with 4wt.% graphite (Gr) as reinforcement particles. The composite was prepared by liquid stir casting method. The microstructure

and mechanical behavior of composites was studied. It is observed the movement of the reinforcement in the melt leading to uniform distribution of reinforcement particles in the matrix. This uniform distribution of reinforcement reduced the agglomeration and segregation of particles, and porosity. Good wetting between particles and molten bronze matrix avoid present of casting defects such as porosity, cracks and shrinkages. Brinell hardness test values shown increasing from 54 to 61 BHN with increasing in graphite content .The tensile strength and yield strength of composites be higher than that of base matrix due to addition of reinforcements.

In 2020, **Yang & Kim [80]** the compressive deformation behavior was studied of a cast Cu-10 wt.% Sn alloy in the high-temperature (570–720 °C) and in the strain rate range of (10^{-3}-10) s^{-1}. Where Cu-10Snalloy showed drag creep at low strain rates and high temperatures, where a viscous glide of dislocations due to their interaction with solute atoms, the rate deformation mechanism at strain rates below (10^{-4}) s^{-1} and the power law breakdown (PLB) at high strain rates and low temperatures,. The results of Cu-10Sn alloy showed a better hot workability and better microstructures before deformation, compared to the pure Cu where the main deformation mechanism is dislocation climb creep. Recrystallization occurred at 570°C, while discontinuous dynamic recrystallization occurred at 720°C.

In 2021, Kathiresan [81] studied Cu-Sn alloy based composite Cu-2%Sn, Cu-5%Sn and Cu-10%Sn reinforced with 5wt.% of SiO2 were prepared through powder metallurgy. The study included the influence of the sintering temperature and pressure duration on the density, the hardness and the microstructure of the prepared composite. The tests results observed the addition of tin improves the mechanical properties, because tin wets the copper grains well at elevate temperature, this reduce the

porosity and increase the hardness of the prepared samples. Also notes that the density increased with the temperature and the pressure increases.

2.11. Summary of The Literature Reviews:

Previous studies showed that:

1. The literature shows that Bronze alloys including (Cu10Sn**)** reinforced with SiC, WS_2, TiO_2 and graphite to improve mechanical and tribological properties.
2. The poor wetting of graphite has not been studied, which lead to formation of graphite particles agglomerations in the matrix.
3. Did not use hot press in three directions (hot squeezing), and did not studied the squeezing enhancement on the grain size and mechanical properties.

Chapter Three

Experimental Part

3.1. Introduction:

This chapter explains the experimental work starting from preparing the samples of the study and their thermo- mechanical treatment. The chapter also describes all the condition under which the tests were carried out. This includes the materials and the apparatus used. Mechanical and physical tests and the program of the machining experiments will be presented. These tests include: Micro-structure test, X-Ray Diffraction, X-Ray Fluorescence, Brinell hardness test, grain size measurement, wear test and SEM-EDS test**.**

3.2. Program of The Current Study:

Figure (3.1) illustrates the program of the present study and the procedure used in the preparation of the samples.

3.3. Materials and Samples Preparation:

Table (3.1) demonstrates the materials used to prepare the samples of the study.

Table (3.1); Materials used to prepare the samples.

Materials	Company
Copper	USA. Oxford LABORATORY REAGENT (iso:9001-2008)
Tin	USA. San Mateo, CA94403.
Graphite	HENAN STAR METALLURGY CO., LTD. China. The particles size 6.3693 μm.

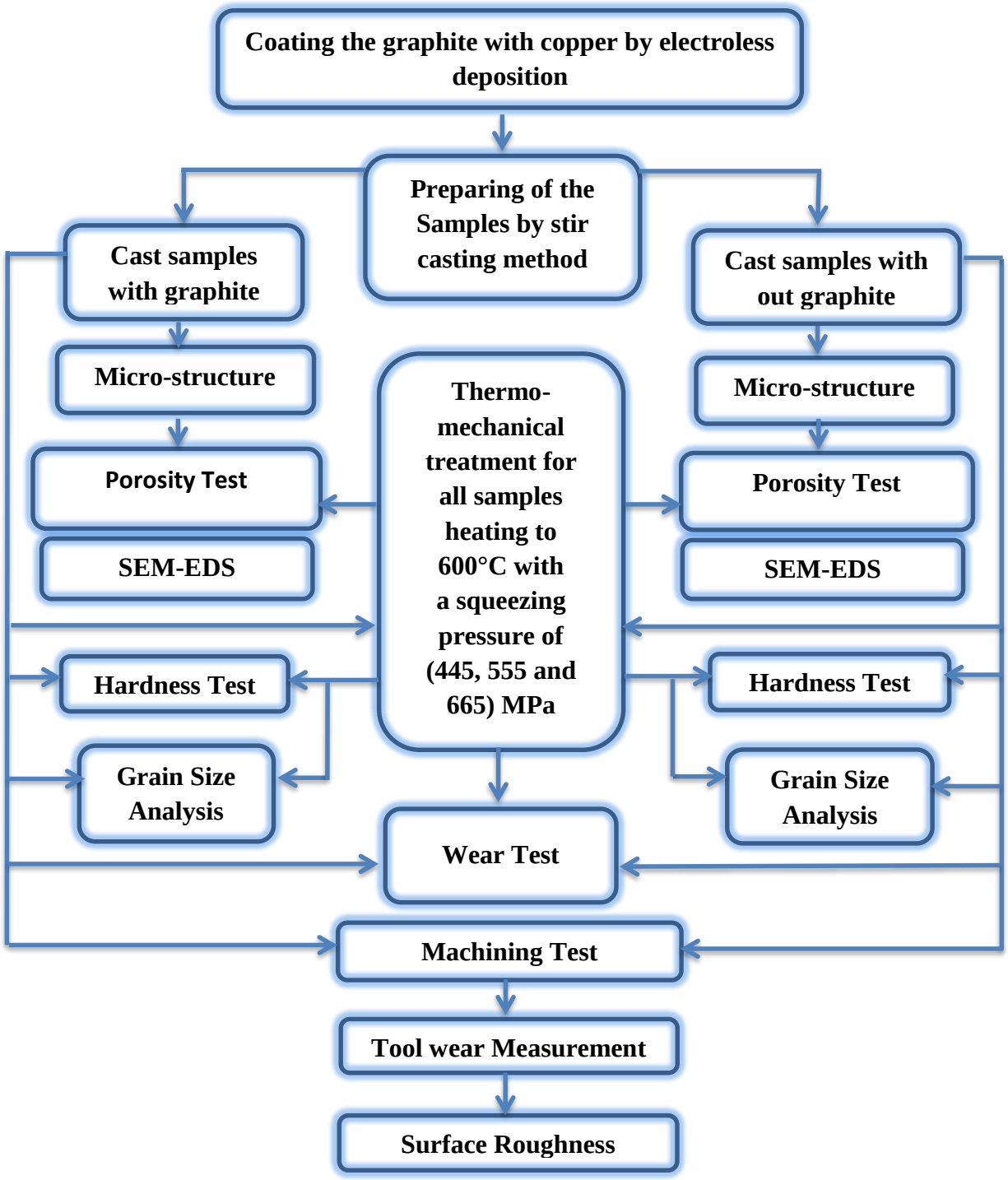

Figure (3.1): Experimental program of the present study.

The average graphite particle size was 6.393μm. The test was achieved via laser particle size analyzer type (Bettersize 2000) shown in Figure (3.2) Particle size analysis was carried out at the University of Babylon /

College of Materials Engineering / Ceramics and Building Materials Labs. The particle size analysis report is shown in Figure (3.3).

Figure (3.2): Laser Particle Size Analyzer type (Bettersize 2000).

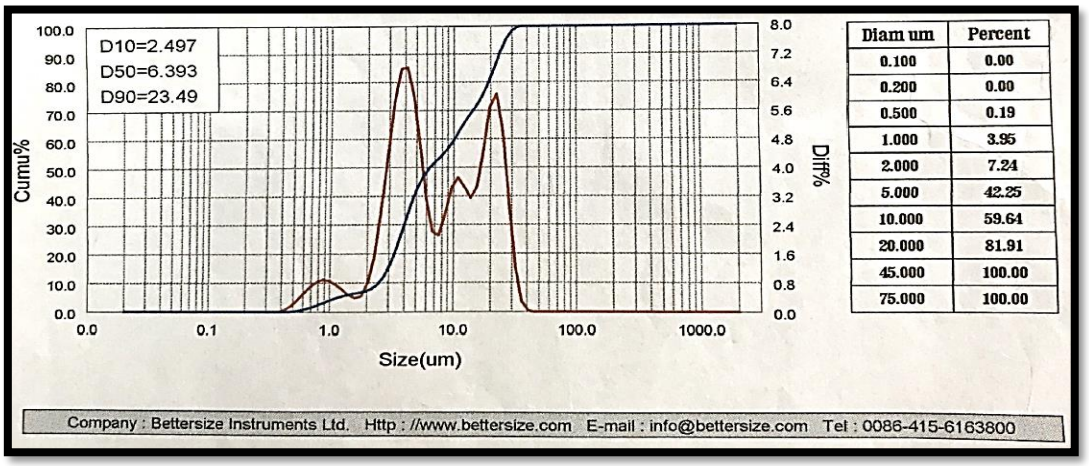

Diam um	Percent
0.100	0.00
0.200	0.00
0.500	0.19
1.000	3.95
2.000	7.24
5.000	42.25
10.000	59.64
20.000	81.91
45.000	100.00
75.000	100.00

Figure (3.3): Particle Size Analysis of the used graphite.

3.3.1. Preparation of Coated Graphite:

One of the main problems in casting Cu-Sn base-graphite composite was the poor wetting of the graphite particles with copper and the difficulty of adding these particles to the molten metal due to the difference density between them. Therefore, the graphite particles were coated with copper by using electroless deposition method at room temperature.

Table (2) contains the materials used in the electroless deposition process [82].

Table (3.2): Materials used in electroless deposition [82].

Material	Weight
Copper sulfate, pentahydrate	13.8 gr/L
Sodium potassium tartrate, tetrahydrate	69 gr/L
Formaldehyde (36% w/v 121%CH,OH)	40 ml/L
Mercaptobenzothiazole	0.003%
Sodium hydroxide	20 gr/L

Electroless deposition was carried out through the following steps :

a) Copper sulfate mixed with the required amount of hot water then left to cool down, then formaldehyde was added to the mixture;

b) Mixing sodium hydroxide with the amount of hot water then adding Rochelle salt to the mixture.

c) Mixing the two above solution

d) By adding the required amount of graphite (100g) to the solution with mixing, the color will be change to the red, which means that Cu coated graphite. The coated graphite was filtered and dried for two hours using an oven at a temperature of (50°C) with inert gas .

3.3.2. Preparation of The Samples By Stir Casting Method:

The alloy samples (Cu10Sn) were prepared by stir casting method. High purity copper was melted in a ceramic crucible via gas furnace at 1100°C in an inert gas atmosphere. The temperature was controlled using infrared camera type (SMART SENSOR AR882). Tin (in the form of particles) or the coated graphite (if required) enveloped separately by

copper foil and added gradually to the copper melt. During the process, the melt was stirred using electric stirrer rotating with a speed of 750rpm. Preheated to 300°C cast iron mold with a cylindrical cavity of 16mm diameter and 220 mm height was used. The samples were cast with (0, 1, 3 and 5wt.%) of coated graphite and coded as B0, B1, B3, B5 respectively. The obtained samples were heated to (650°C) for 3hrs in an electric furnace type (Sola Basic SB Lindberg) for homogenization. The homogenized samples were left to cool inside the furnace.

3.4. Thermo-Mechanical Treatment of The Samples:

To investigate the effect of hot forming on the studied properties, specimens of the cast samples were subjected to different amounts of squeezing pressure (445, 55 and 665 MPa) at 600 °C. The pressure was kept for 10 minutes at the elevated temperature to reach the active effect of the process. Cylindrical specimens with 13mm - diameter and 14mm-height was fitted in a cylindrical steel die with the same diameter and subjected to the axial squeezing load. The squeezing process was performed via an electric press type (CARVER), shown in Figure (3.4). The heating was performed by a heating specially designed and built device shown in Figure (3.5).The die and the specimens are shown in Figure (3.6). The treatment was carried out at Babylon University College of Materials Engineering- Dept. of Metallurgical Engineering

Figure (3.4): press type (carver) used to perform squeezing of the specimens.

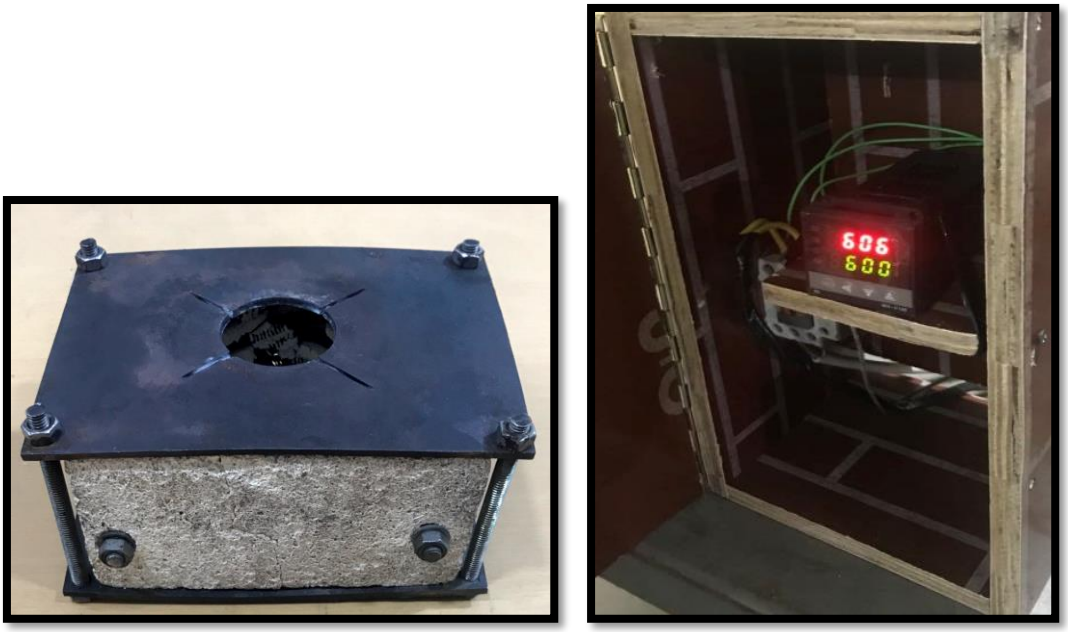

(a) **(b)**

Figure (3.5): (a) The designed heating element; (b) the controller of temperature.

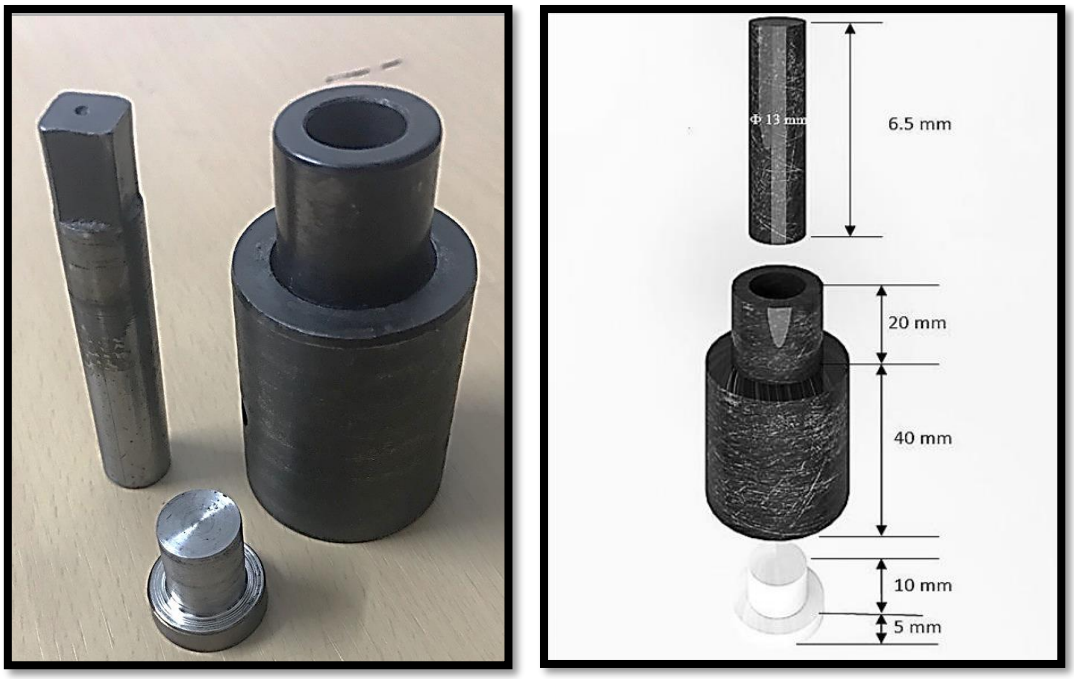

(a) **(b)**

(c) **(d)**

Figure (3.6): The die and the specimen: (a) die parts; (b) dimensions of the die parts; (c) specimen before pressing; (d) specimen after pressing.

3.5. Mechanical and Physical Tests:

3.5.1. Chemical Composition Test:

The optical emission spectrometer is the chemical composition analysis for the prepared samples was carried out in the General Company for Examination and Rehabilitation Engineering-Baghdad via the testing device type (Bruker AXS- ID76187 Karisruhe).

3.5.2. Optical Microscope Analysis:

Specimens with 13mm diameter and 14mm height machined from the prepared samples were ground and polished according to ASTME3 by using paper grits as (180, 400, 800, 1000, 1200, 2500 and 3000) and diamond solution with 0.25µm. The specimens then were etched with a solution consisting of (95 ml + 8ml HCl + 5g FeCl3) at room temperature [83], washed by distilled water and dried via electric drier. Optical microscope model YJEYE01 captured the microstructure of the surface.

3.5.3. X-Ray Diffraction (XRD):

The X-Ray diffraction was used in order to identify the phases of the cast samples, and then compare it with the standard charts. The speed used was (2deg/min), the step was (0.02deg), and the angle 2θ used is from 20 to 100º with Cu target, wave length of 1.54060 Aº, voltage and current are 40 KV and 30 µA respectively. This test was carried out in the Center of Nanotechnology at University of Technology, via the X-ray diffractometer type model: "XRD 6000" shown in Figure (3.7).

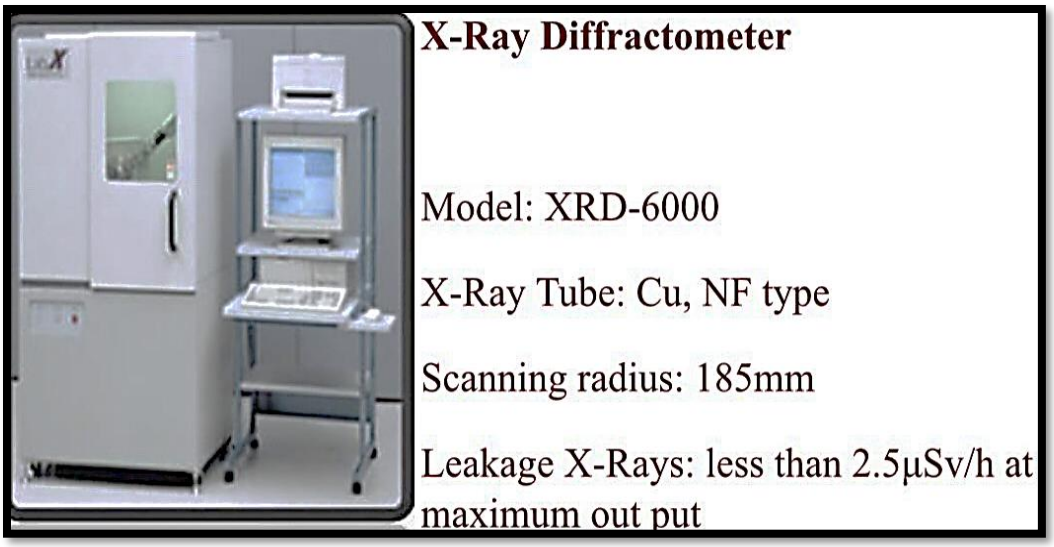

Figure (3.7): X-Ray Diffractometer.

3.5.4 Scanning Electron Microscopy (SEM- EDS) Analysis:

The specimens were prepared as the same followed procedure in the optical microscopic test. The test was carried out via a scanning electron microscope type (INSPECTS550) shown in Fig (3.8). Energy dispersive spectrometer (EDS) determined the mean value of the chemical composition for the micrograph of the specimen.

Figure (3.8): Scanning electron microscope type (INSPECTS550).

3.5.5. Grain Size Measurement:

Grain size measurement achieved by using the ―Image J version software. The software is able to effectively analyze the image and receive the detailed technical data. It supports most of the image formats and has a set of editing tools. The software enables to produce the various geometric transformations, create the density histograms, conduct 3D visualization, perform the logical and arithmetic operations between images, etc. The program can measure the area of a single grain as well as the areas of the total grains in relation to the microstructure. It can measure the number of total grains in relation to the total area. This ability will be used in this work.

3.5.6. Porosity Test:

The tests were carried out for specimens the cast samples. The test was performed for the specimens before and after the hot deformation. Porosity determined according to the ASTM (B 328 – 96), the following equation was used [84].

$$\text{Porosity (apparent)} = [\,(Ww - Wd\,) \div (Wsat - Wg)] \times 100 \quad \ldots\ldots\ldots (3\text{-}1)$$

Where: W_d:- dry weight of the specimen; W_w:- wet weight of the sample (the sample was weighed after immersing it for 24 hours in distilled water); W_{sat} :- saturated weight (the sample was weighed after immersing it for 5hrs. in pure water at 80°C); W_g :-.suspended weight (weighing the suspended sample in distilled water).

3.5.7. Brinell Hardness Test:

The test was performed in accordance with ASTM (E10-15a) using a ball indenter of (2.5mm) diameter and a load of (62.5kg) for 30 seconds [85]. A suitable specimen size was cut from each type of the cast

samples and well prepared for this test. The hardness was recorded as an average of three measurements for each specimen. The test was performed via a Brinell hardness tester type (Wilson Hard REICHERTER UH 250) the University of Babylon/College of Materials Engineering- Dept. of Metallurgical Engineering.

3.5.8. Wear Test:

Pin-on-disk device was utilized to determine the coefficient of the friction and the wear rate of the prepared samples. Specimens of 13mm in diameter and of 14mm thickness were used based on ASTM (G99-104) [86]. The specimens were ground and polished suitably by using emery paper so that the average of surface roughness was 0.8μm. The weight loss of the specimens due to the test was measured via sensitive electric balance model (M254A) with ±0.0001 accuracy. The test was performed via a wear tester device type (MT-4003, version 10.0) shown in Figure (3.9). The specimen was set as a pin against standard rotating steel disk with a hardness of 850HV and a diameter of 30mm. The wear rate was determined by the following equation [87]:

$$W_r = \Delta w / 2\pi r n t \quad \ldots\ldots\ldots\ldots\ldots\ldots\ldots\ldots\ldots\ldots\ldots\ldots\ldots\ldots \quad (3.2)$$

Where: W_r - wear rate (g/mm.rev); ΔW- weight lost (g) which is the difference in weight of the specimen before and after the test; t- Sliding time (20min.); r- the radius of the specimen to the center of the disc (5mm); and n- disk rotational speed (400rpm).

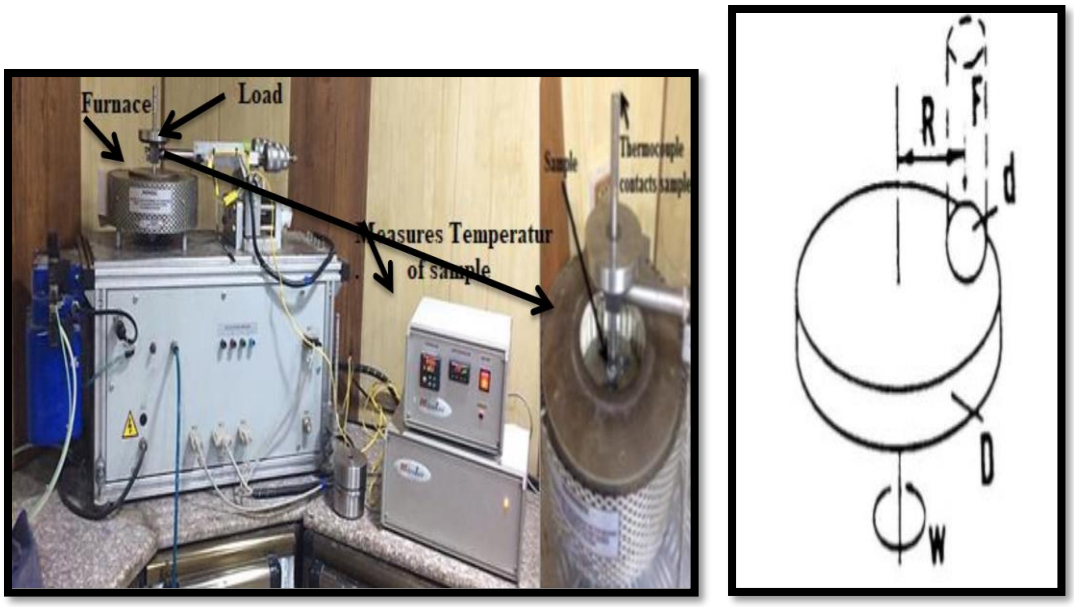

Figure (3.9): (a) wear tester device type (MT-4003), version 10.0; (b) Schematic of Pin-on-disk Wear Test System [87].

During the test the pin (diam. =10mm) was subjected to a normal force of 10 and 20N for a sliding time of 20 min

3.6. Machining Test:

Facing turning was used for all machining experiments. The turning was achieved on a machine type (ZMM-Sliven/Bulgaria) with a power of 2.2 kw and a spindle speed of (20-2000 rpm) and feed rate of (0.015-0.6 mm/rev). The machining tests had been carried out using cemented carbide tips type P10 with a chemical composition of (65% W, 9% Co, 26% (TaC + TiC) [88]. The tip has two cutting edges with tool angle of (55°) and a nose radius of (1.6mm). The tool holder type (AG.CO Tools) and dry cutting conditions at a constant depth of cut d=0.01 mm, were used. Four spindle speeds (80, 125, 315 and 500 rpm) with a feed rate of (0.15 mm/rev) were used as the machining conditions.

3.6.1. Measurement of The Tool Life:

During the machining operations measurements related to the tool wear and surface roughness had been carried out. A maximum width of (VB max = 0.3 mm) for the flank wear was used as a criterion for the tool life according to ISO 3685 [89]. One minute-short time test was used to find the tool life. In this method the cutting conditions will be continued for "1.0"min, and then the operation will be stopped to measure the width of the flank wear. The process will be repeated under the same cutting conditions and using the same cutting edge until the width of the flank wear reaches its criterion limit. Optical microscope type (1280XEQ-MM300TUSB) of 100X magnification was used to measure the flank wear width.

3.6.2. Surface Roughness Measurement:

For each cutting operation under the required cutting conditions, the surface roughness (Ra) was measured via a roughness type ((HSR 210 Roughness Tester, china). All measurements were carried out after the first minute of machining. In each case the sample was mounted on a flat base then the distance to be tested was appointed and the probe of the measuring instruments was attached by special lever to the surface of the sample, after that the instrument was switched on with continuous movement of the probe into front and behind. The instrument registration board gives the roughness value directly and the maximum reading was recorded. The specimen was turned and the measurement was repeated. An average of three readings was considered in this test.

Chapter Four

Results & Discussion

4.1. Introduction

Chapter four records all results of the physical and mechanical tests carried out in this study. These results are scientifically discussed to choose the best the addition of graphite and the best conditions of thermo mechanical treatment on the output parameters or responses of the self-lubricant tin-bronze cast composite.

4.2. Chemical Composition Analysis:

The chemical composition analysis for all prepared samples are demonstrated in the table (4.1). The results indicate that all the prepared sample have the required composition.

Table (4.1): Composition of the prepared samples.

Samples Code	Elements											
	Cu%	Sn%	Zn %	Ni%	Al%	Sb%	Fe%	Si%	Mn%	Mg%	Ag%	Other %
B0	88.55	9.53	0.81	0.42	>0.168	<0.1	0.060	0.043	0.026	<0.002	0.005	0.286
B1(with 1% coated graphite)	87.97	10.34	0.67	0.57	0.005	<0.1	0.19	0.037	<0.003	<0.002	<0.005	0.108
B3(with 3% coated graphite)	87.01	10.6	1.22	0.48	0.042	<0.1	0.345	0.039	<0.003	<0.002	0.007	0.152
B5(with 5% coated graphite)	87.42	10.16	1.25	0.394	0.003	<0.1	0.336	0.04	0.005	<0.002	0.008	0.282

4.3. Optical Microscope Analysis:

Figures (4.1) to (4.4) show the microstructures of the samples before and after the hot pressing. The dark region in the figure represents the graphite particles around the grain boundaries. The microstructures exhibited the homogeneous distribution of solid lubricant in the bronze matrix and the fine microstructure with increasing the pressing load.

After the homogenization treatment conducted at 650°C for 3 hours for all specimens , one-phase microstructure is noticed, which represents the α-phase of the alloy matrix [90].

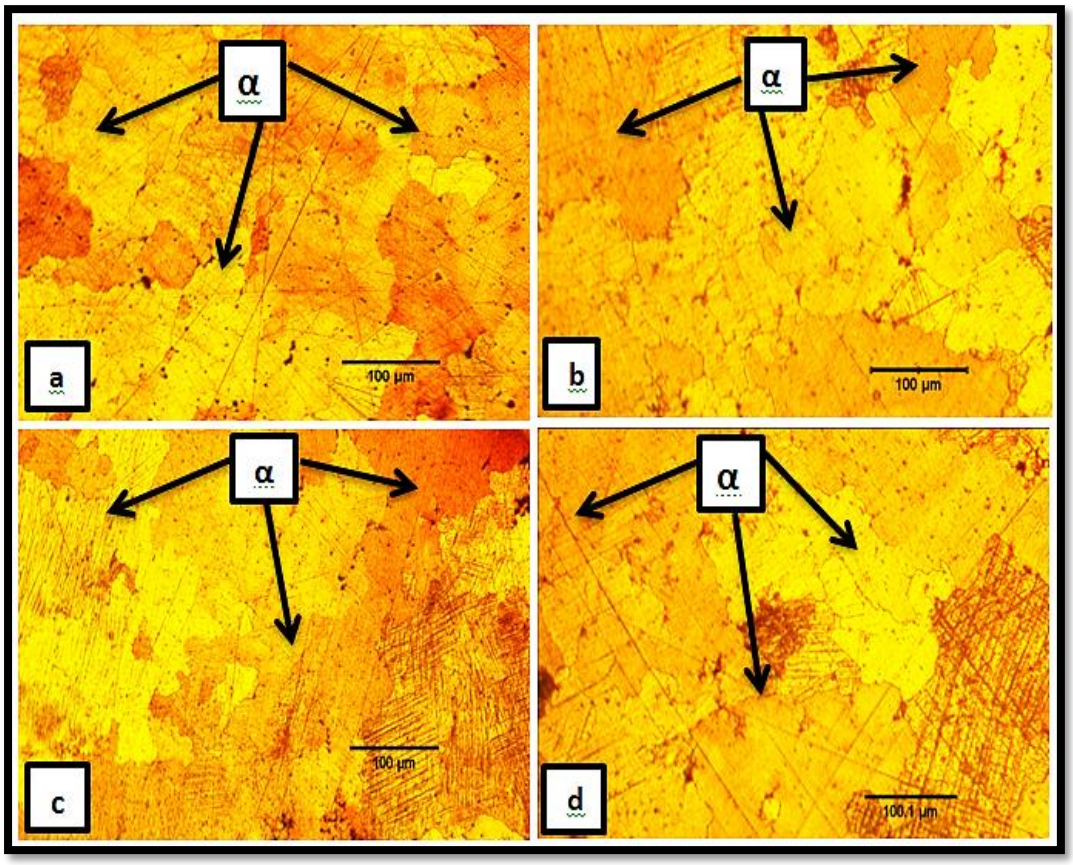

Figure (4.1): Microstructure (100x) of Cu-10Sn alloy: (a) before the hot pressing and after hot press with; (b) 445MPa; (c) 555MPa; and (d) 665MPa.

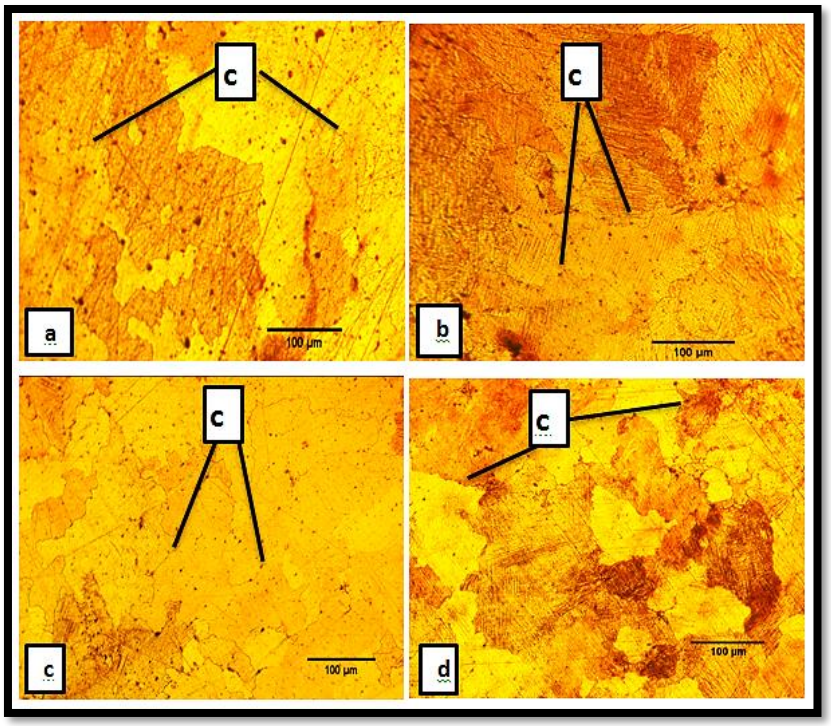

Figure (4.2): Microstructure (100x) of Cu-10Sn with 1wt.% of coated graphite: (a) before the hot pressing and after hot press with; (b) 445MPa; (c) 555MPa; and (d)665MPa.

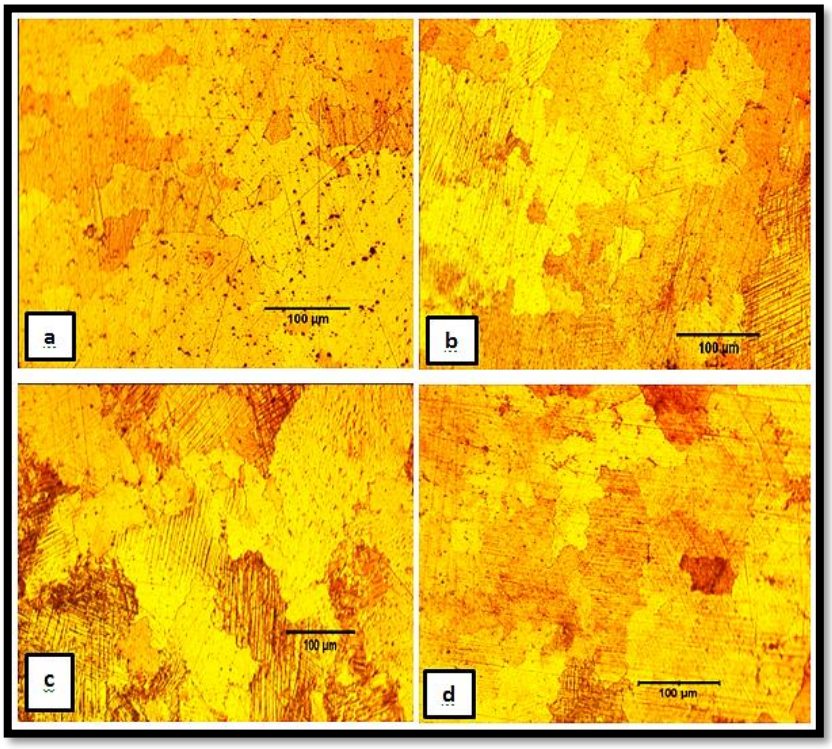

Figure (4.3): Microstructure (100x) of Cu-10Sn with 3 wt.% coated graphite: (a) before the hot pressing and after hot press with; (b) 445MPa; (c) 555MPa; and (d) 665MPa.

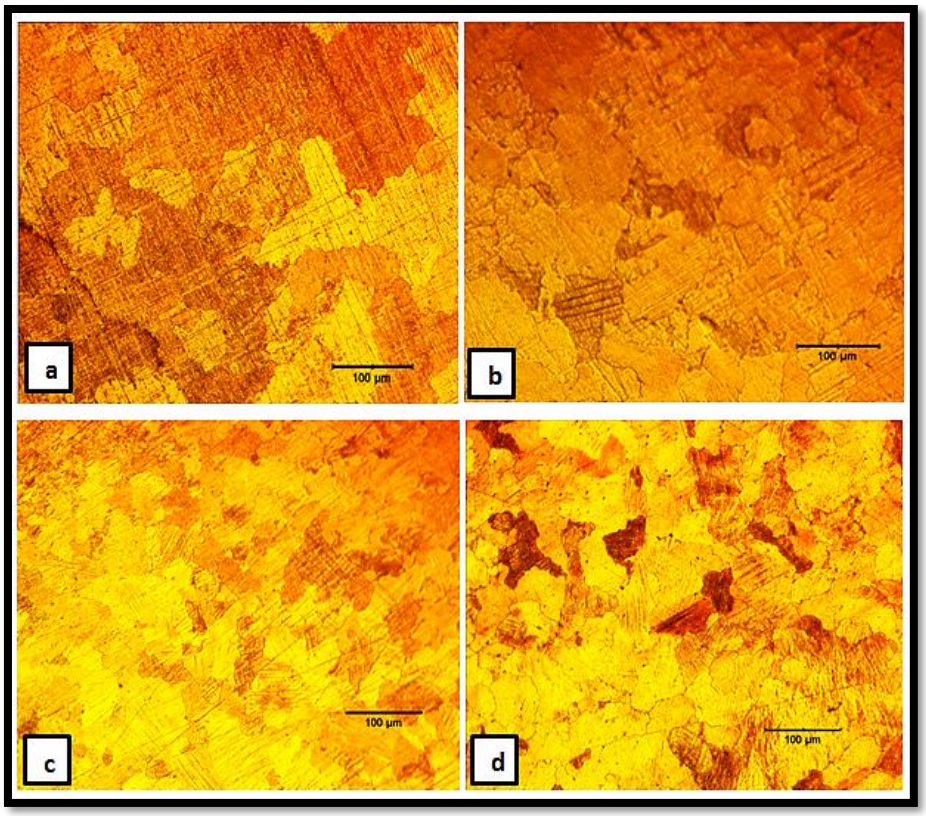

Figure (4.4): Microstructure (100x) of Cu-1Sn with 5 wt.% coated graphite: (a) before the hot pressing and after hot press with; (b) 445MPa; (c) 555MPa; and (d) 665MPa.

4.4. X-ray Diffraction (XRD) Analyses:

Figure (4.5) and (4.6) demonstrates samples of the identical resulted patterns. The results of the X-Ray diffraction analyses insure the presence of one phase (α-phase) in all of the alloy samples before and after the hot pressing. The formation of ε (Cu_3Sn) phase was avoided due to the high temperature homogenization. Furthermore the avoidance of δ ($Cu_{41}Sn_{11}$) phase formation which is hard and brittle insure the 10wt% of the tin in the prepared samples. The (α-cu)-phase samples of the result patterns are shown in figure (4.5) for the base alloy and figure (4.6) for the composite having 5 wt. % of the coated graphite. The peaks match with the standard chart of the X-ray diffraction for each phase. All the patterns and the slandered chart are shown in appendix (A1).

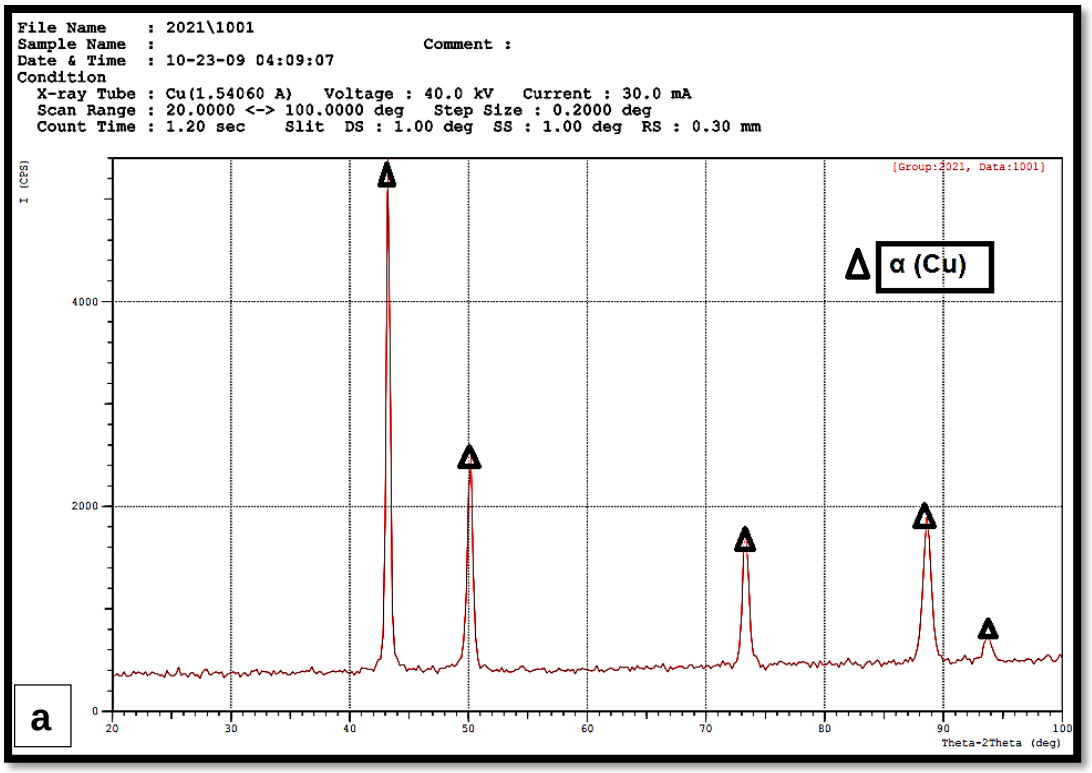

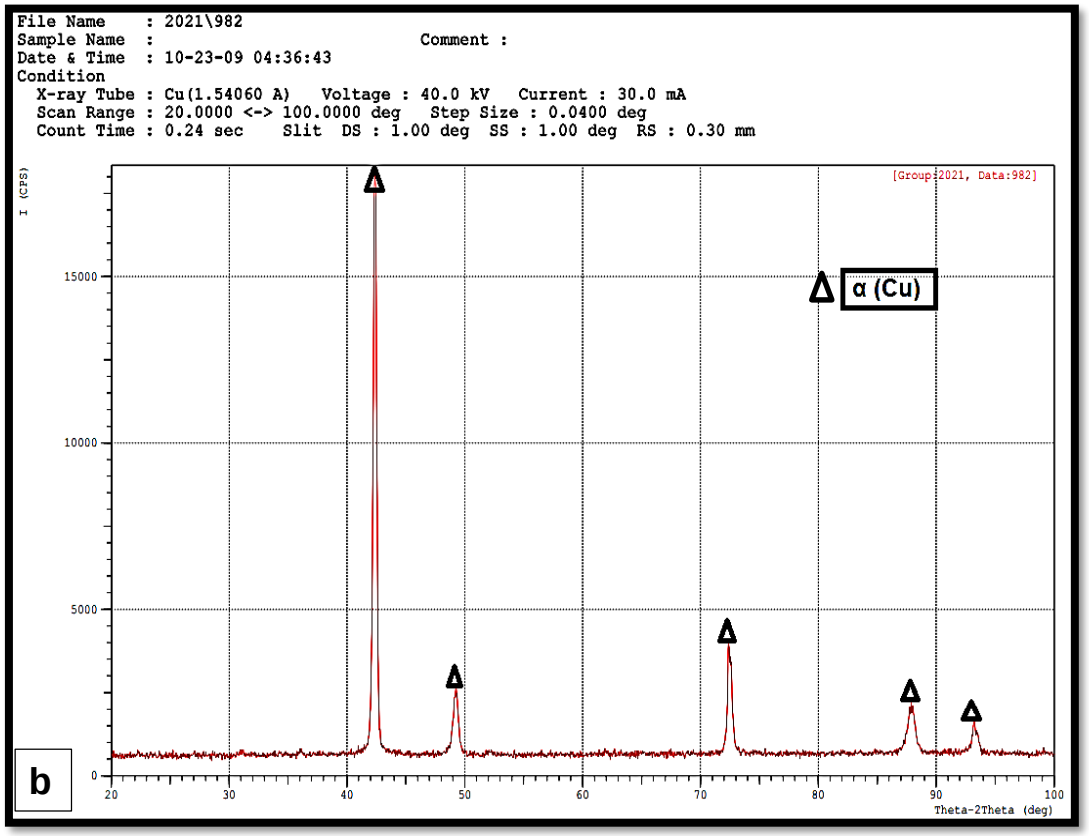

Figure (4.5): XRD patterns before hot pressing for: (a) alloy sample B0, (b) composite sample B5 having 5wt.% of coated graphite.

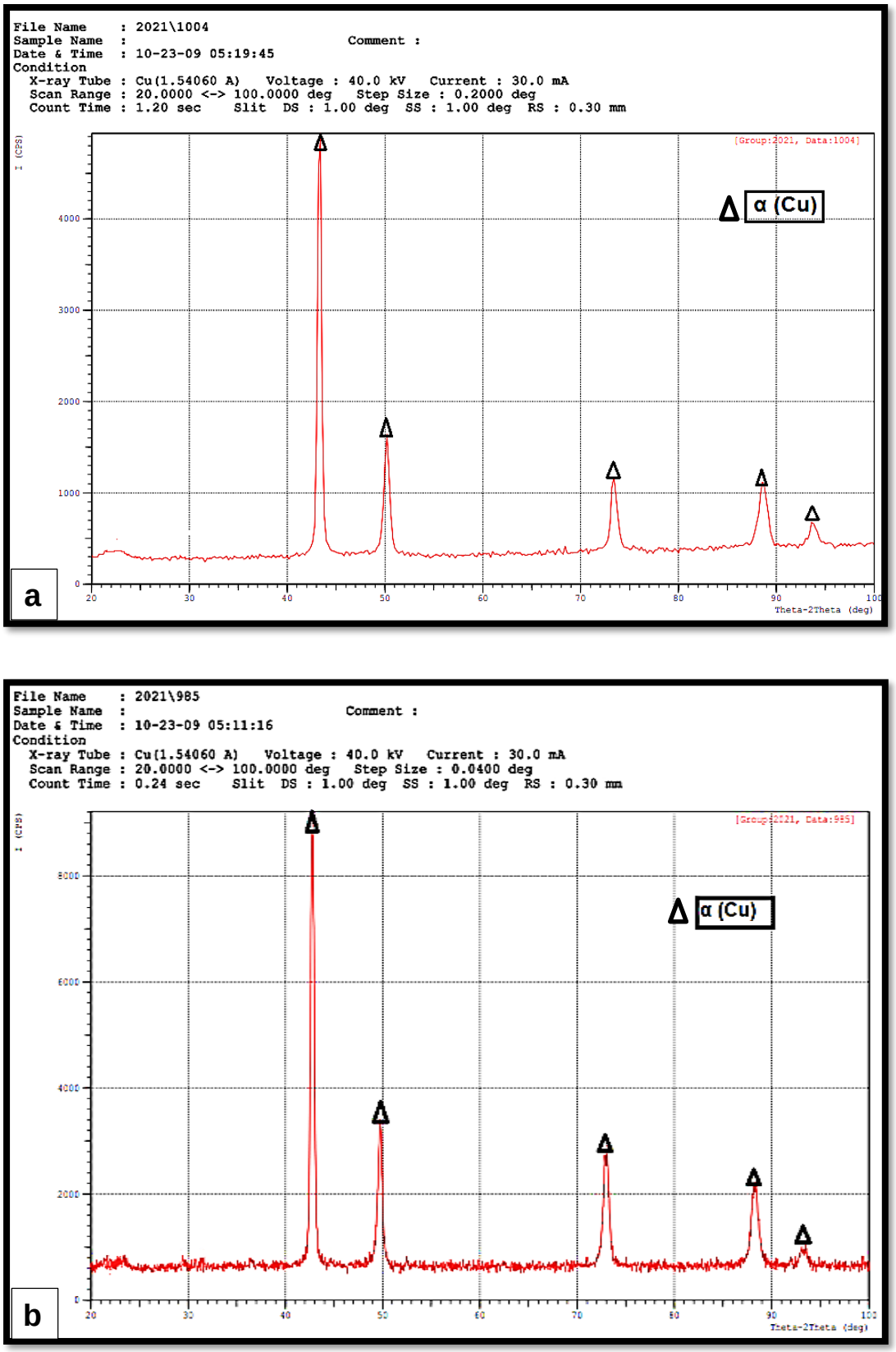

Figure (4.6): XRD patterns after the hot pressing for: (a) alloy sample B0; (b) composite sample B5 having 5wt.% of coated graphite.

4.5. SEM-EDS Analysis:

Figure (4.7) and (4.8) shows respectively the results of the SEM analysis for the prepared Cu10Sn alloy sample and for the reinforced sample with 5wt.% graphite. The results indicate the presence of graphite in the specimens. The SEM images of the Cu10Sn and Cu10Sn with 5wt.% graphite show, homogeneous microstructures containing deformed and smaller grain size, in comparison with the composites and the alloys before hot press [91]. SEM image observed the arrangement of graphite particles as a compact agglomerates at grain boundaries in the matrix.

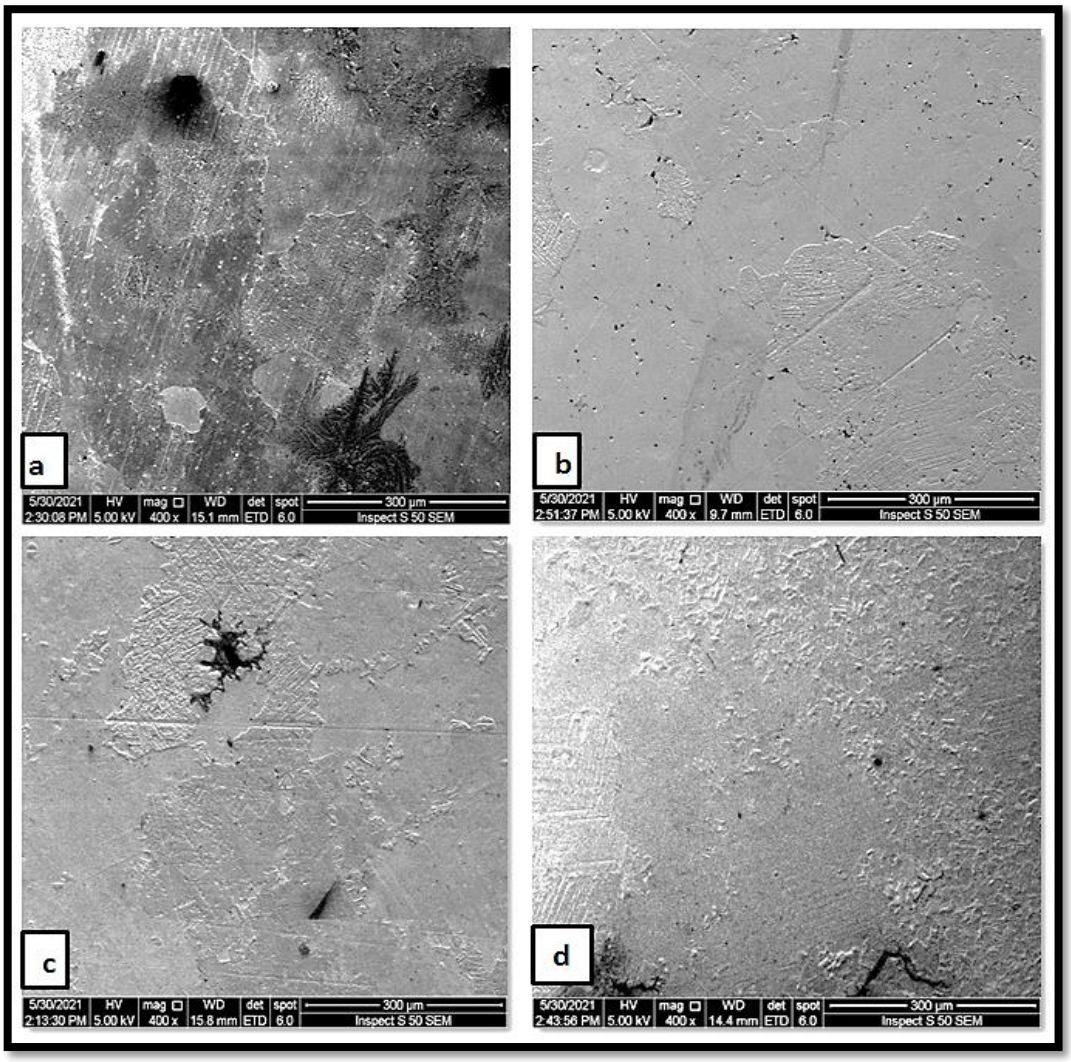

Figure (4.7): SEM image of B0 sample: (a) before hot press(b) 445MPa; (c) 555MPa; and (d) 665MPa.

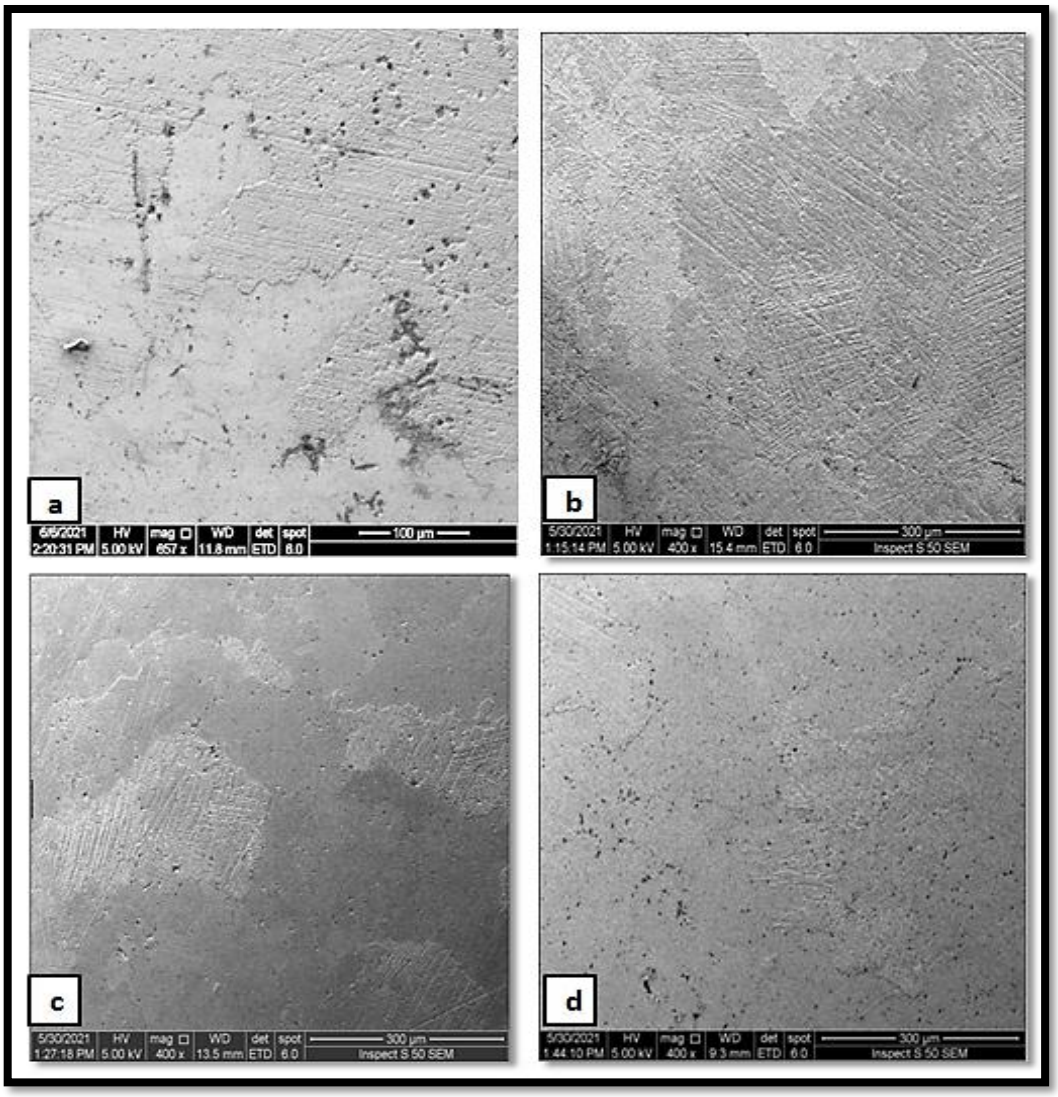

Figure (4.8): SEM image of B5 sample: (a) before hot press; (b) 445MPa; (c) 555MPa; and (d) 665MPa.

Figure (4.9) shows samples for the EDS analyses of the prepared alloy and composite. The analyses indicate the presence of the graphite with the designed percentage in the composite .The SEM images and the EDS analyses for all of the samples are shown in appendix (A5).

a

Application Note

BRUKER

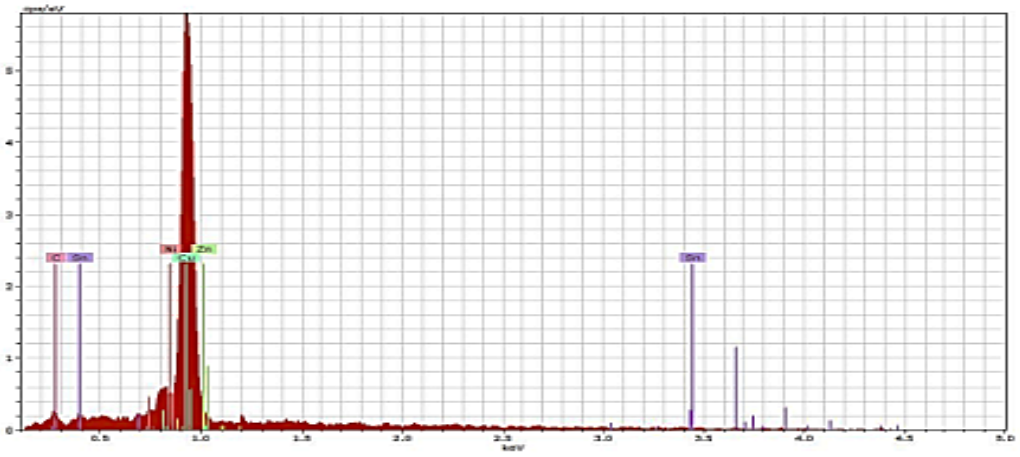

Spectrum: Acquisition 4193

El	AN	Series	unn. C [wt.%]	norm. C [wt.%]	Atom. C [at.%]	Error (1 Sigma) [wt.%]
Cu	29	L-series	98.23	98.23	96.51	16.73
Sn	50	M-series	1.22	1.22	0.64	1.44
C	6	K-series	0.55	0.55	2.85	0.50
Zn	30	L-series	0.00	0.00	0.00	0.00
Ni	28	L-series	0.00	0.00	0.00	0.00
		Total:	100.00	100.00	100.00	

b

Application Note

BRUKER

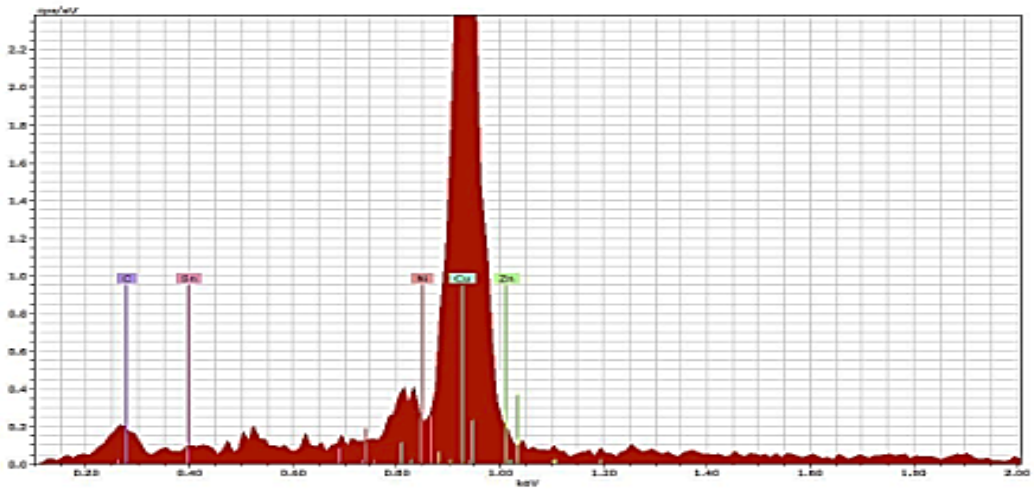

Spectrum: Acquisition 4194

El	AN	Series	unn. C [wt.%]	norm. C [wt.%]	Atom. C [at.%]	Error (1 Sigma) [wt.%]
Cu	29	L-series	94.81	94.81	89.21	17.41
Sn	50	M-series	3.36	3.36	1.69	2.86
C	6	K-series	1.83	1.83	9.10	1.10
Zn	30	L-series	0.00	0.00	0.00	0.00
Ni	28	L-series	0.00	0.00	0.00	0.00
		Total:	100.00	100.00	100.00	

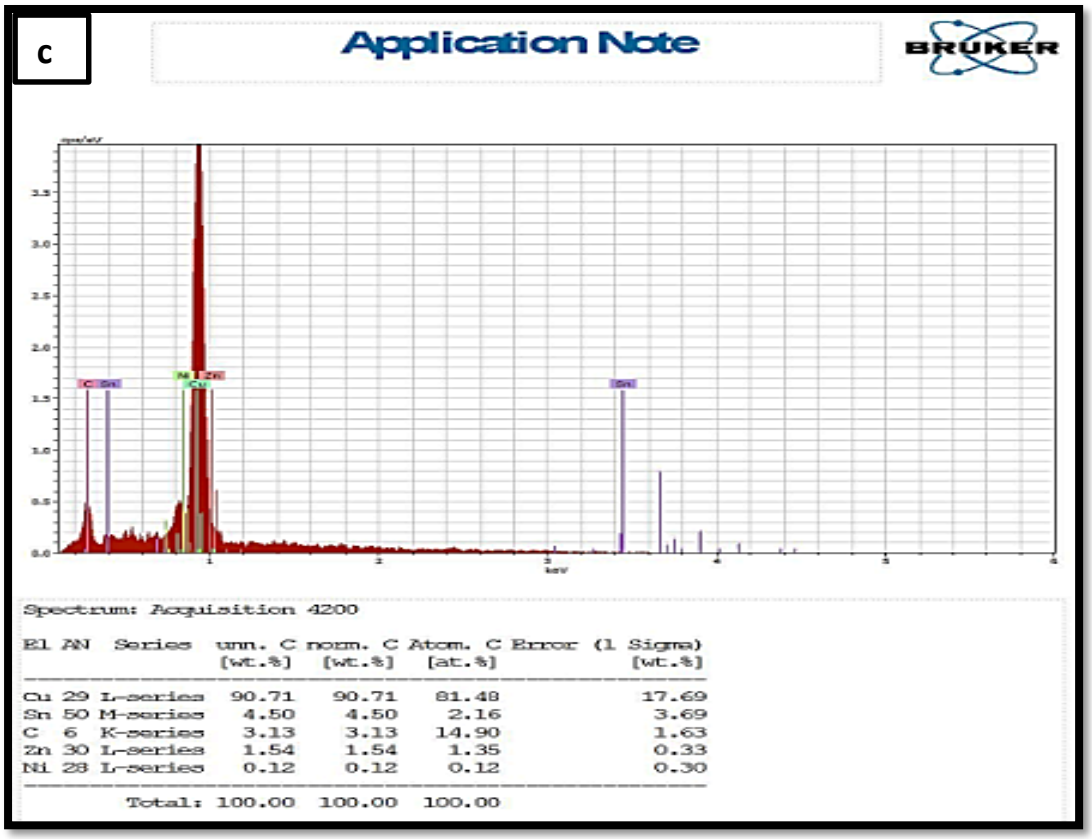

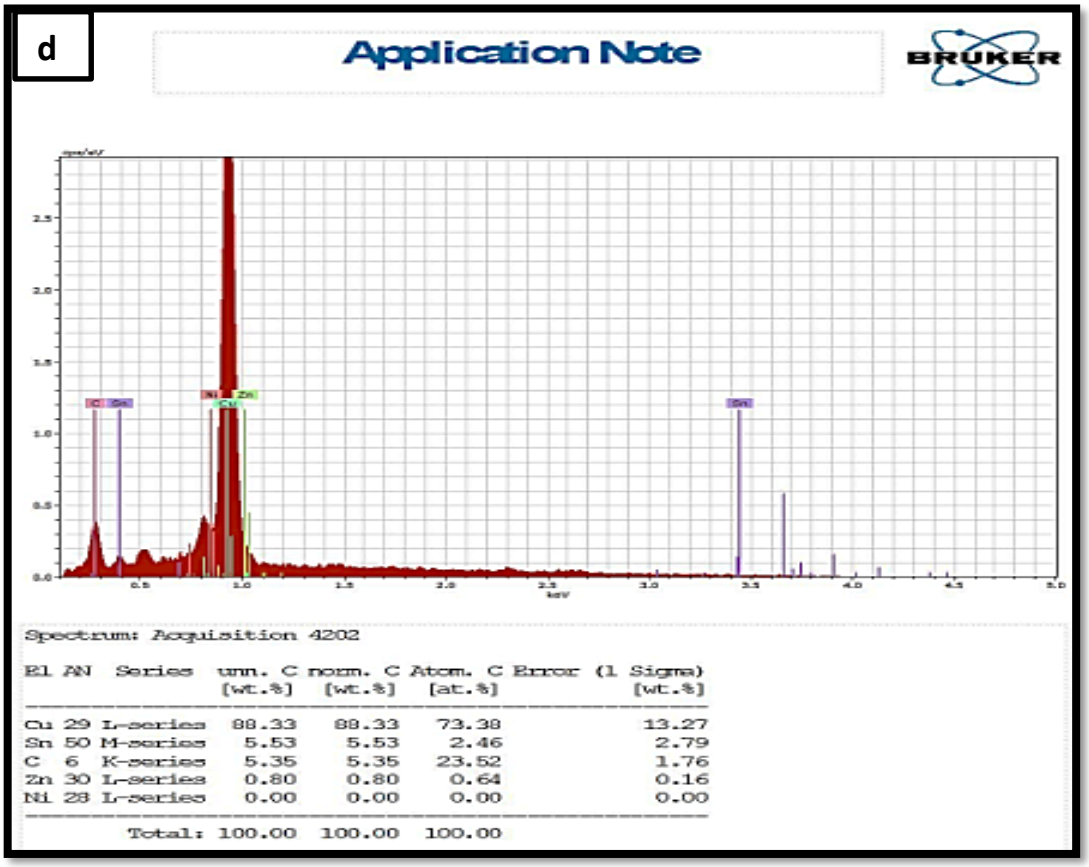

Figure (4.9): The EDS analyses for all specimenes after hot pressing at 665MPa : a) sample B, 665MPa, b) sample B1, 665MPa, c) sample B3, 665MPa, d) sample B5, 665MPa

4.6. Grain Size Measurement:

Grain size affects the physical and the mechanical properties of the alloy and it's composite. The superior mechanical properties can observe in materials with the smaller grain size. It is observed the increase in the graphite content leads to increase in the number of grains (i.e. to small grains size).This may be attributed to the higher number of nucleation center by the insoluble graphite particles.

Figure (4.10) shows the grain size of the prepared specimens before the hot pressing. The results were obtained by using the Image J- application software version 1.53. The results as recorded and appeared by the program are shown in appendix (A19).

Figure (4.10) Grain size of specimens before hot press.

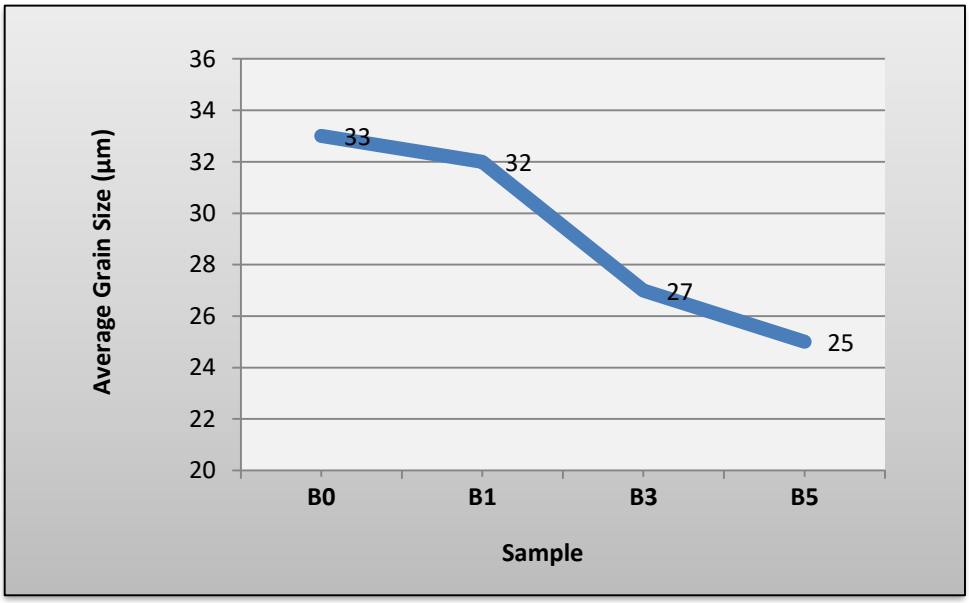

Figure (4.11) demonstrate the grain size of the hot pressed alloy specimens and the reinforced specimens by 5wt.% of coated graphite. The results indicate the following:

The reinforced specimen have a smaller grain size; hot pressing has significant effect in reducing the grain size of the tested specimens;

increasing the amount of hot pressing lead to further decrease in the grain size.

The grain produced with the effect of 3-dimensional hot pressing are not only fine but they are close to be equiaxed. The squeezing action of the applied loading prevents the grain growing more and also reduces the formation of porosity.

Figure (4.11): Grain size of (B0 and B5) specimens after hot press.

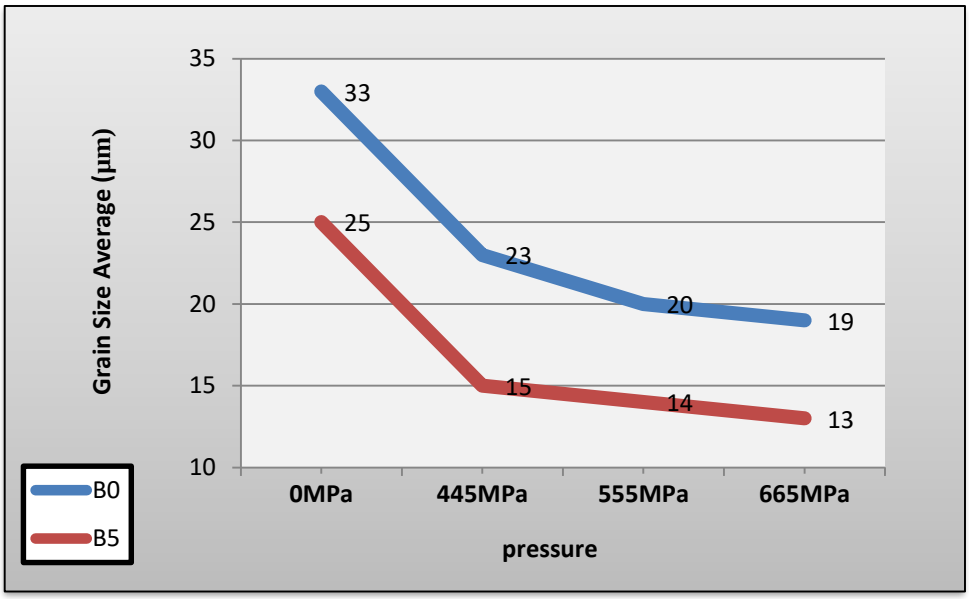

4.7. Porosity Results:

The results of the porosity test, shown in table (4.2), indicate that the specimens with the addition of graphite have higher density and lower porosity compared with those without it. The cast samples have a larger grains size. The hot pressing refines the grain which affects on the porosity formation with increasing the density. The lowest porosity and the lager density value were recorded for samples with 5wt.% coated graphite and hot pressed by **665MPa**.

Table (4.2): Porosity results before and after hot press for all specimens.

		Sample			
		B0	**B1**	**B3**	**B5**
Before Hot Press	Porosity %	**3.45**	**3.32**	**3.28**	**3.11**
After hot pressing by 445MPa	Porosity %	**3.3**	**3.15**	**3.08**	**2.87**
	Reduction in porosity %	**4**	**5**	**6**	**8**
After hot pressing by 555MPa	Porosity %	**3.23**	**2.94**	**2.78**	**2.61**
	Reduction in porosity %	**6**	**11**	**15**	**16**
After hot pressing by 665MPa	Porosity %	**2.93**	**2.75**	**2.64**	**2.5**
	Reduction in porosity %	**15**	**17**	**19**	**20**

4.8. Brinell Hardness Results:

The Brinell hardness increased with increasing of graphite This increase are attributed not only to the higher order content interfacial strength between the copper and coated graphite but also to the relatively and finer microstructure to improved of graphite reinforced composites [91]. The hardness of all samples increases with the increase in weight percentage of graphite particles up to 5 wt.%. This is true due to the fact that copper is a ductile material and the reinforced particle contributes positively to the hardness of the composites. The presence of graphite reinforcement leads to the increase in constraint to plastic deformation of the matrix. Thus increase of hardness of composites could be attributed to the relatively graphite particles itself which acting as barriers to dislocations

motion and contribute to bearing a part of the loading. The interstitial spaces of the bronze metal matrix are sated with reinforcement particles which hinder the grain dislocation thus improving the cumulative strength of the composite [91]. The hot deformation mechanism can be done by slipping and twinning in copper alloys, dislocations generated by continuous twins boundary. It can hinder the dislocations movement. Addition reinforcement particles can grain refinement and preventing the grain growth, leading to improve mechanical properties [92].

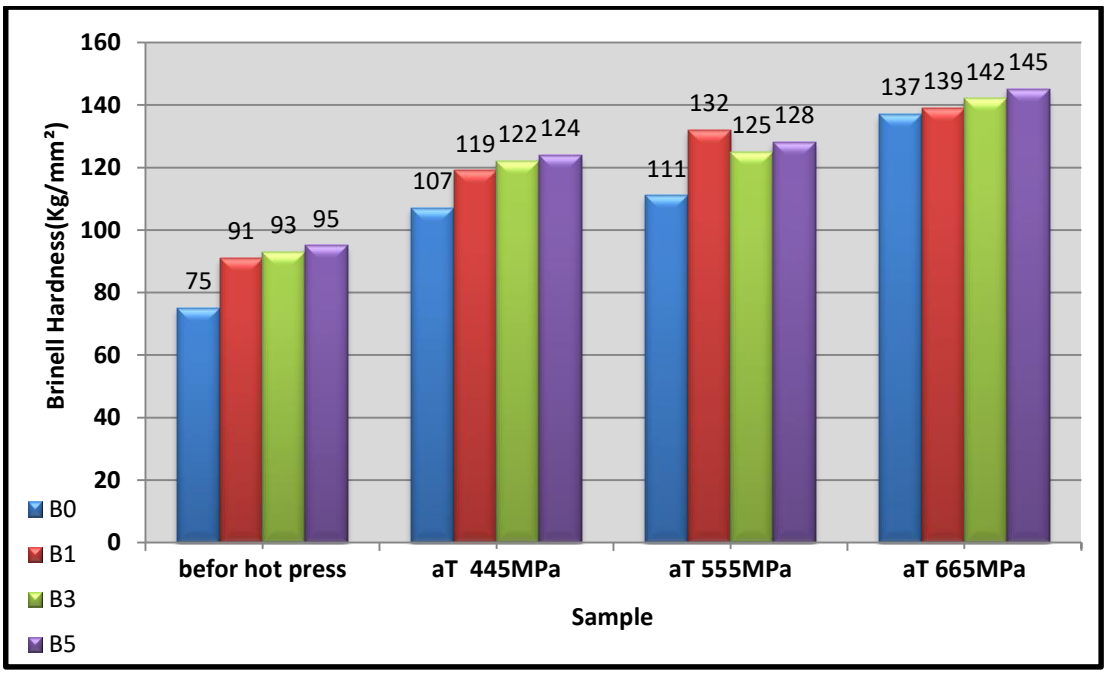

Figure (4.12): Brinell hardness for all specimens before and after Hot prress.

4.9. Wear Test:

Results showed that the lowest average value of the wear rate, coefficient of friction and weight loss was observed in the Cu-10Sn with 5%wt. graphite composite because the natural lubricating behavior of graphite. The highest average value of the wear rate, coefficient of friction and weight loss was reached with the Cu-10Sn alloy. Mainly affected self-

lubrication was by size, volume content, and distribution of graphite particles. The higher strength bonds between the matrix and coated graphite, lower porosity, higher hardness and finer microstructure, which improved, the wear resistance of graphite reinforced composites. Coated graphite particles, as the reinforcement particles and lubricant decreases the wear rate. Hot pressing enhance and refine the grain size of the composite materials, and lead decreasing of porosity and improving mechanical and wear properties. Figure (4.13) indicated to the reducing in wear rate by the effect of graphite in Cu 10Sn alloy before the hot. Figure (4.14) indicated the effect of the hot pressing, which increase the reduction of wear rate in Cu 10Sn alloy. The maximum reduction in the wear rate can be noticed in the specimen having 5wt.% coated graphite and hot pressed by 665MPa. This maximum percentage reduction in the wear rate was 54% and 48%. Calculated for 10N and 20N respectively after a wearing time at 20 minutes.

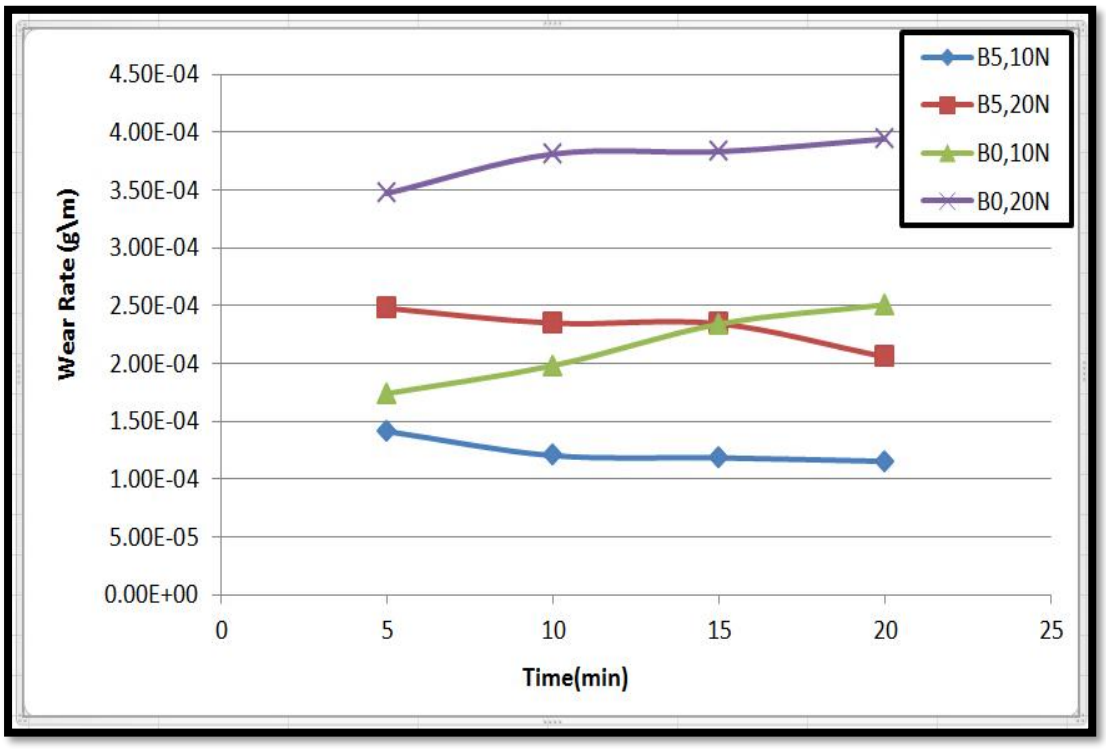

Figure (4.13): Wear Rate of samples B0 and B5 before hot pressing.

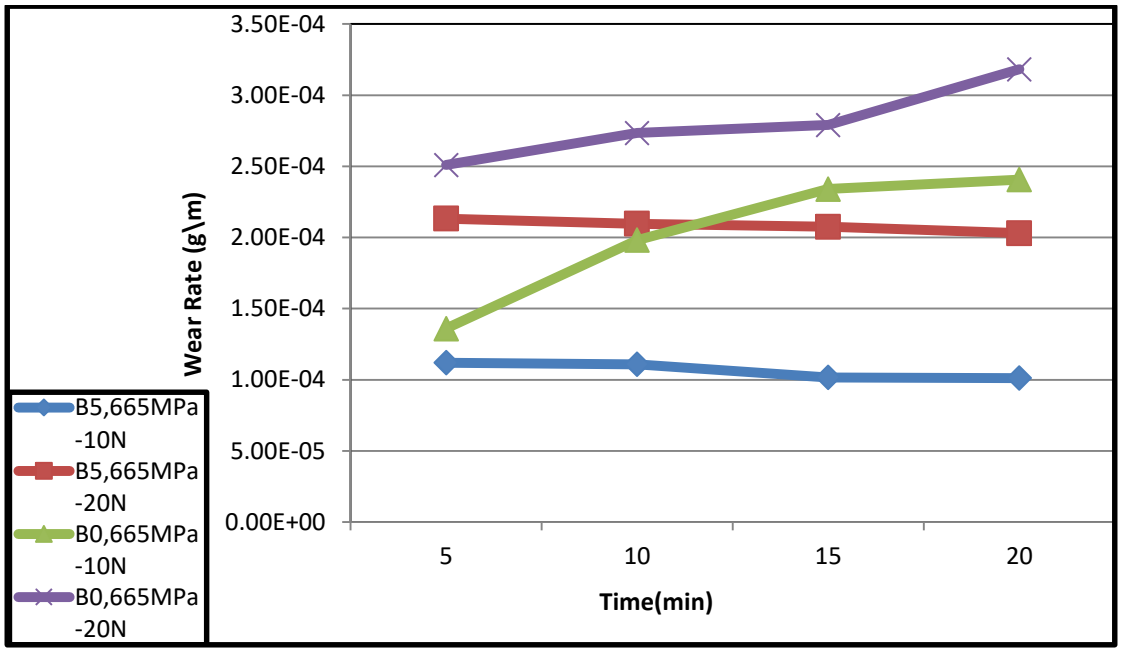

Figure (4.14): Wear Rate of samples B0 and B5after hot pressing.

Optical Microscope images shown in figure (4.15) and figure (4.16) indicate the wear track of samples before and after the hot press. The lowest level traces of the surface sample observed in composites material with increasing in the lubricating phase (coated graphite) and the applied hot squeezing, i.e. in the specimen containing 5wt.% of coated graphite. The surface sample observed in composites material containing 5wt.% of graphite, shows a uniform, relatively shallow trace with increasing in the lubricating phase(coated graphite). This indicated to smooth wearing process, the traces show regular course that means the squeezing of graphite out from the subsurface and spread over the worn surface during the sliding process [93-94].

All the results of the wear tests are recorded and appeared by tables in appendix (A20).

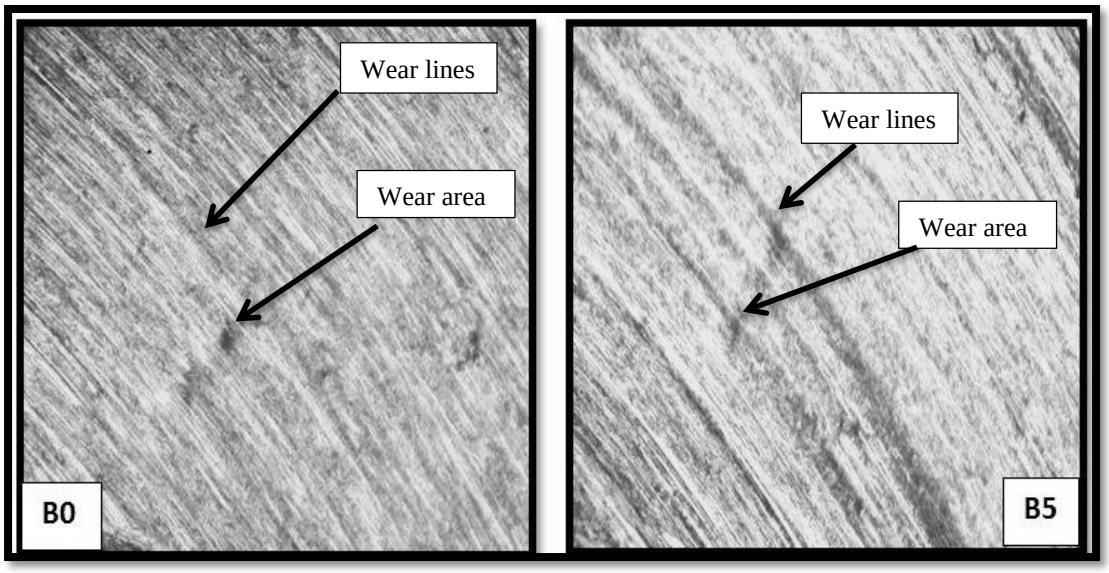

Figure (4.15): Optical Microscope of Wear track (100x) of sample before hot press: (a) B0; (b) B5.

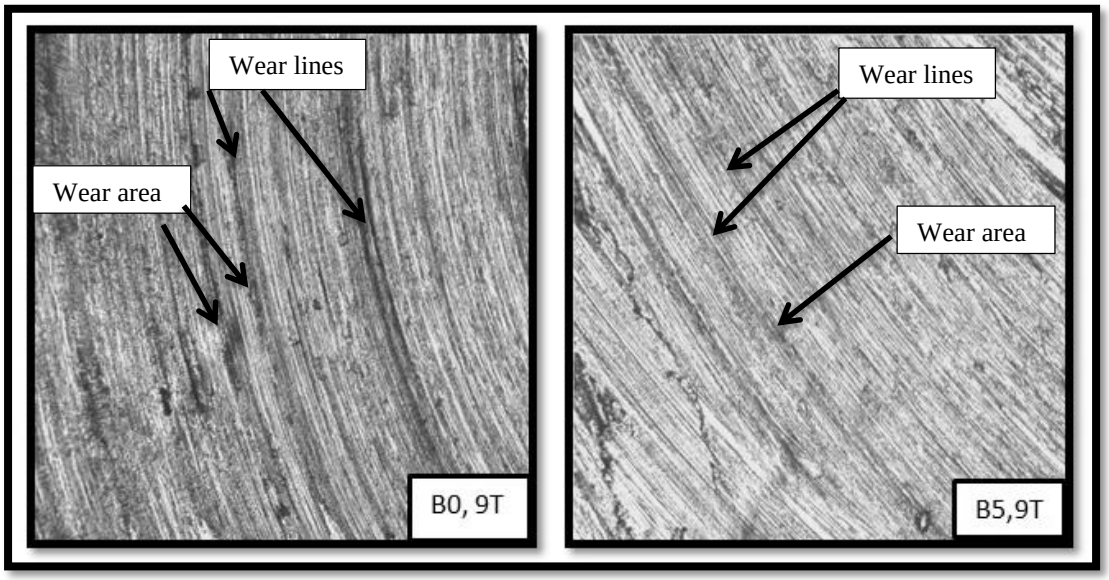

Figure (4.16): Optical Microscope of Wear track (100x) of sample after hot press: (a) B0,665MPa; (b)B5,665MPa.

Figure (4.17) and (4.18) indicated to the effect of lubricating characteristic of graphite which reduces the friction coefficient from 0.76 to 0.48 for the specimen with out hot forming and from 0.72 to 0.44for the hot formed specimen.

The friction coefficients of the hot treated specimens Cu10Sn alloy with 5wt.% coated graphite is lower than that untreated specimens because

the hot pressing decreased porosity and reinforced the based which decreased the friction coefficient and improved mechanical properties and wear resistance [91], the friction coefficients for each alloy sample set in each cutting conditions are tabulated in appendix (A21).

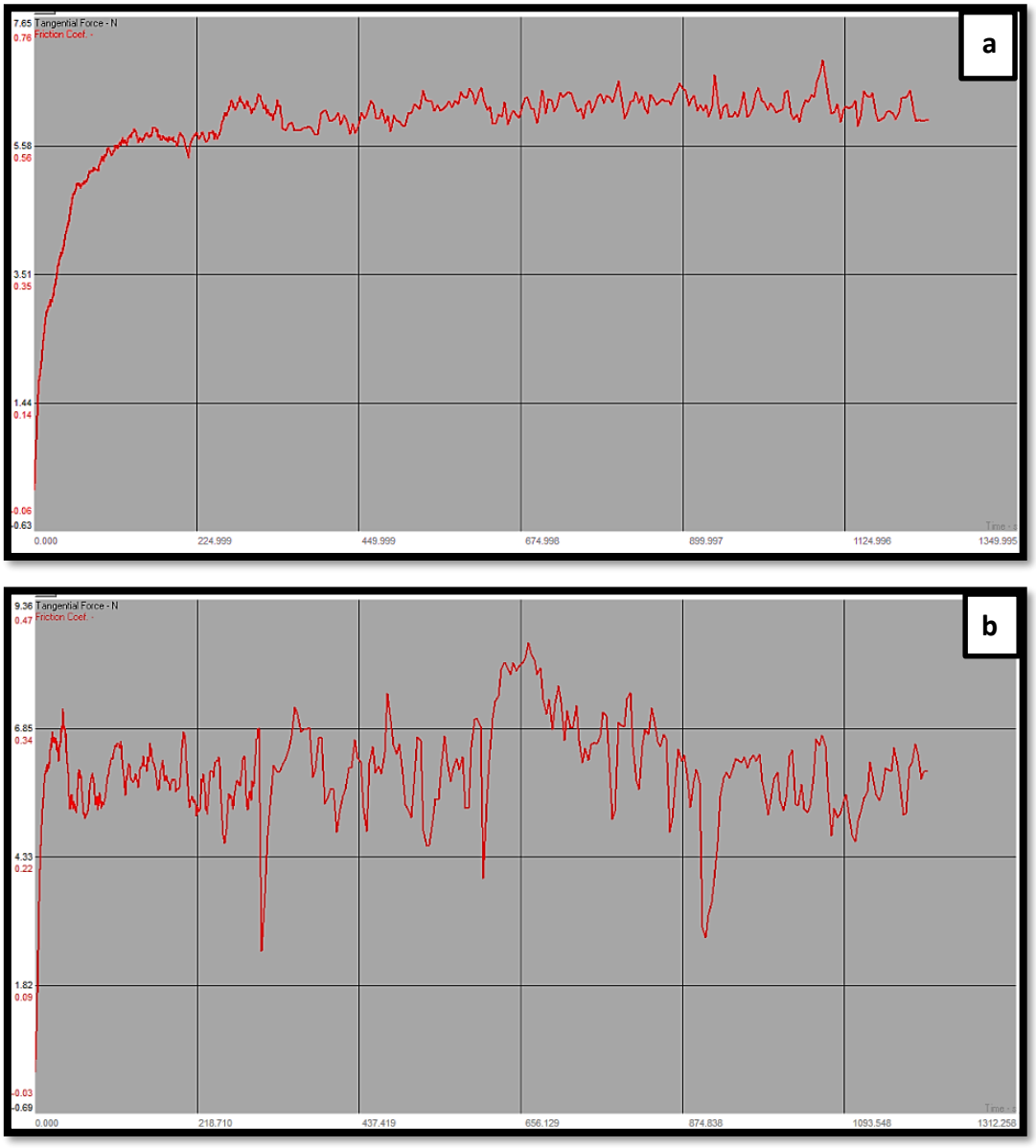

Figure (4.17): Friction Coefficient of samples: a) B-10N; b) B5-10N before hot pressing.

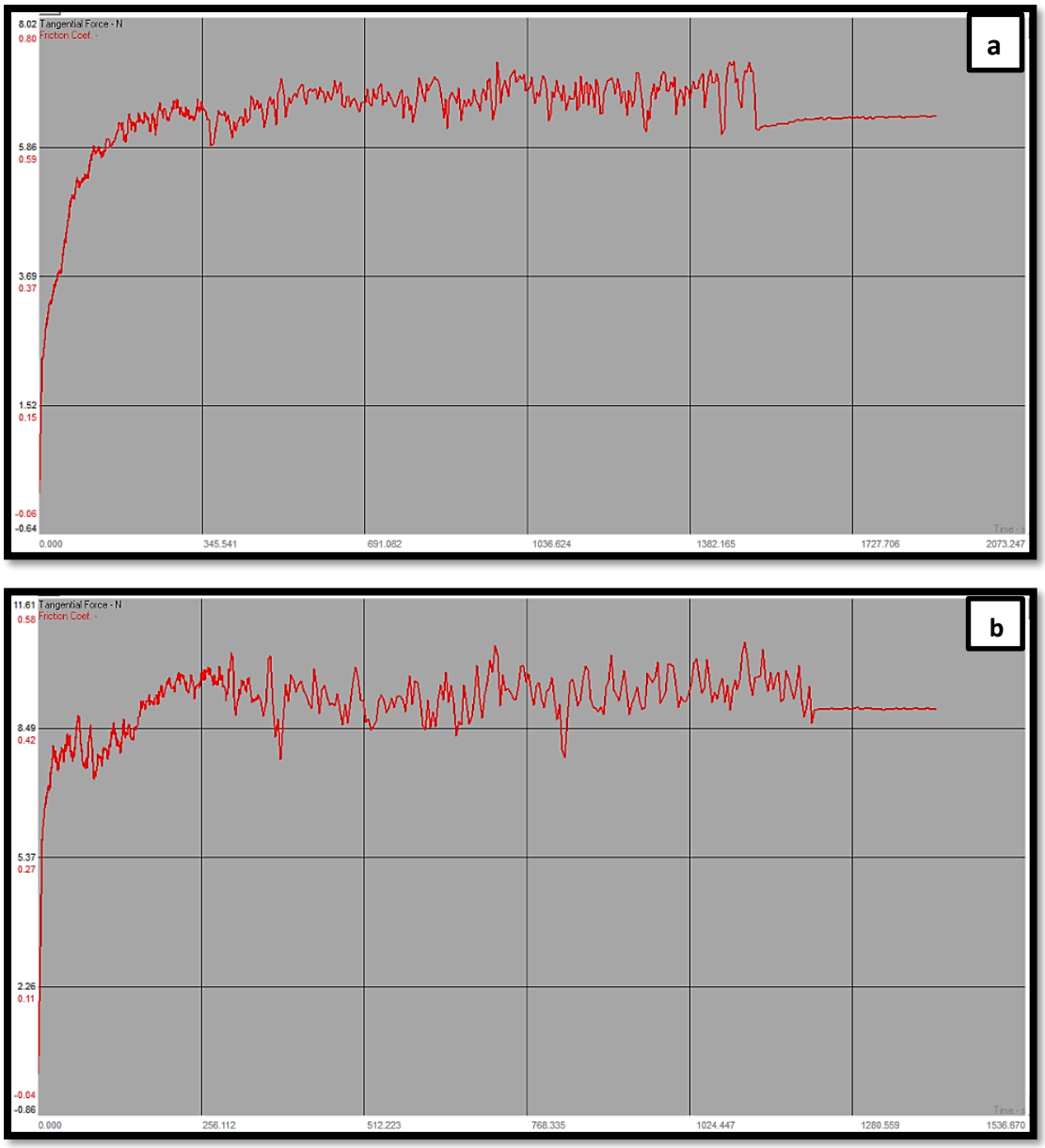

Figure (4.18): Friction Coefficient of samples: a) B-10N; b) B5-10N after hot pressing and at665MPa.

4.10. Results of Machining Experiments:

According to the planed program, the machining experiments were carried out for the Cu10Sn samples and Cu10Sn with 5wt.% coated graphite before and after hot pressed by 665MPa to study the effect of reinforcing by graphite particles and thermo-mechanical treatment on the tool life and the roughness of the machined surface. The results of the machining experiments are tabulated in appendix (A21).

4.10.1. Results of The Flank Wear and The Tool Life:

A maximum width of flank wear tool (VB max = 0.3mm) for the flank wear was considered as a criterion for the tool life [89].

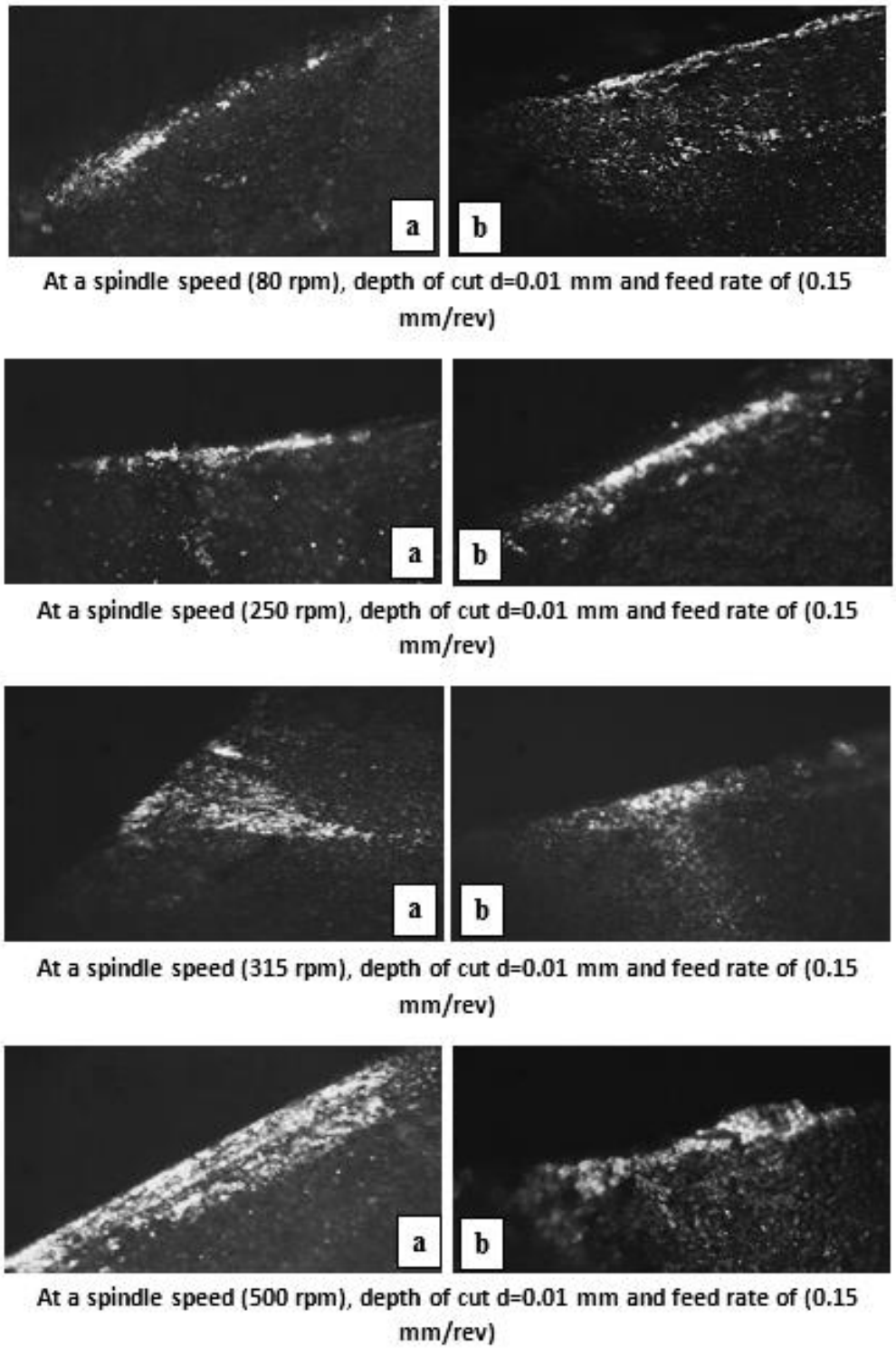

Figure (4.19): Tool Flank Wear for sample (B0): (a) before hot pressing; (b) after hot pressing at 665MPa.

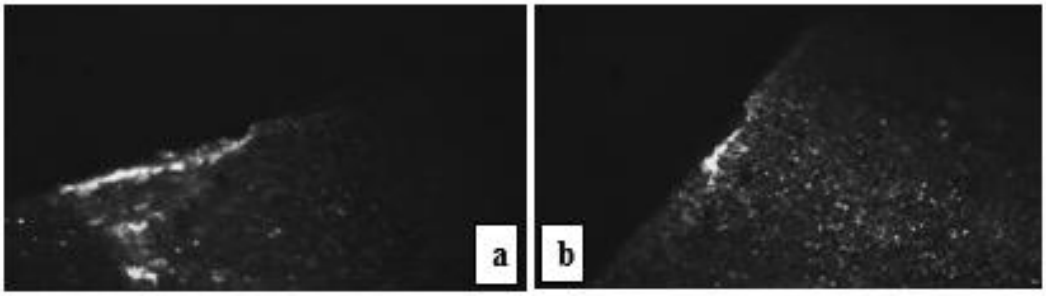

At a spindle speed (80 rpm), depth of cut d=0.01 mm and feed rate of (0.15 mm/rev)

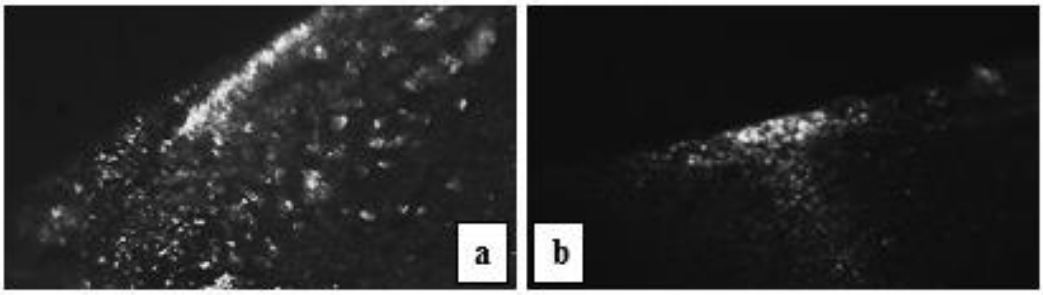

At a spindle speed (250 rpm), depth of cut d=0.01 mm and feed rate of (0.15 mm/rev)

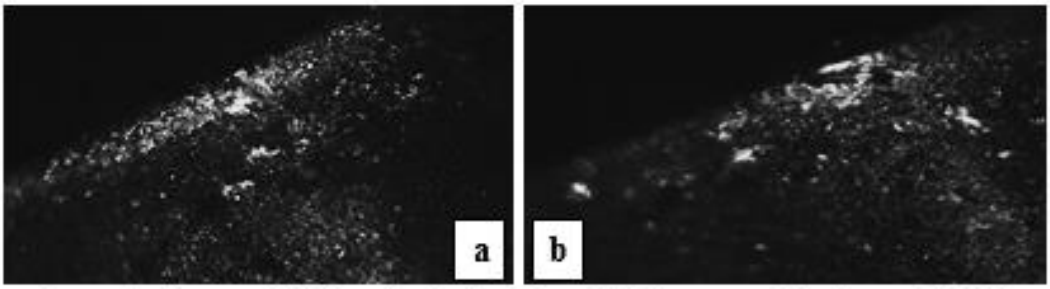

At a spindle speed (315 rpm), depth of cut d=0.01 mm and feed rate of (0.15 mm/rev)

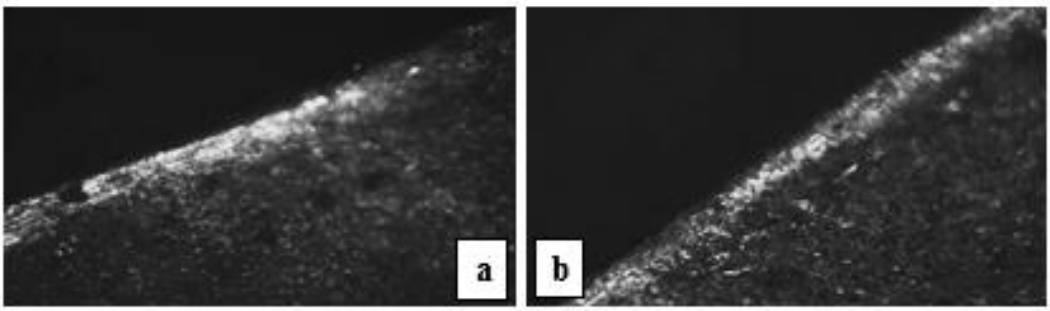

At a spindle speed (500 rpm), depth of cut d=0.01 mm and feed rate of (0.15 mm/rev)

Figure (4.20): Tool Flank Wear for sample (B5): (a) before hot pressing; (b) after hot pressing at 665MPa.

Figures (4.19) and (4.20) show the wear occurred at the flank surface of the tool during different machining conditions in samples Cu 10Sn and Cu 10Sn with 5wt.% coated graphite before and after the hot pressing. The optical images (100x) observed lower flank wear widths in hot squeezed samples containing the coated graphite in comparison with the non squeezed base alloy samples, the reason for this reduction in flank wear due to the self-lubricating characteristics of graphite that which dispersed in the alloys and the effect of hot pressing to improved the mechanical properties and wear resistance and lower the friction coefficient, which lead to lowered the flank wear width and increasing the tool life. Figure (4.21), (4.22) represents an example for the method used in determining the tool life.

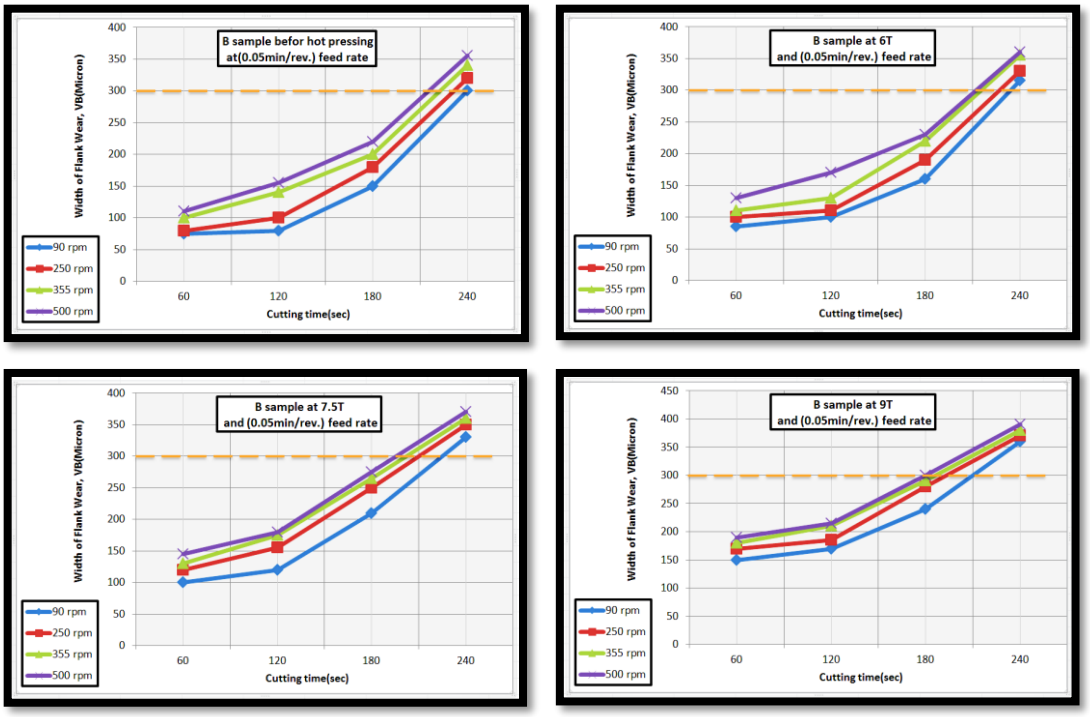

Figure (4.21): Estimation the tool life in machining B0 sample before and after the hot pressing.

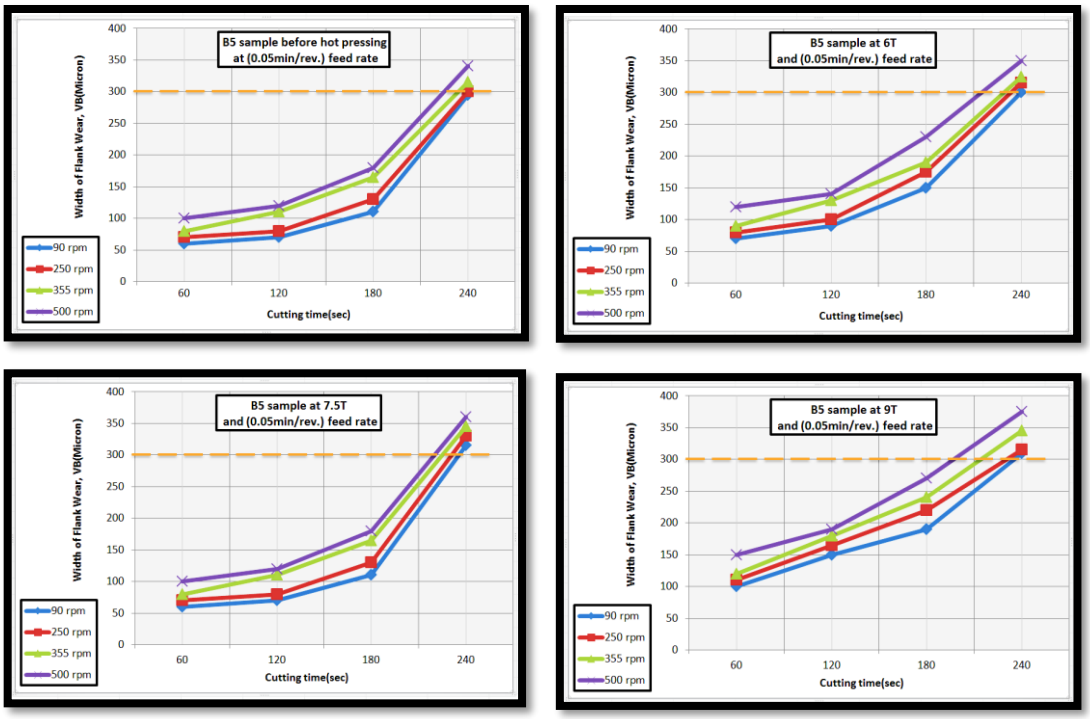

Figure (4.22): Estimation the tool life in machining B5 sample before and after the hot pressing.

Table (4.3) demonstrate the determined tool life for the samples due to the used machining conditions.

Table (4.3): The tool life for the test specimens due to depth of cut d=0.01 mm and feed rate of (0.15 mm/rev).

Tool life (Sec.)								
Spindle speed (rpm)	Base alloy (B0)				Sample with 5wt.% coated graphite (B5)			
	Before hot press	After hot press			Before hot press	After hot press		
		445MPa	555MPa	665MPa		445MPa	555MPa	665MPa
90	235	230	215	210	250	240	235	230
250	230	225	210	195	240	235	230	220
315	225	215	200	190	230	225	220	210
500	218	210	196	180	225	215	210	200

In figures (4.23), (4.24) also indicate that a higher cutting speed causes a higher value of VB. This is due to the increase in cutting temperature accompanying the increase in cutting speed and this causes increase in adhesion wear on tool cutting edge, also the increase in temperature may soften a very thin surface layer of the tool cutting edge. In addition to that a higher cutting speed means a higher repeated contact between the machined surface and the flank surface which increases the abrasive wear and the scratching action of machined material [95].The tool life increasing with increasing the hot squeezed samples containing the coated graphite in comparison with the non squeezed base alloy samples, due to the lubricating of graphite. The lower friction coefficient in hot squeezed samples containing the coated graphite in comparison with the non squeezed base alloy samples, the reason for this reduction in flank wear due to the lubricating of coated graphite and the effect of hot pressing to enhance the wear resistance and lowered the frictional coefficient.

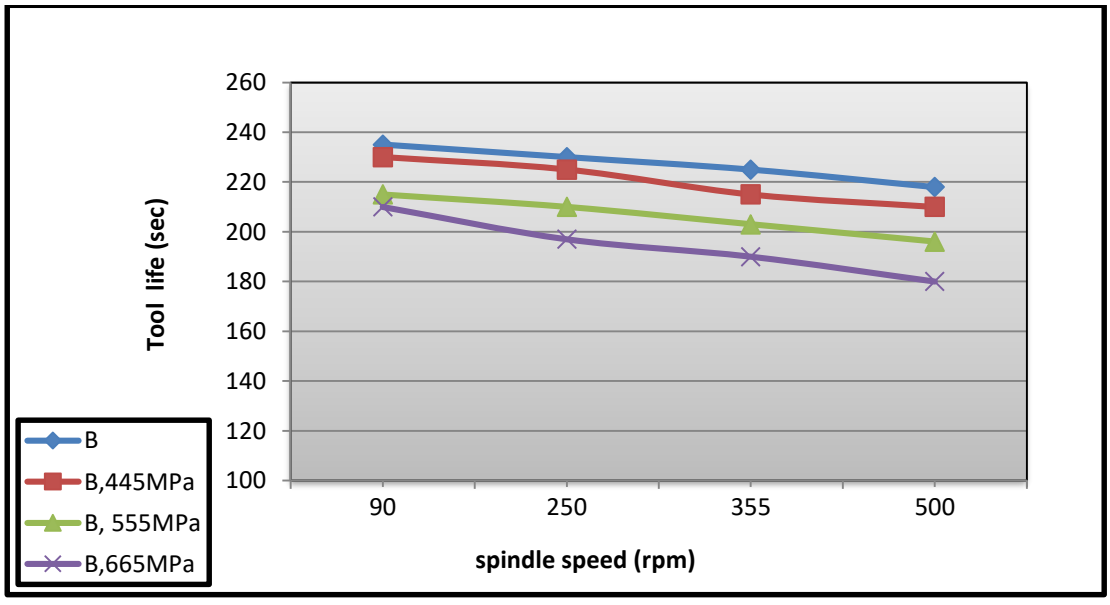

Figure (4.23): Effect of spindle speed on the tool life of sample B0 before and after the hot pressing used depth of cut d=0.01 mm and feed rate of (0.15 mm/rev).

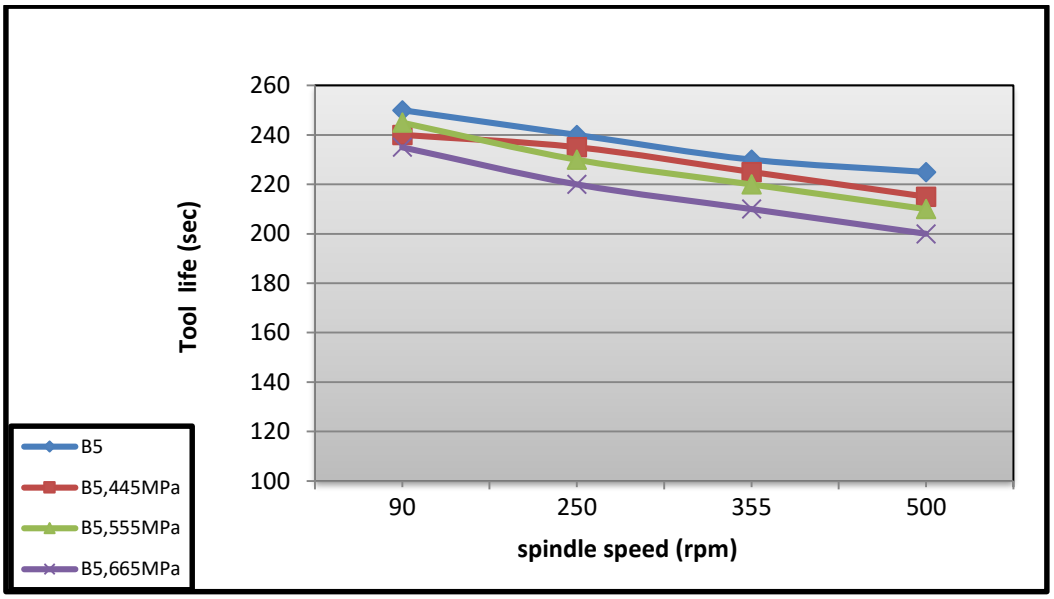

Figure (4.24): Effect of spindle speed on the tool life of sample B5 before and after the hot pressing used depth of cut d=0.01 mm and feed rate of (0.15 mm/rev).

4.10.2. Results of Surface Roughness:

The measured surface roughness for each sample due to the considered cutting conditions, are demonstrated in the table (4.4). Figure (4.25) and (4.26) show the variation of the surface roughness with used cutting speeds at constant feed rate and depth of cut. The increase in cutting speed improves the machined surface quality. When the spindle speed is between 90 rpm and 500 rpm, surface roughness is decreasing slightly because of the lubricating effect of graphite particles and good mechanical properties of the hot squeezing samples where the surface roughness improved with an increase in the hardness samples. Reduction of porosity in hot treated specimen eliminated/ reduces the vibration during the machining process. This leads to a lower surface roughness. In Cu10Sn samples with 5wt.% coated graphite the recorded values of surface roughness are lesser than that recorded for the Cu10Sn samples. This is due to the presence of graphite which has lubricating effect that

reduces the amount of friction between the tool and the work piece. This also reduces the machining temperature, which reduce the surface roughness [96].

Table (4.4): The surface roughness for the sample due to depth of cut d=0.01 mm and feed rate of (0.15 mm/rev).

Spindle speed (rpm)	Surface Roughness of base alloy (B0)				Surface Roughness of sample with 5wt.% coated graphite (B5)			
	Before hot press	After hot press			Before hot press	After hot press		
		445MPa	555MPa	665MPa		445MPa	555MPa	665MPa
90	0.479	0.456	0.419	0.385	0.363	0.348	0.315	0.293
250	0.463	0.436	0.395	0.368	0.358	0.343	0.311	0.289
315	0.455	0.425	0.378	0.356	0.349	0.333	0.305	0.281
500	0.432	0.413	0.367	0.339	0.315	0.295	0.261	0.227

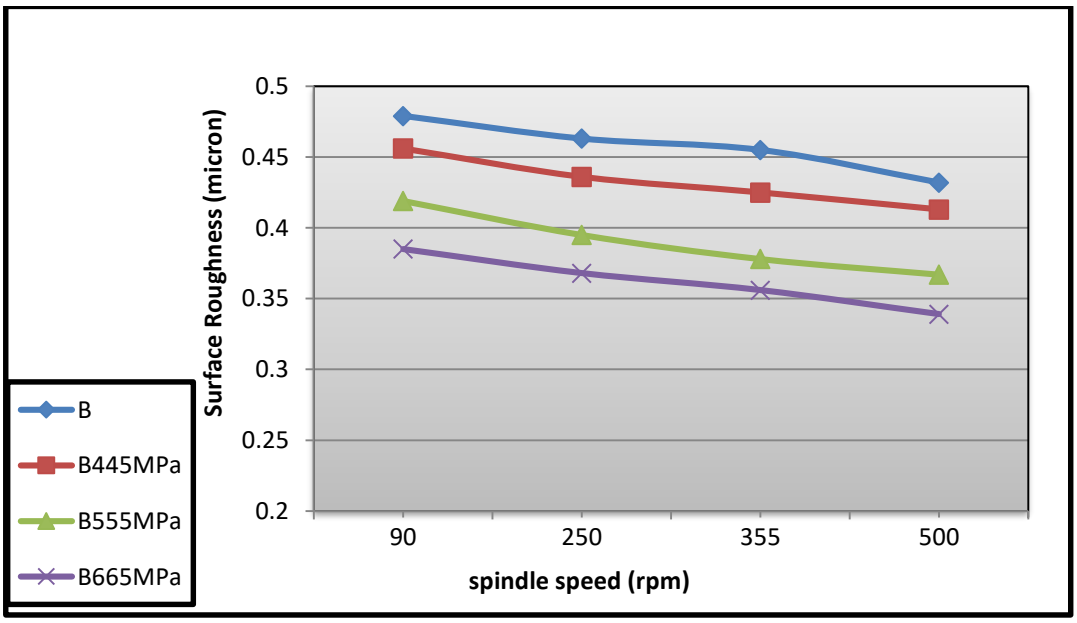

Figure (4.25): Effect of spindle speed on the surface roughness of sample B before and after hot pressing used depth of cut d=0.01 mm and feed rate of (0.15 mm/rev).

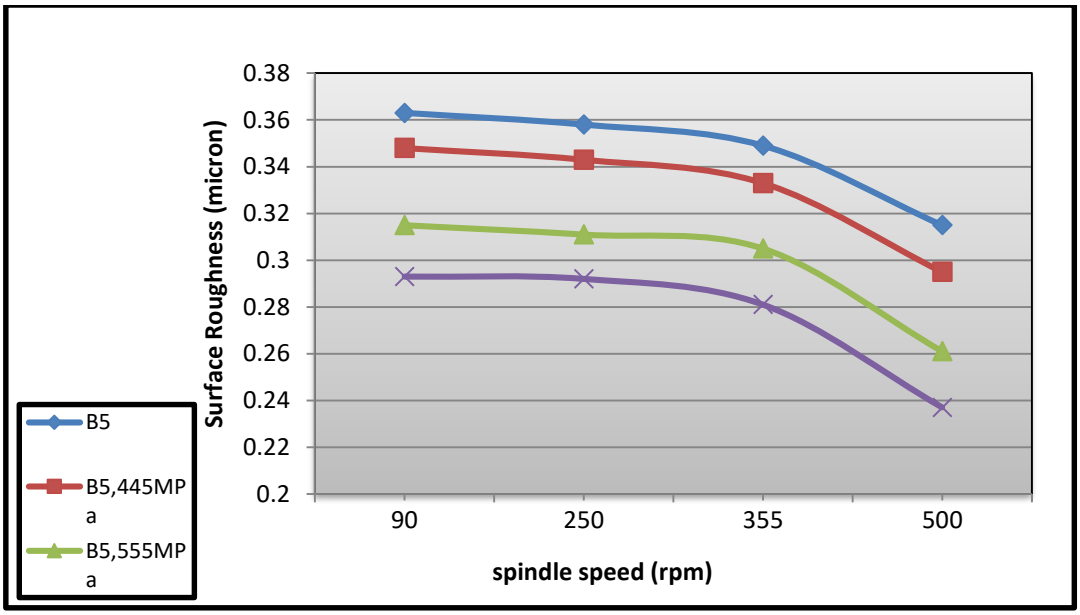

Figure (4.26): Effect of spindle speed on the surface roughness of sample B5 before and after hot pressing used depth of cut d=0.01 mm and feed rate of (0.15 mm/rev).

4.11. Abbreviation of Mechanical and Physical Properties Results:

The enhancement of mechanical, physical and tribological properties by the effect of the hot pressing and the addition of coated graphite in the matrix Cu 10Sn alloy and hot squeezed by 665MPa Cu 10Sn with 5wt.% graphite demonstrated in the table (4.5) and the change percentage in these properties.

Table (4.5): Mechanical and physical properties of matrix and composite materials with change percentage.

Samples	Brinell Hardness (kg/mm²)	Average Grain Size (µm)	Density (g/cm3)	Porosity (%)	Friction coefficient	Wear Rate (g/m) 10Nnload	Tool life (sec)	Surface Roughness (micron)
Cu 10Sn with out graphite	75	33	8,8551	3.45	0.72	2.06×10^{-4}	218	0.432
Cu10Sn+5wt.% coated graphite	95	25	8.8695	3.11	0.44	1.74×10^{-4}	225	0.315
Hot pressed by 665MPa Cu 10Sn	137	19	8.8894	2.94	0.76	2.51×10^{-4}	180	0.339
Hot pressed by 665MPa Cu10Sn+5wt.% coated graphite	145	13	8.9997	2.5	0.48	1.01×10^{-4}	200	0.227
Enhancement Percentage (%)	93 ↑	61 ↓	2 ↑	28 ↓	33 ↓	51 ↓	8 ↓	47 ↓

Chapter Five

Conclusions and Recommendations

5.1. Conclusions:

According to the results of the present work, the following can be concluded:

1- All tin-bronze samples (90 wt.% Cu , 10 wt.% Sn) with (1,3,5)wt.% adding coated graphite, prepared by stir casting can provide a reasonable homogenous distribution of graphite particles in Cu10%Sn.

2- The homogenization treatment has been done at (650°C) for 3hours, hot squeezing was performed in (445, 555 and 665 MPa) at (600°C) for period (10 min) have a microstructure consisting of one phase α–phase as the matrix of the alloy.

3-Graphite can serve effectively as reinforcement in Cu10%Sn alloy. Adding of graphite improves in mechanical and physical properties of the Cu10%Sn alloy. Addition of coated graphite particles to Cu10%Su alloy causes best results in mechanical and physical properties of the composite alloy.

4- The mechanical properties such as hardness increased from (75 kg/mm²) to (91 kg/mm²) with 1wt.% coated graphite, increased to (93 kg/mm²) with 3wt.%coated graphite and increased to (95 kg/mm²) with 5wt.% coated graphite.

5- The hot squeezing causes increase in density by 2% and decreasing in grain size by 61% and porosity by 28% of Cu10%Sn alloy composite with 5wt.% coated graphite at 665MPa.

6- 665MPa hot squeezing pressure applied on Cu10Sn alloy with 5wt.% coated graphite reduced the wear rate by (51%), and reduced the friction coefficient by 33%.

6- Hot squeezing of the base alloy and the reinforced by 5wt.% coated. Enhancement the machining properties .The surface roughness was reduced from (0.479) to (0.227) according to the used machining conditions. The tool life was decreased by (8%).

5.2. Recommendations for future work:

1- Studying the other properties to alloys that used in this study such as (Compressive and fatigue strength).

2- Adding of other metals to the base alloy with 5wt% graphite, and see the effect on mechanical, physical and machining properties.

3- Carrying out the machining experiment with different feed rate, depth of cut and tool geometry.

4- Study the effect of adding ceramic oxides.

Appendix

X-ray Diffraction (XRD):

B-6T

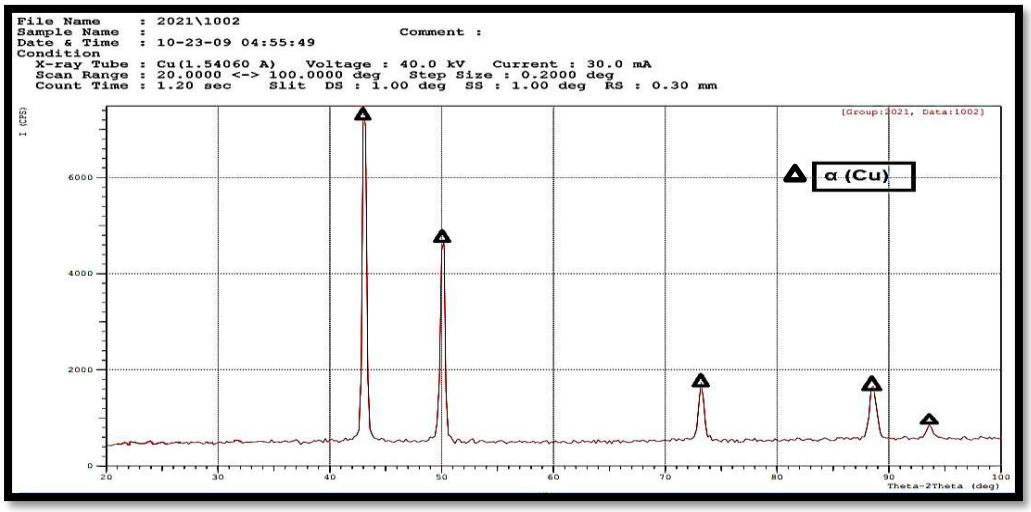

B-7.5T

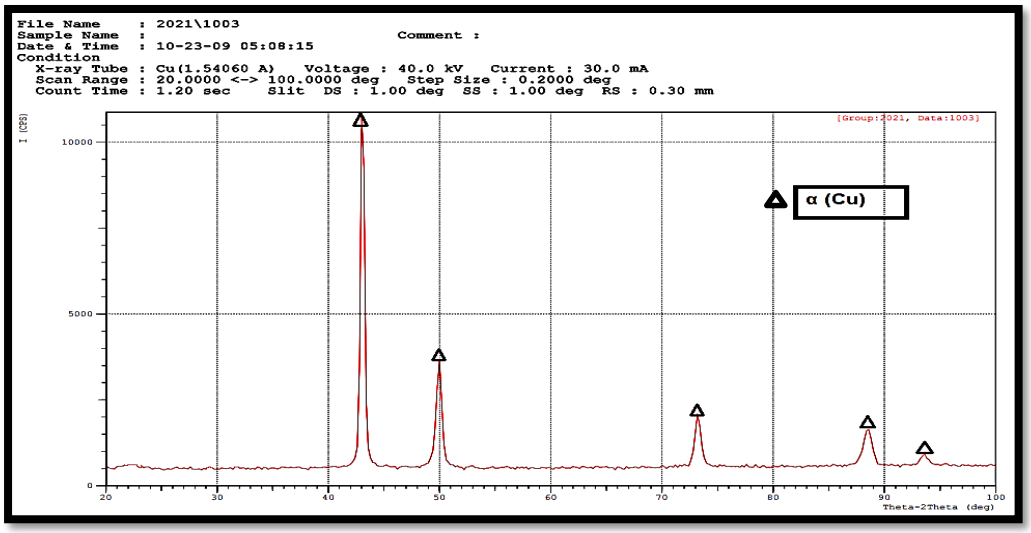

B1-befor hot press:

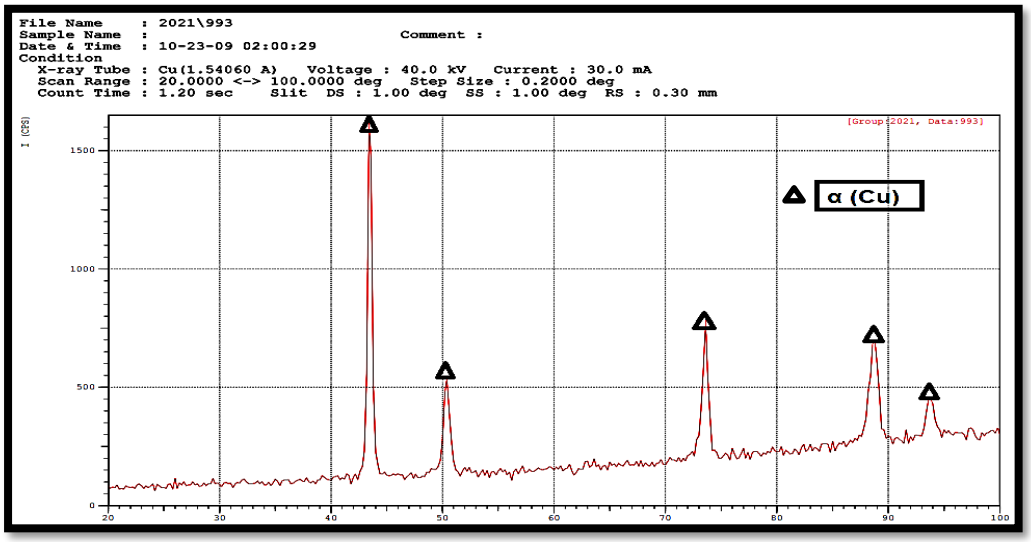

B1-6T

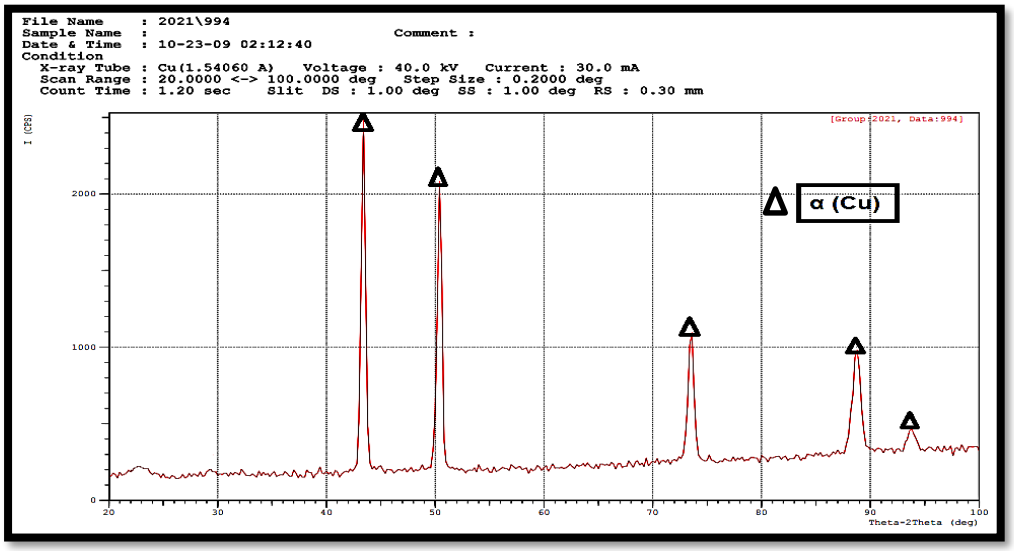

B1-7.5t

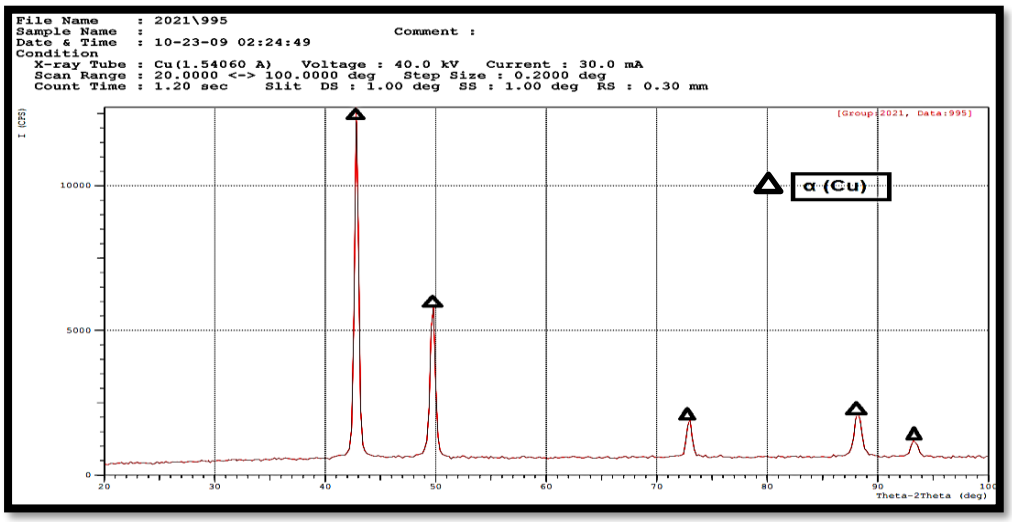

B1-9T

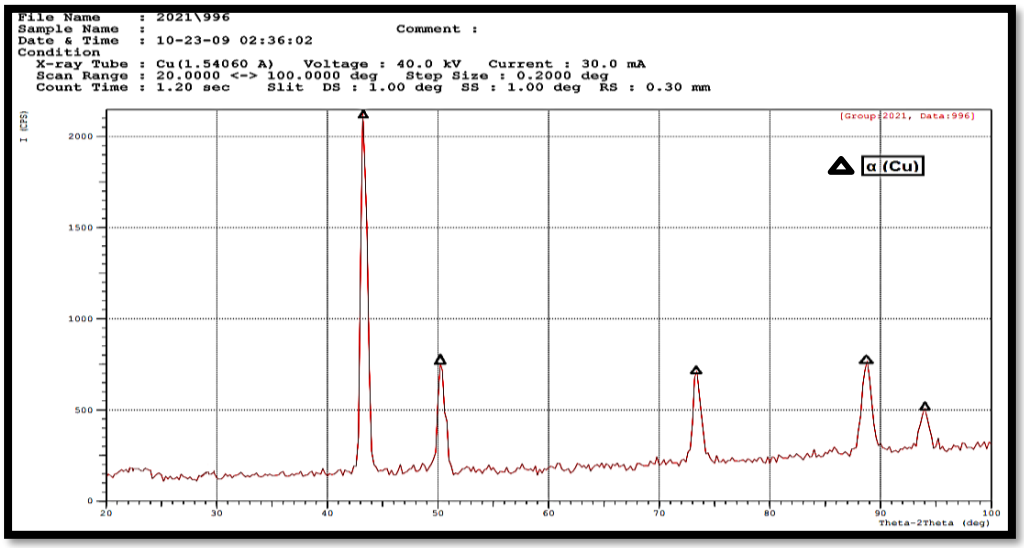

B3-before hot press:

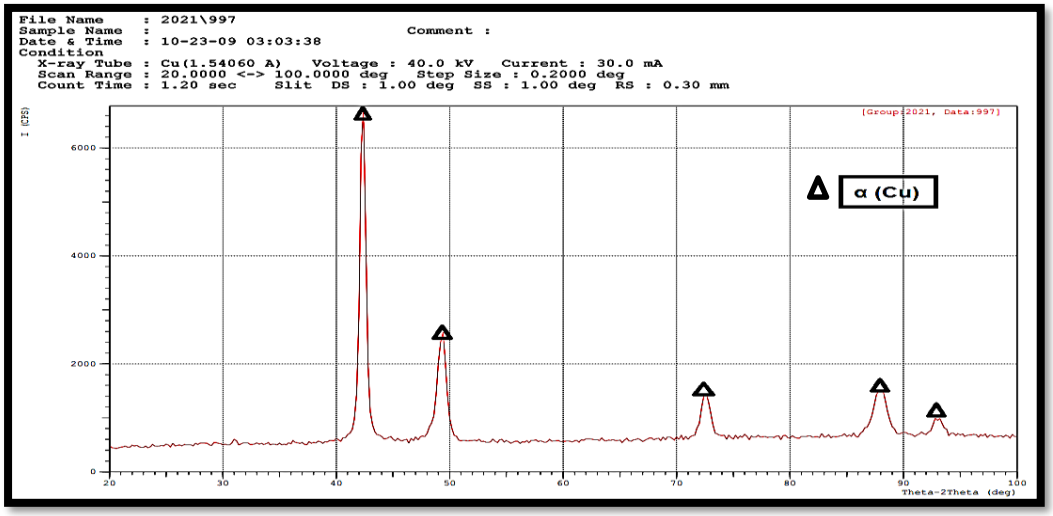

B3-6T

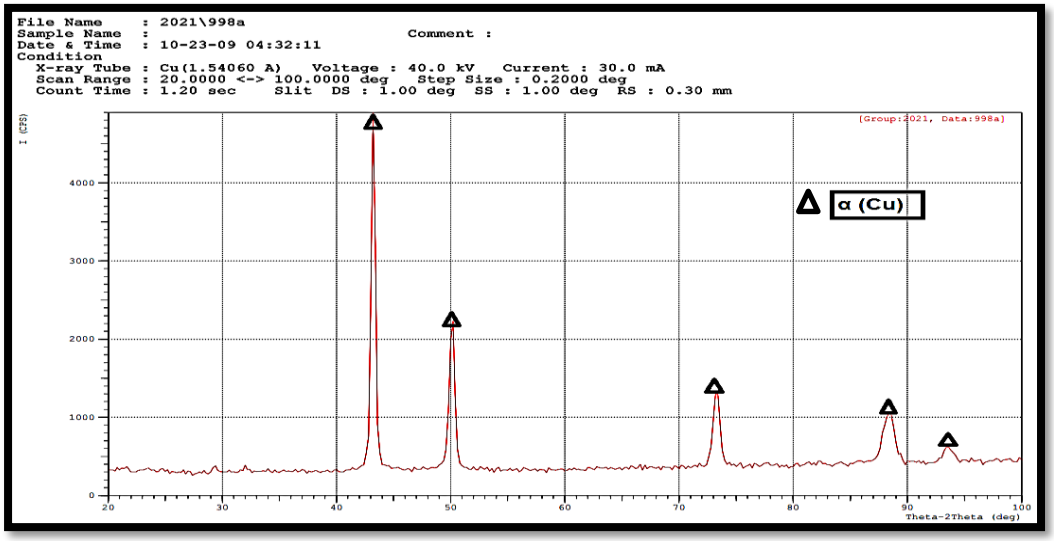

B3-7.5T:

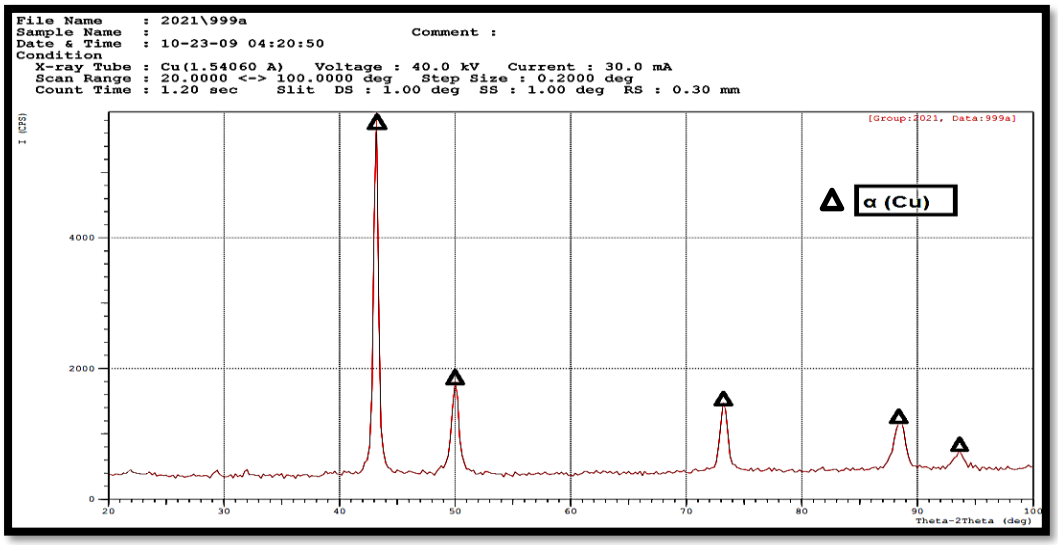

B3-9T:

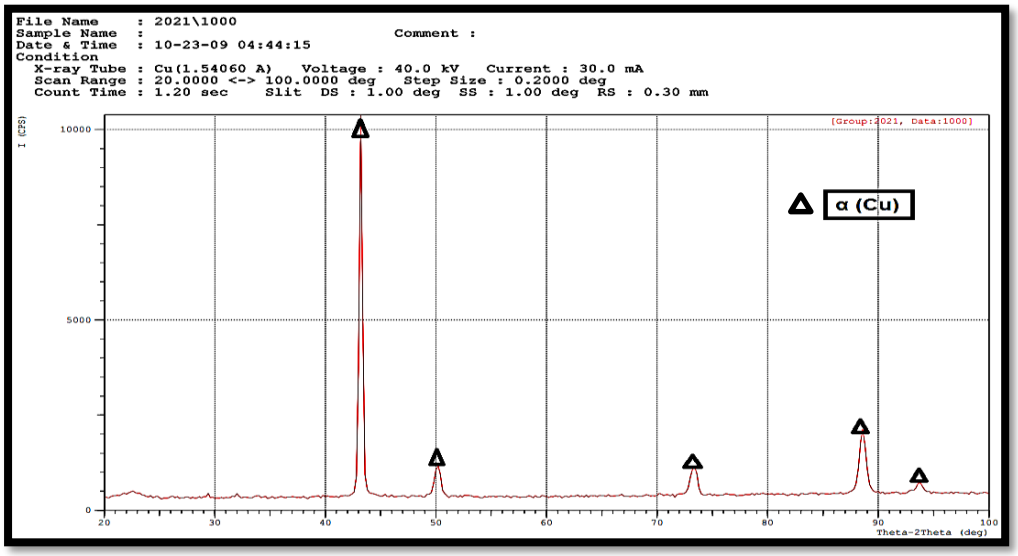

B5-6T:

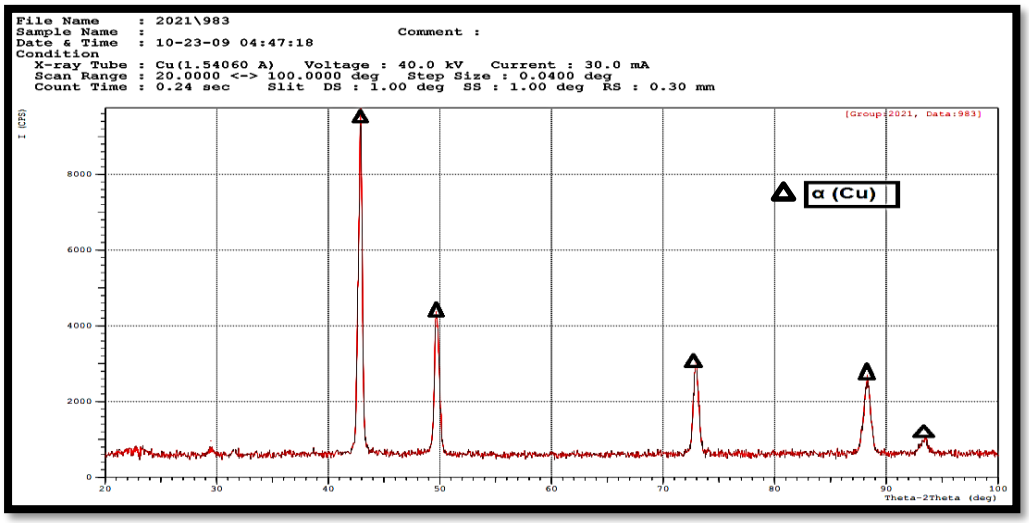

B5-7.5T:

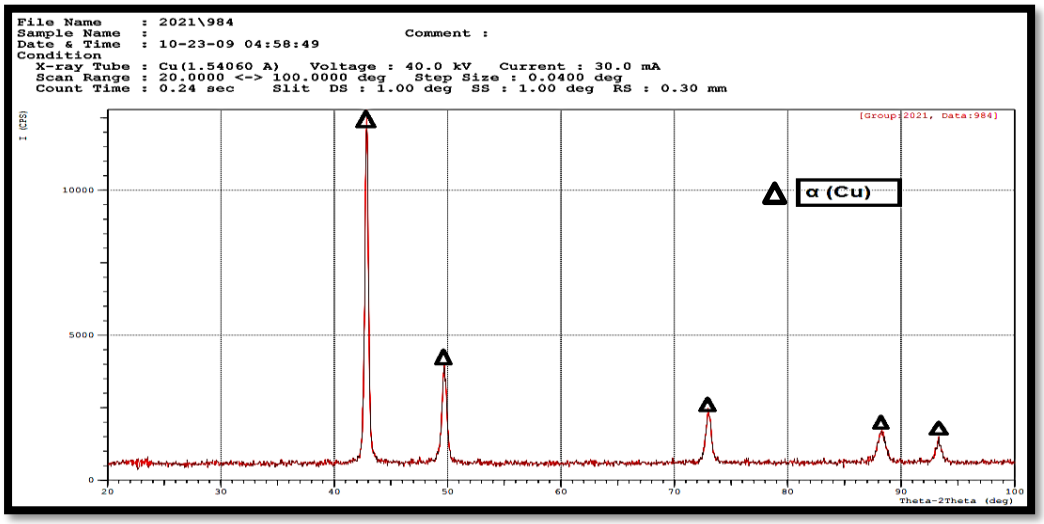

SEM-EDS Images:

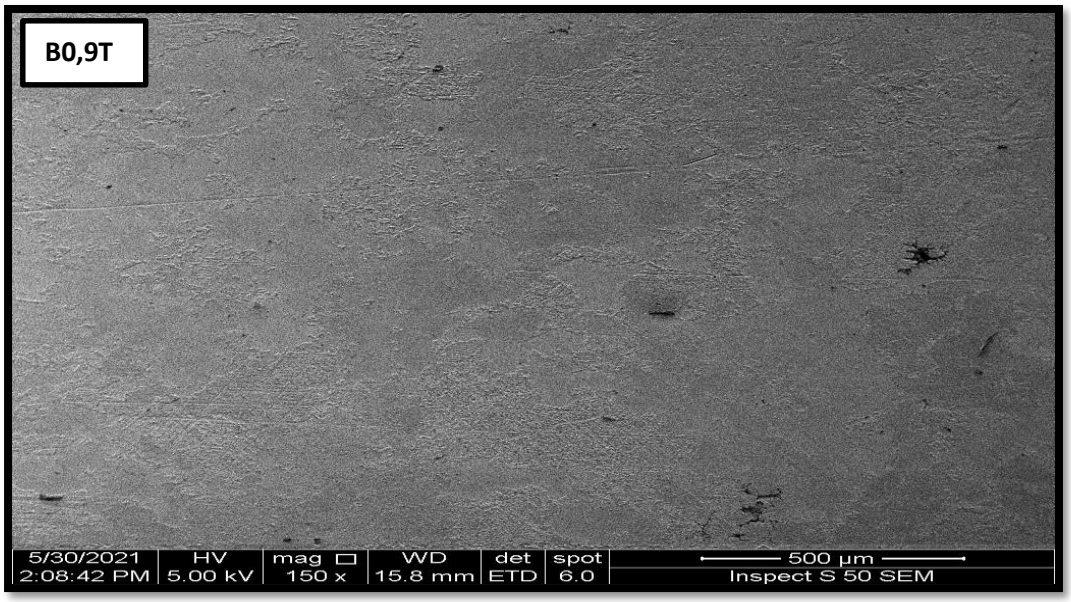

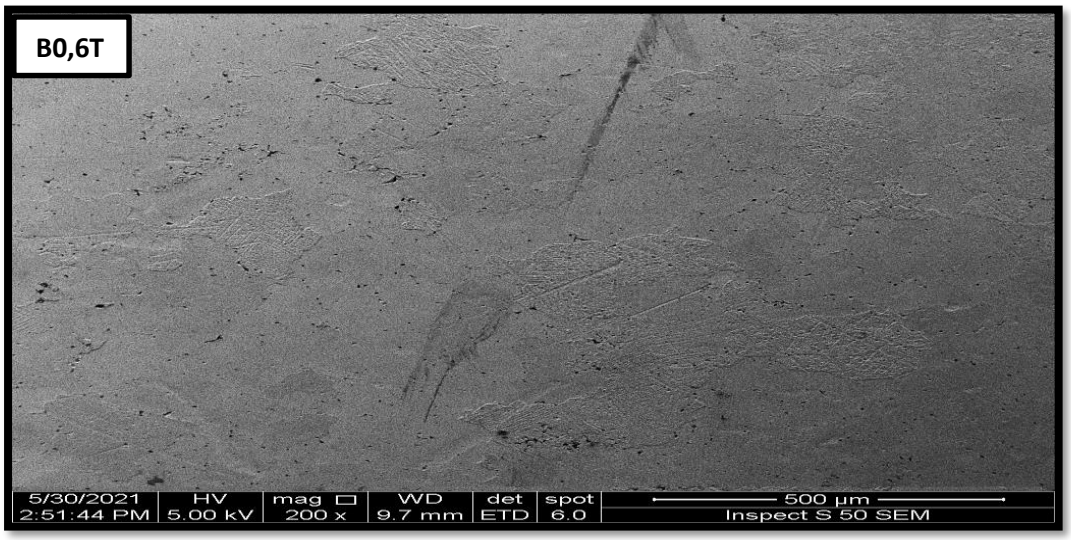

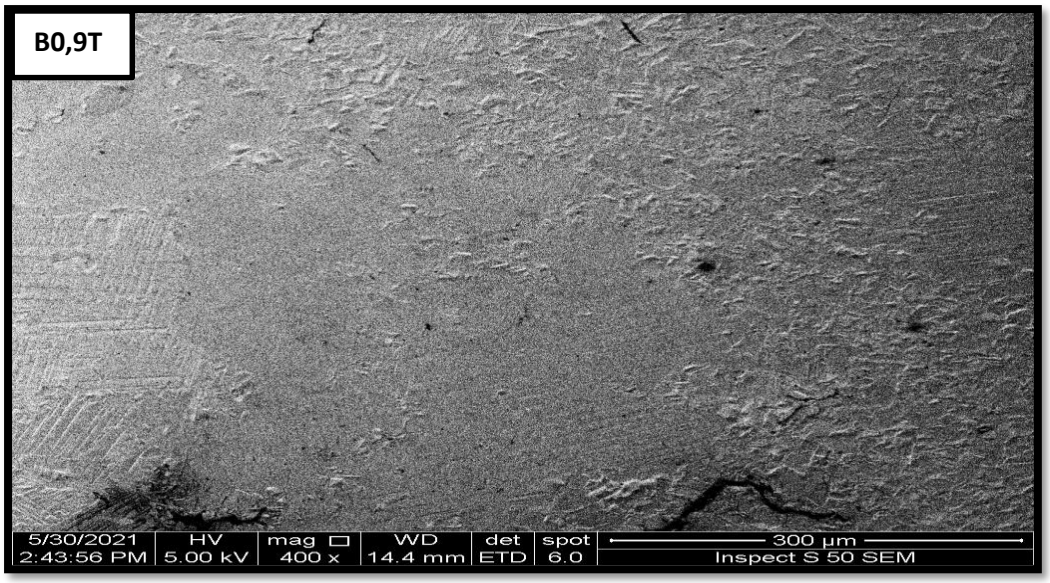
B0,9T
5/30/2021
2:43:56 PM
HV
5.00 kV
mag
400 x
WD
14.4 mm
det
ETD
spot
6.0
300 µm
Inspect S 50 SEM

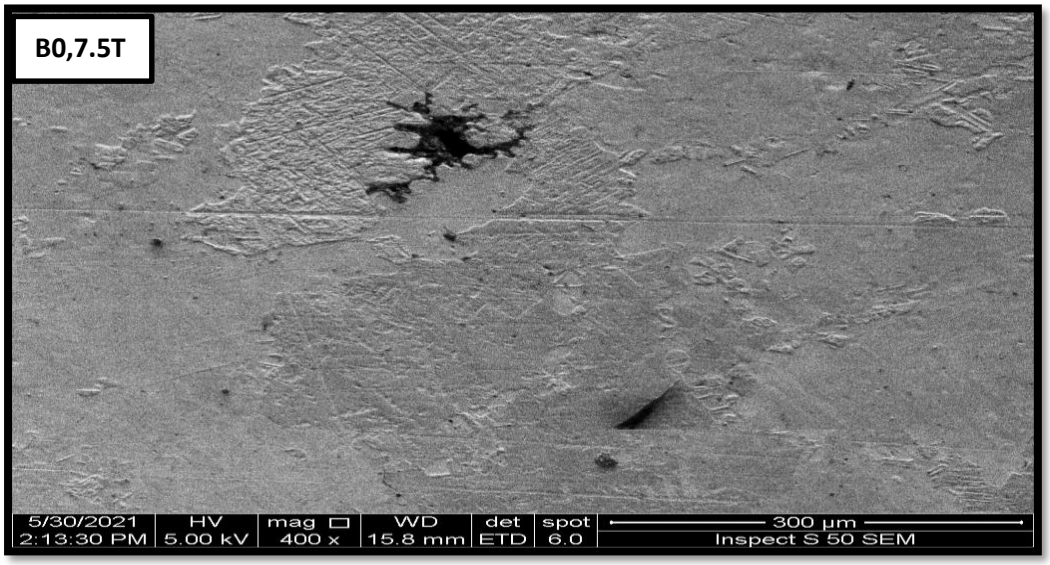
B0,7.5T
5/30/2021
2:13:30 PM
HV
5.00 kV
mag
400 x
WD
15.8 mm
det
ETD
spot
6.0
300 µm
Inspect S 50 SEM

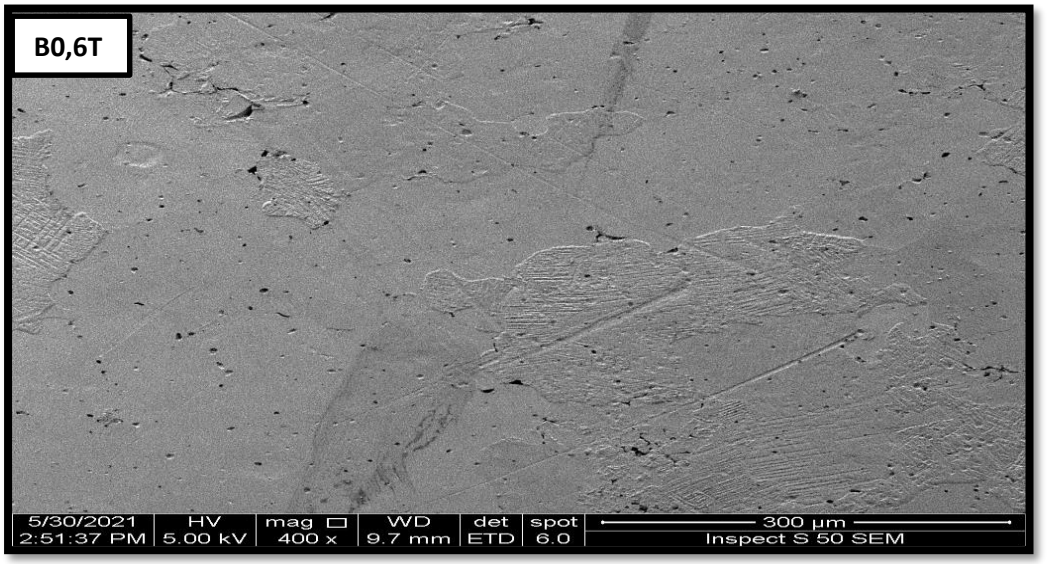
B0,6T
5/30/2021
2:51:37 PM
HV
5.00 kV
mag
400 x
WD
9.7 mm
det
ETD
spot
6.0
300 µm
Inspect S 50 SEM

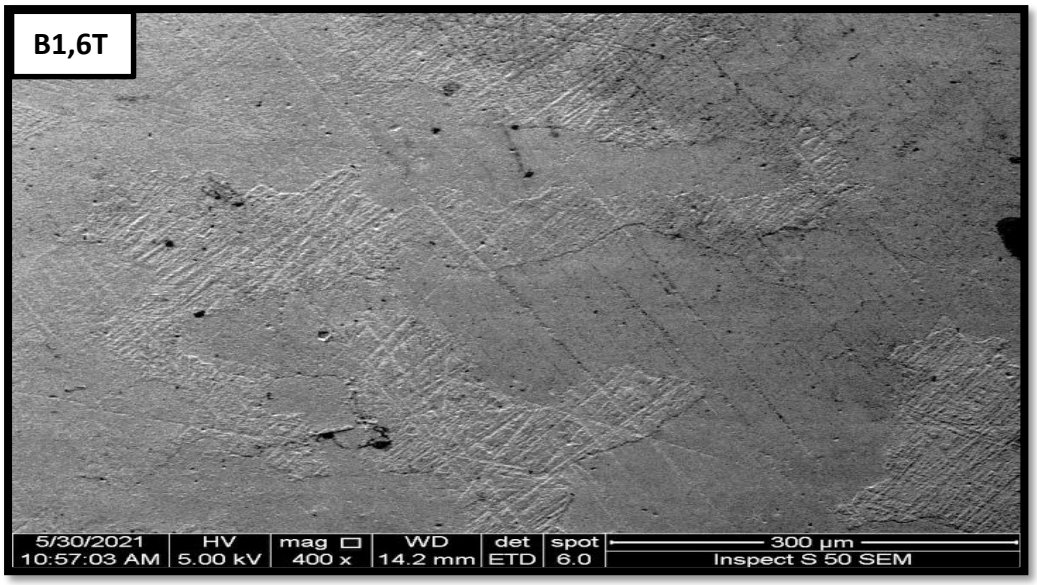
B1,6T
5/30/2021
10:57:03 AM
HV
5.00 kV
mag
400 x
WD
14.2 mm
det
ETD
spot
6.0
300 µm
Inspect S 50 SEM

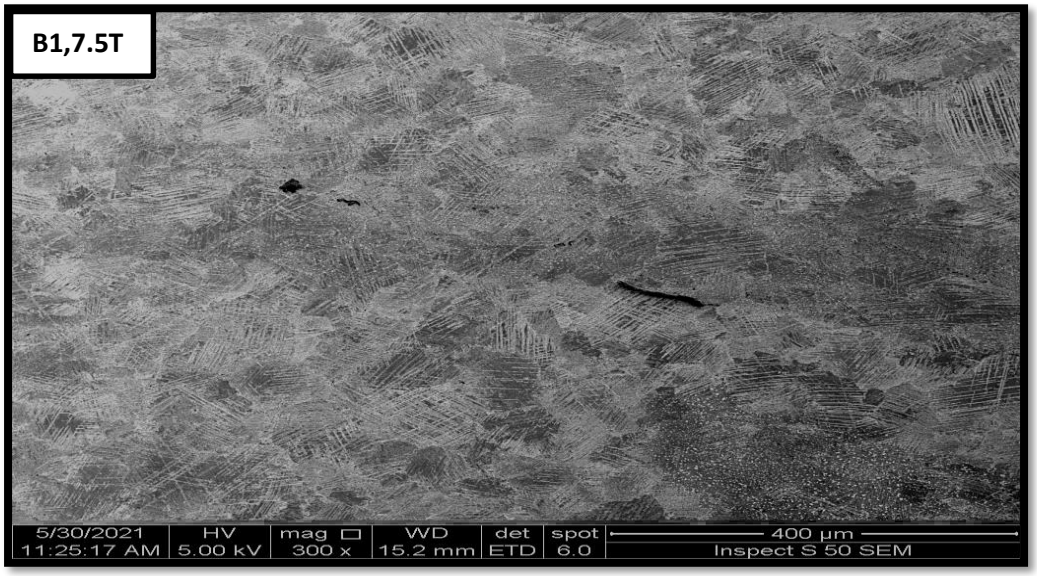
B1,7.5T
5/30/2021
11:25:17 AM
HV
5.00 kV
mag
300 x
WD
15.2 mm
det
ETD
spot
6.0
400 µm
Inspect S 50 SEM

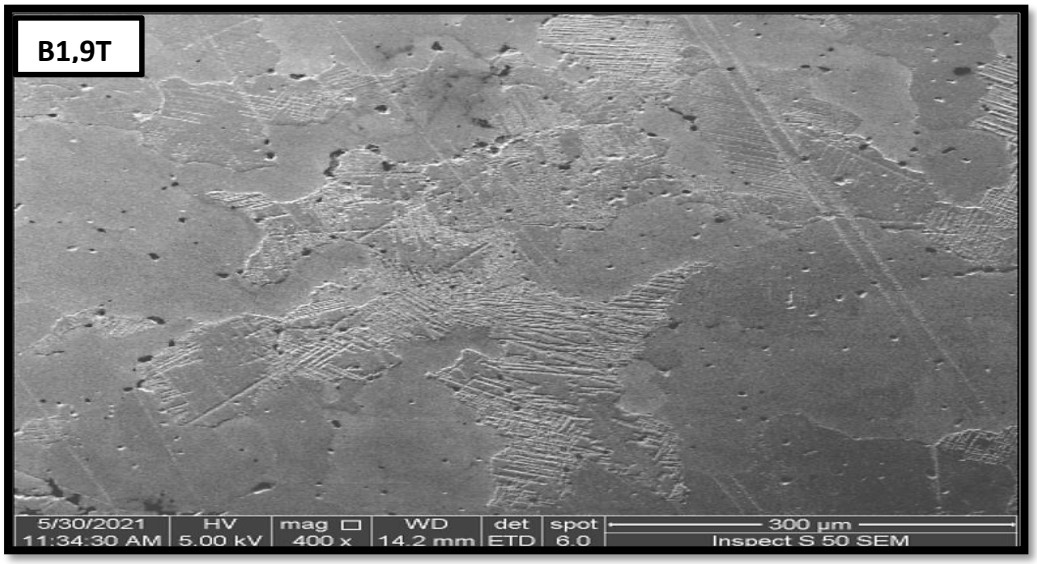
B1,9T
5/30/2021
11:34:30 AM
HV
5.00 kV
mag
400 x
WD
14.2 mm
det
ETD
spot
6.0
300 µm
Inspect S 50 SEM

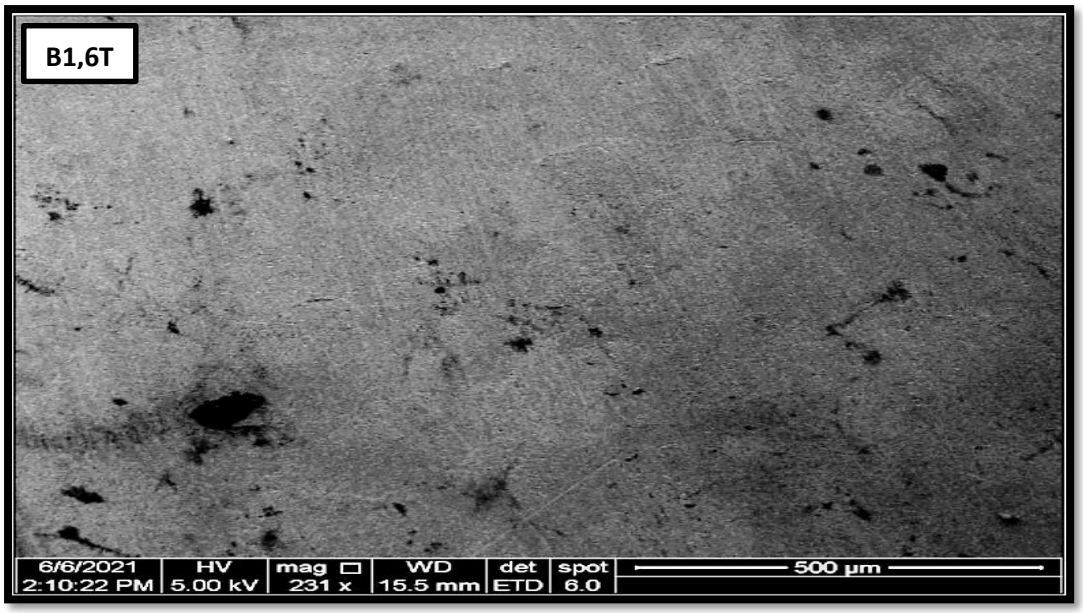
B1,6T
6/6/2021
2:10:22 PM
HV
5.00 kV
mag
231 x
WD
15.5 mm
det
ETD
spot
6.0
500 µm

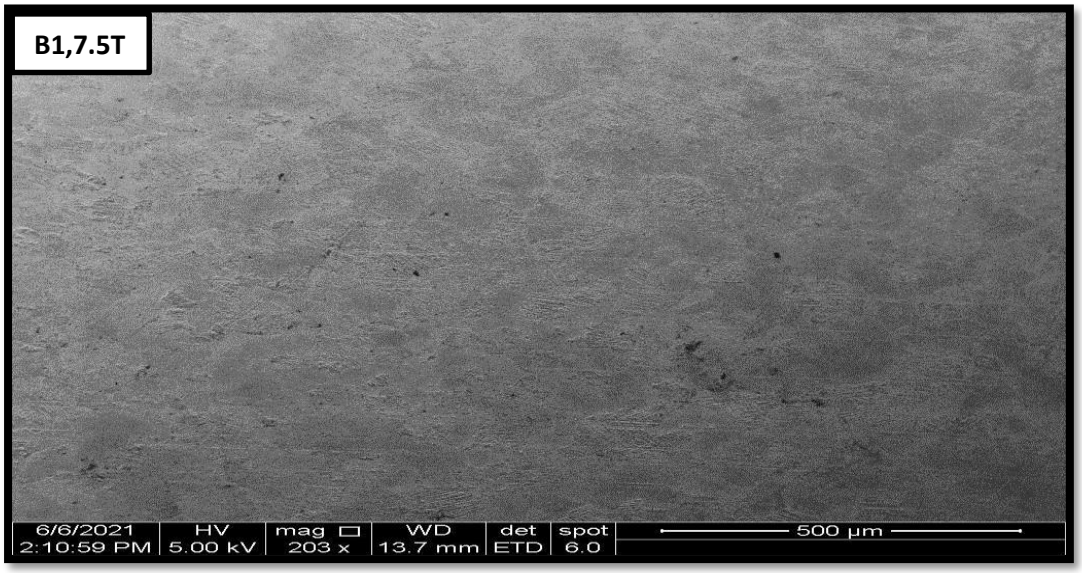
B1,7.5T
6/6/2021
2:10:59 PM
HV
5.00 kV
mag
203 x
WD
13.7 mm
det
ETD
spot
6.0
500 µm

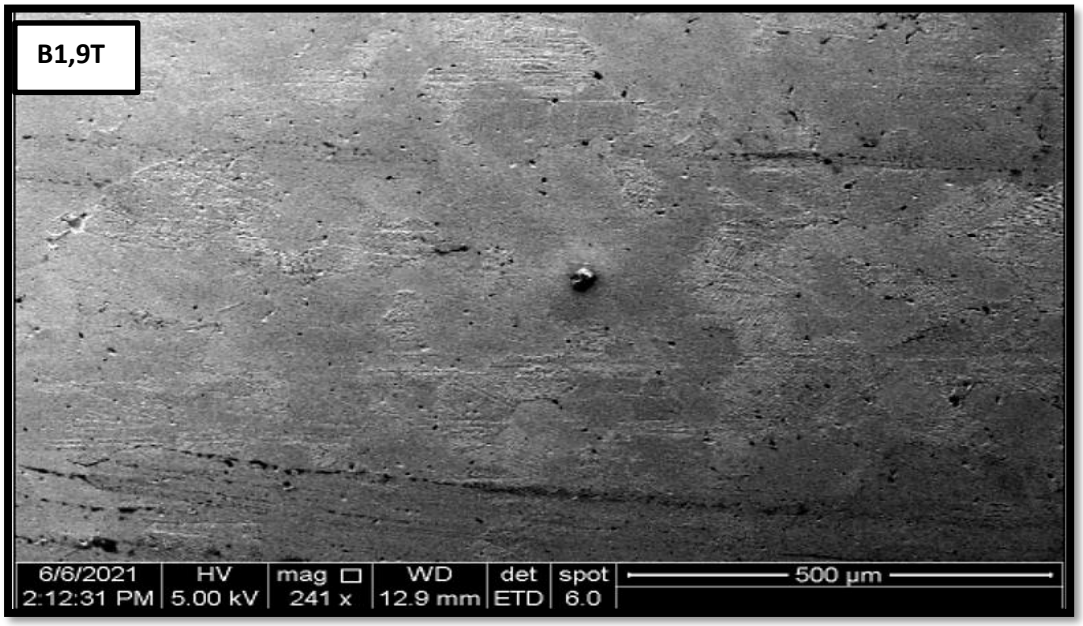
B1,9T
6/6/2021
2:12:31 PM
HV
5.00 kV
mag
241 x
WD
12.9 mm
det
ETD
spot
6.0
500 µm

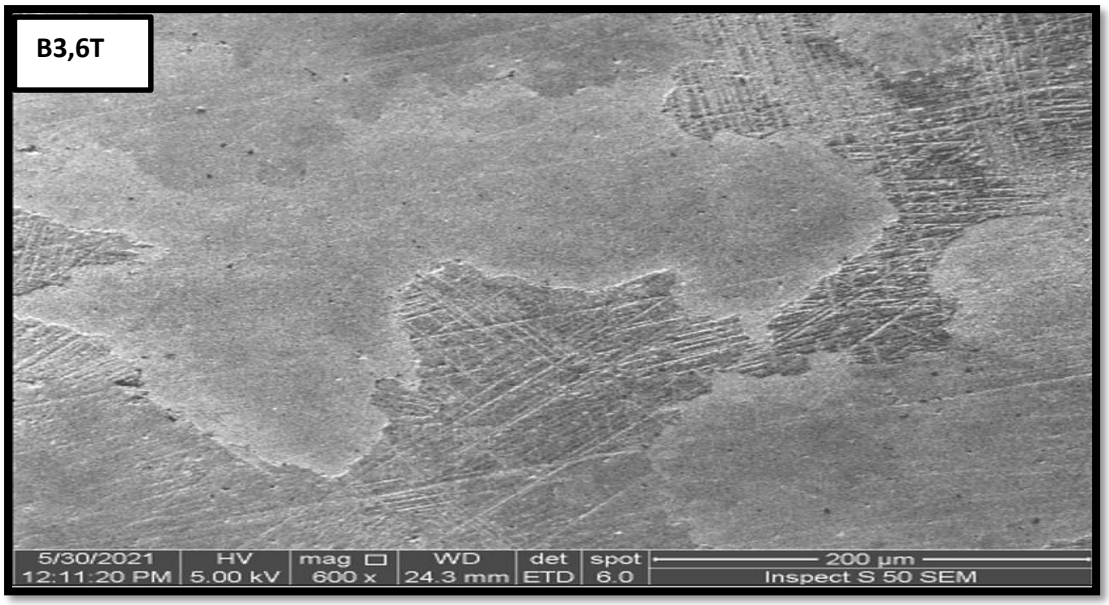
B3,6T
5/30/2021
12:11:20 PM
HV
5.00 kV
mag
600 x
WD
24.3 mm
det
ETD
spot
6.0
200 µm
Inspect S 50 SEM

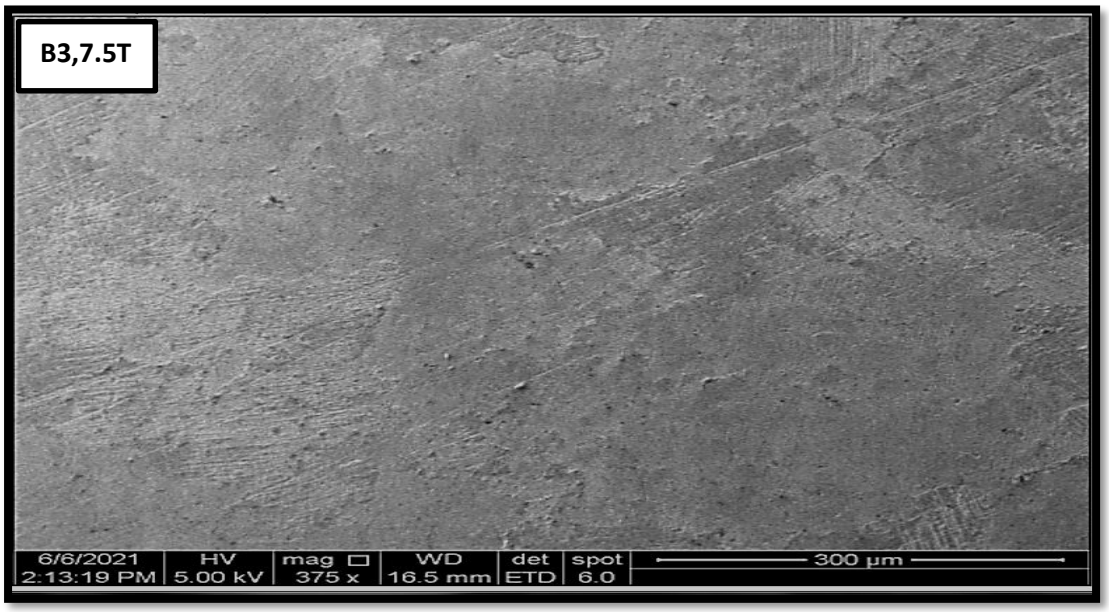
B3,7.5T
6/6/2021
2:13:19 PM
HV
5.00 kV
mag
375 x
WD
16.5 mm
det
ETD
spot
6.0
300 µm

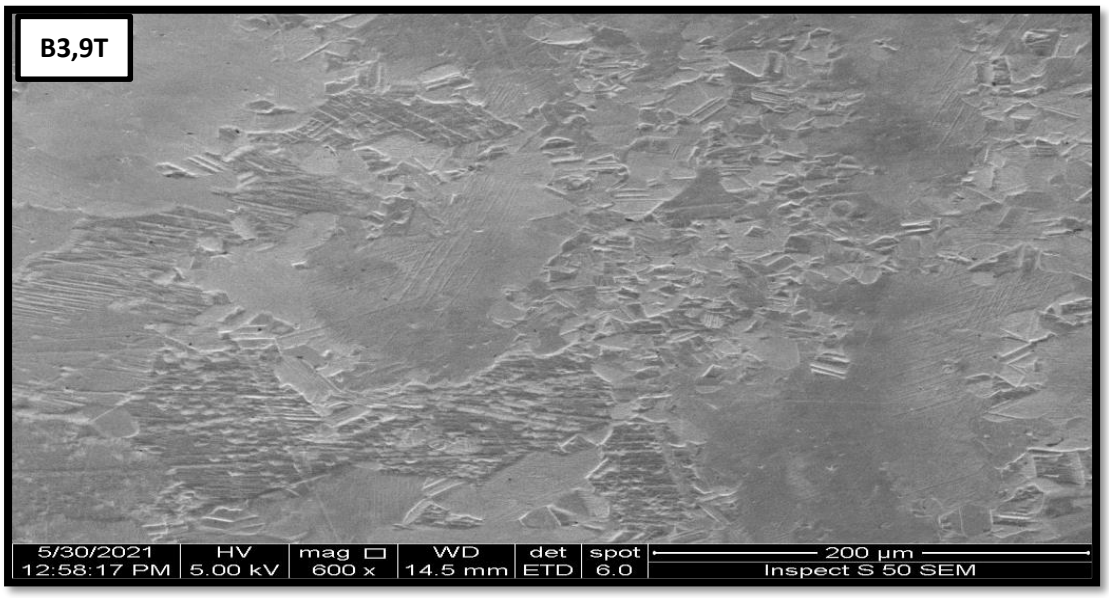
B3,9T
5/30/2021
12:58:17 PM
HV
5.00 kV
mag
600 x
WD
14.5 mm
det
ETD
spot
6.0
200 µm
Inspect S 50 SEM

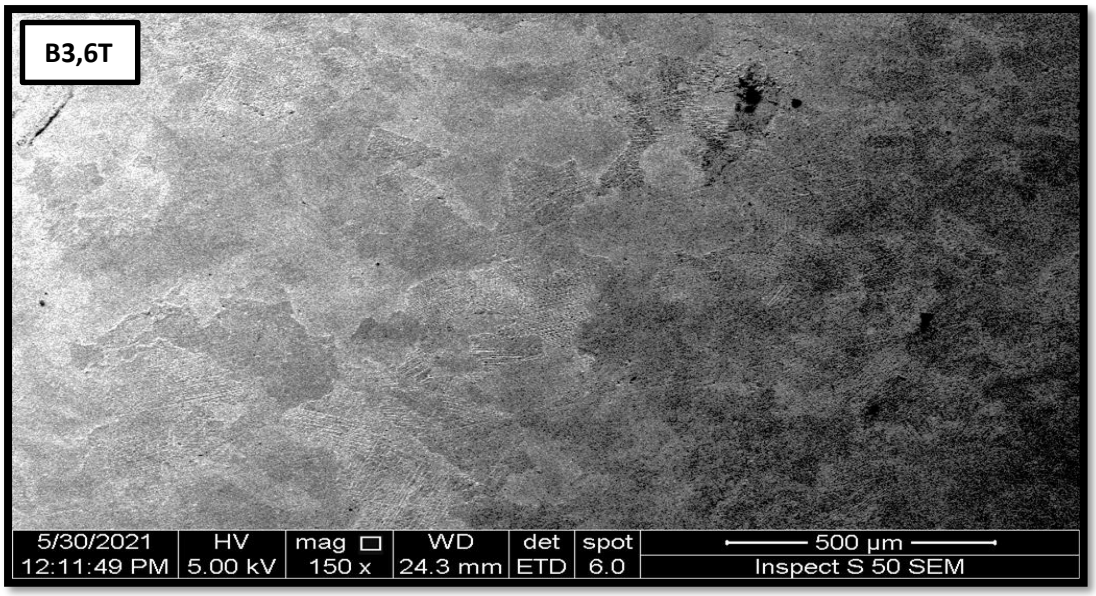
B3,6T
5/30/2021
12:11:49 PM
HV
5.00 kV
mag
150 x
WD
24.3 mm
det
ETD
spot
6.0
500 µm
Inspect S 50 SEM

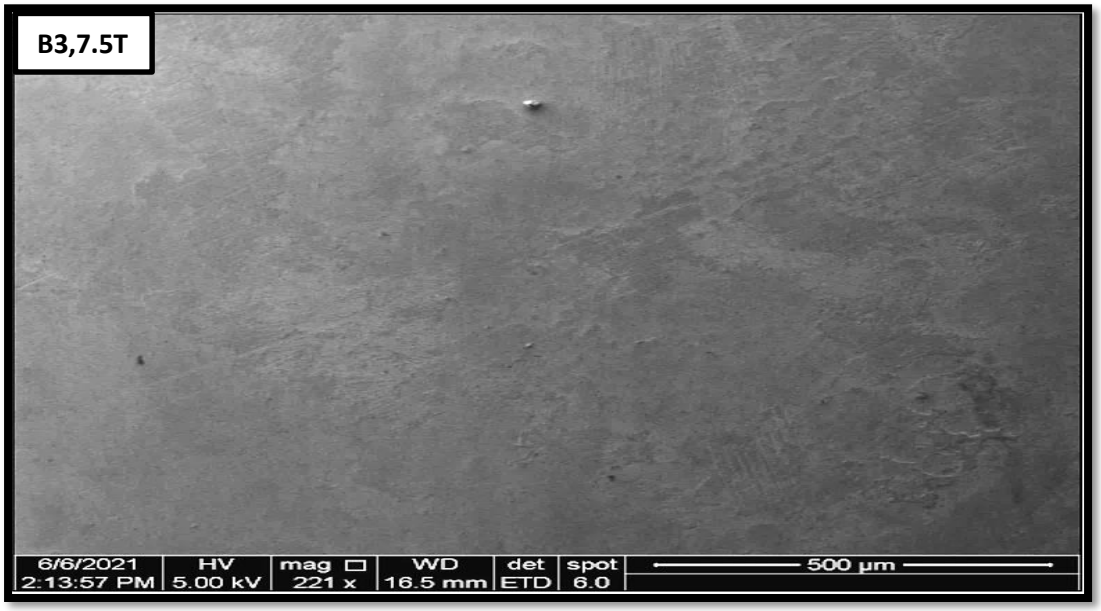
B3,7.5T
6/6/2021
2:13:57 PM
HV
5.00 kV
mag
221 x
WD
16.5 mm
det
ETD
spot
6.0
500 µm

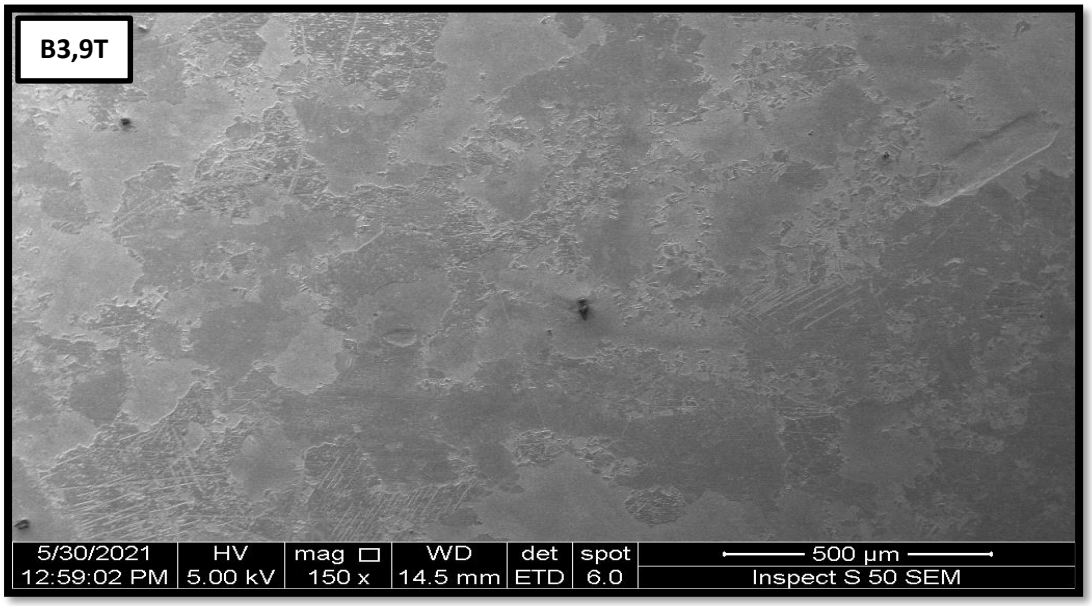
B3,9T
5/30/2021
12:59:02 PM
HV
5.00 kV
mag
150 x
WD
14.5 mm
det
ETD
spot
6.0
500 µm
Inspect S 50 SEM

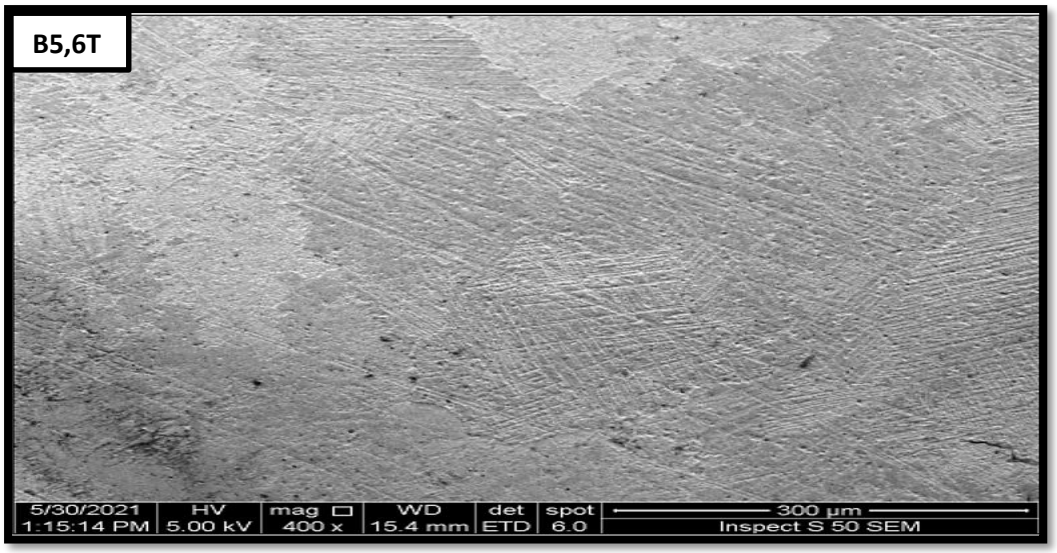
B5,6T
5/30/2021
1:15:14 PM
HV
5.00 kV
mag
400 x
WD
15.4 mm
det
ETD
spot
6.0
300 µm
Inspect S 50 SEM

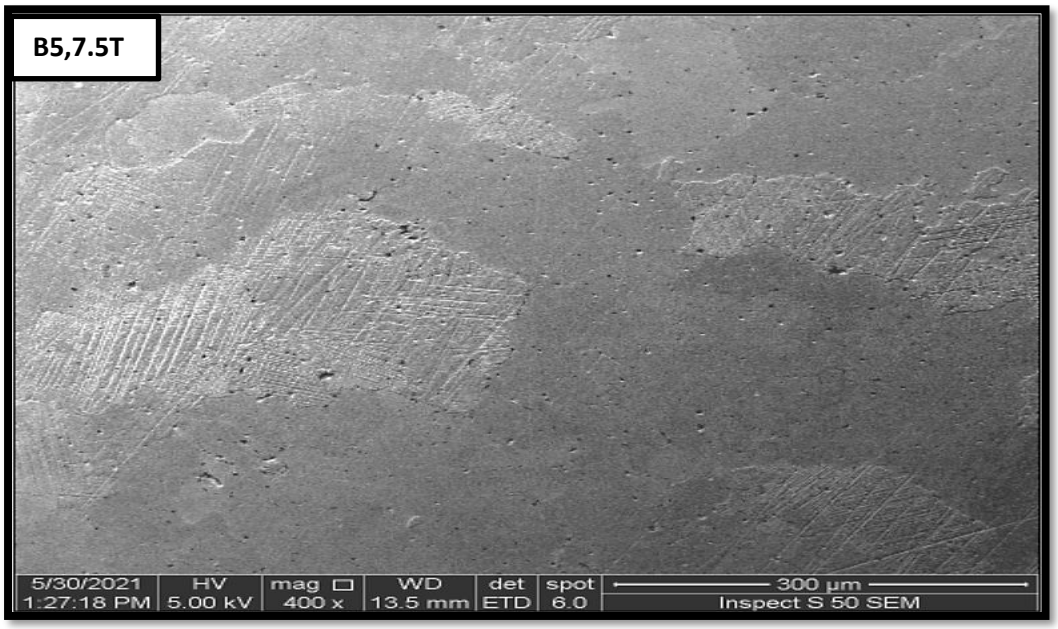
B5,7.5T
5/30/2021
1:27:18 PM
HV
5.00 kV
mag
400 x
WD
13.5 mm
det
ETD
spot
6.0
300 µm
Inspect S 50 SEM

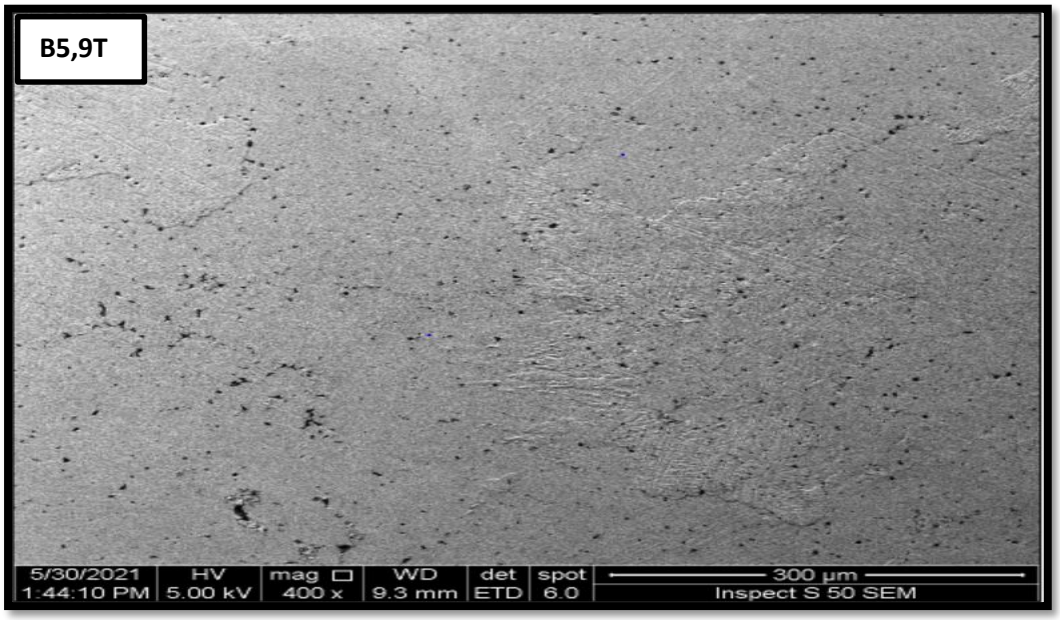
B5,9T
5/30/2021
1:44:10 PM
HV
5.00 kV
mag
400 x
WD
9.3 mm
det
ETD
spot
6.0
300 µm
Inspect S 50 SEM

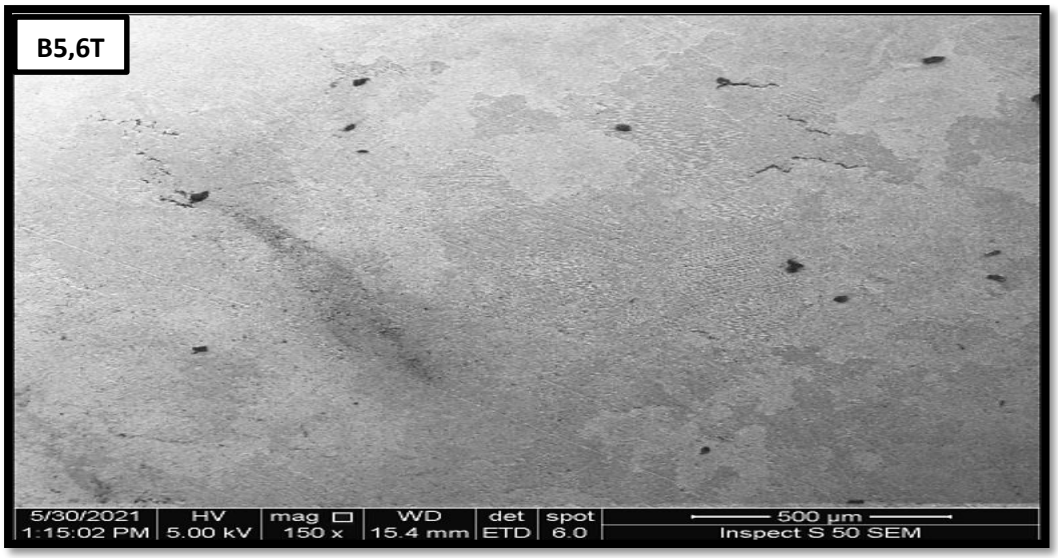
B5,6T
5/30/2021
1:15:02 PM
HV
5.00 kV
mag
150 x
WD
15.4 mm
det
ETD
spot
6.0
500 µm
Inspect S 50 SEM

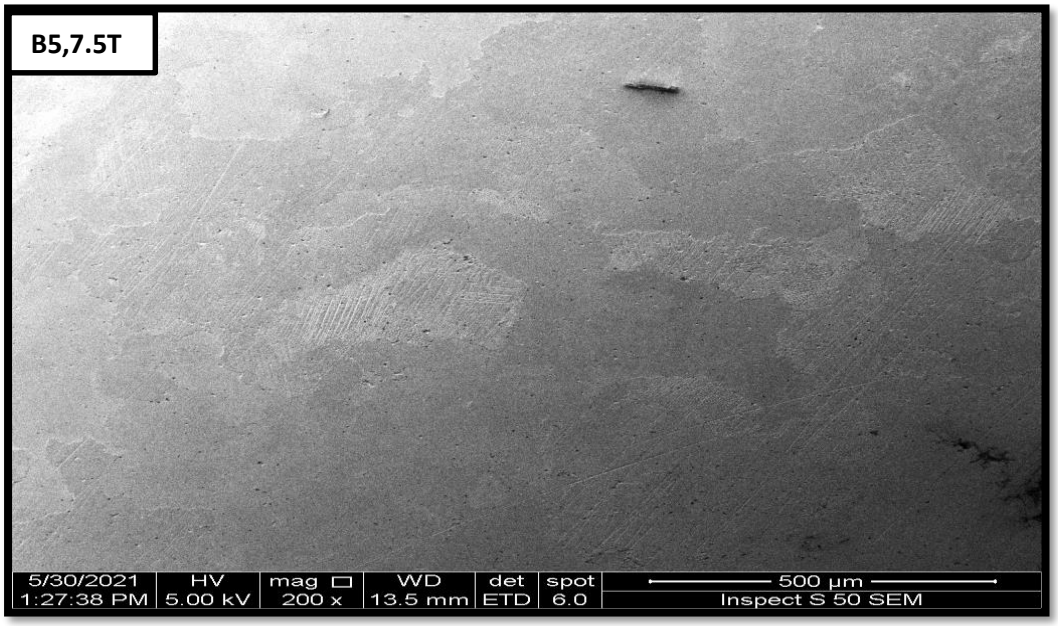
B5,7.5T
5/30/2021
1:27:38 PM
HV
5.00 kV
mag
200 x
WD
13.5 mm
det
ETD
spot
6.0
500 µm
Inspect S 50 SEM

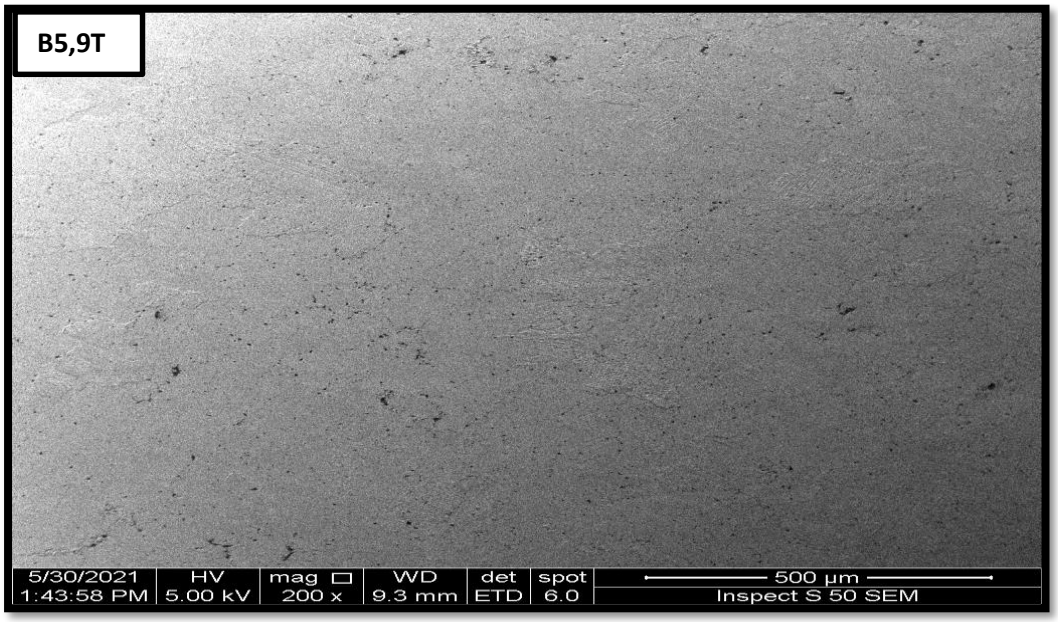
B5,9T
5/30/2021
1:43:58 PM
HV
5.00 kV
mag
200 x
WD
9.3 mm
det
ETD
spot
6.0
500 µm
Inspect S 50 SEM

B0

Application Note

BRUKER

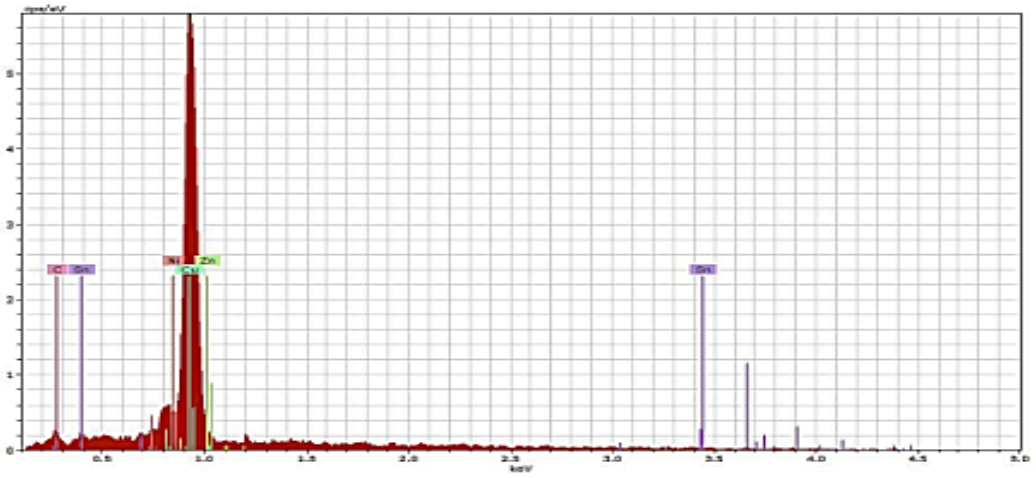

Spectrum: Acquisition 4193

El	AN	Series	unn. C [wt.%]	norm. C [wt.%]	Atom. C [at.%]	Error (1 Sigma) [wt.%]
Cu	29	L-series	98.23	98.23	96.51	16.73
Sn	50	M-series	1.22	1.22	0.64	1.44
C	6	K-series	0.55	0.55	2.85	0.50
Zn	30	L-series	0.00	0.00	0.00	0.00
Ni	28	L-series	0.00	0.00	0.00	0.00
		Total:	100.00	100.00	100.00	

B0,6T

Application Note

BRUKER

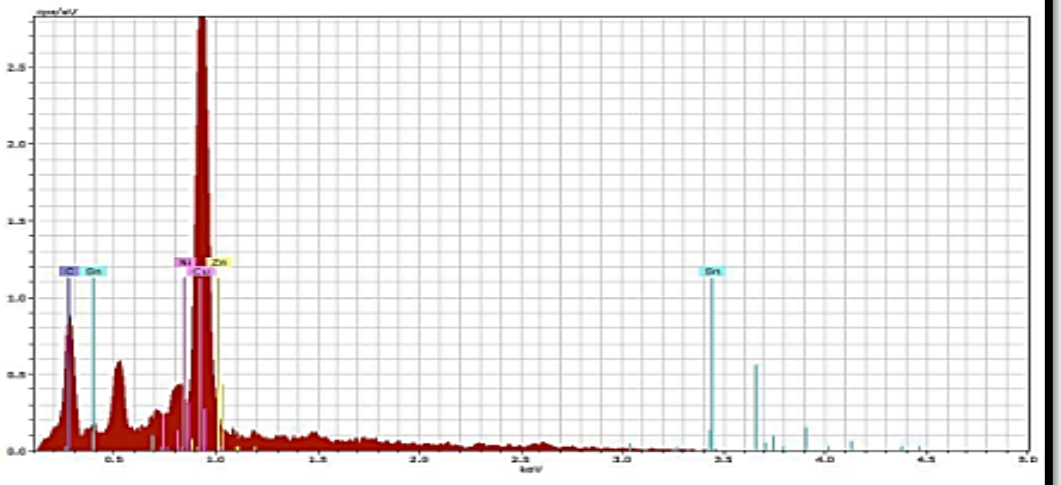

Spectrum: Acquisition 4191

El	AN	Series	unn. C [wt.%]	norm. C [wt.%]	Atom. C [at.%]	Error (1 Sigma) [wt.%]
Cu	29	L-series	91.11	91.11	80.96	17.13
Sn	50	M-series	5.06	5.06	2.41	3.69
C	6	K-series	3.46	3.46	16.28	1.63
Ni	28	L-series	0.35	0.35	0.34	0.48
Zn	30	L-series	0.01	0.01	0.01	0.05
		Total:	100.00	100.00	100.00	

B0,7.5T

Application Note

BRUKER

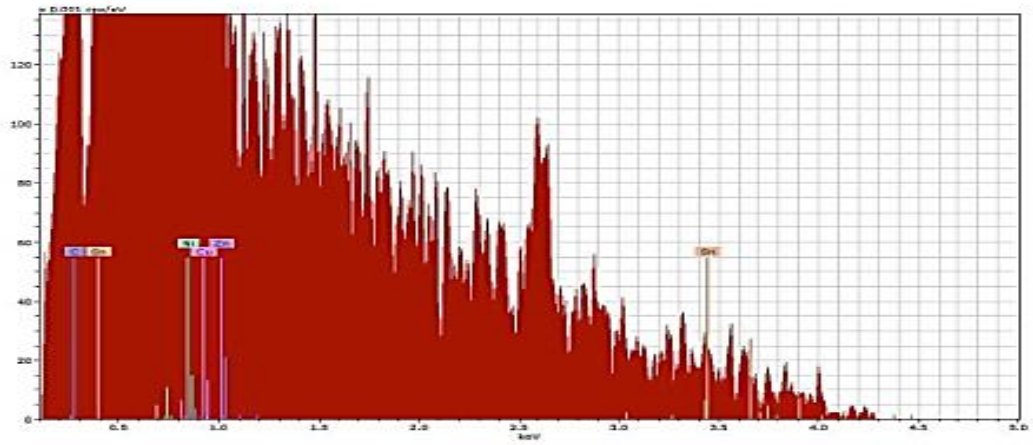

Spectrum: Acquisition 4213

El	AN	Series	unn. C [wt.%]	norm. C [wt.%]	Atom. C [at.%]	Error (1 Sigma) [wt.%]
Cu	29	L-series	94.06	94.06	90.74	15.47
Sn	50	M-series	4.57	4.57	2.36	2.71
C	6	K-series	1.35	1.35	6.88	0.75
Zn	30	L-series	0.02	0.02	0.02	0.05
Ni	28	L-series	0.00	0.00	0.00	0.00
		Total:	100.00	100.00	100.00	

B1

Application Note

BRUKER

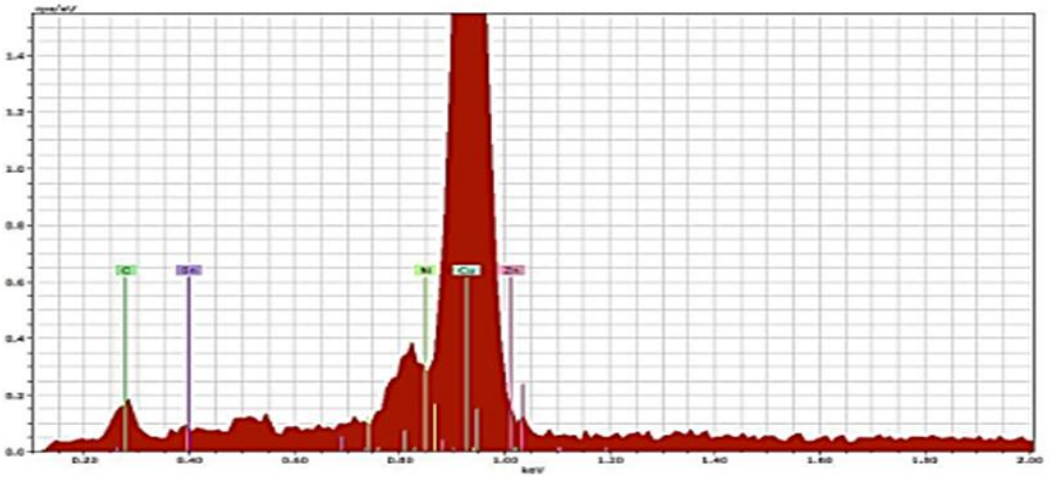

Spectrum: Acquisition 4202

El	AN	Series	unn. C [wt.%]	norm. C [wt.%]	Atom. C [at.%]	Error (1 Sigma) [wt.%]
Cu	29	L-series	94.06	94.06	88.58	13.60
Sn	50	M-series	3.60	3.60	1.81	1.85
C	6	K-series	1.82	1.82	9.07	0.76
Ni	28	L-series	0.52	0.52	0.53	0.34
Zn	30	L-series	0.00	0.00	0.00	0.00
		Total:	100.00	100.00	100.00	

B1,6T

Application Note

BRUKER

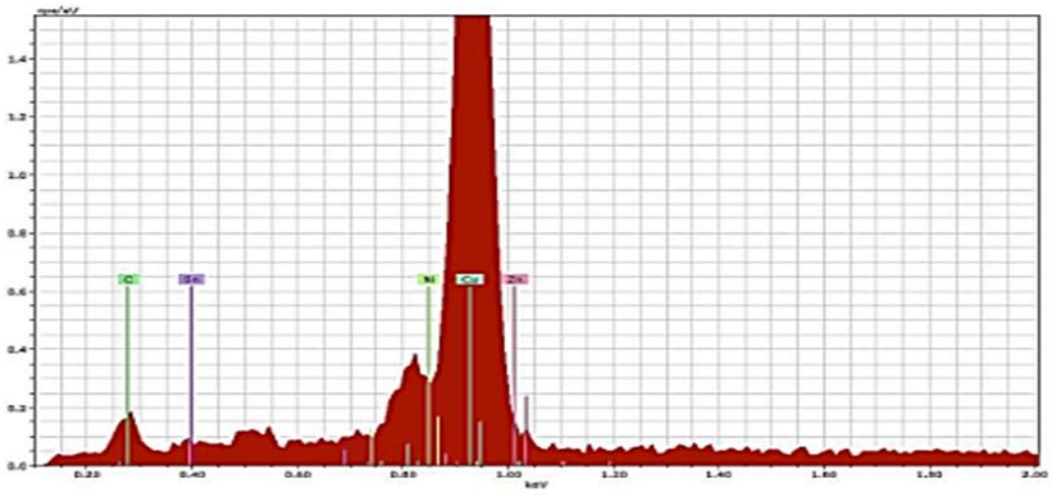

Spectrum: Acquisition 4202

El	AN	Series	unn. C [wt.%]	norm. C [wt.%]	Atom. C [at.%]	Error (1 Sigma) [wt.%]
Cu	29	L-series	94.06	94.06	88.58	13.60
Sn	50	M-series	3.60	3.60	1.81	1.85
C	6	K-series	1.82	1.82	9.07	0.76
Ni	28	L-series	0.52	0.52	0.53	0.34
Zn	30	L-series	0.00	0.00	0.00	0.00
		Total:	100.00	100.00	100.00	

B1,7.5T

Application Note

BRUKER

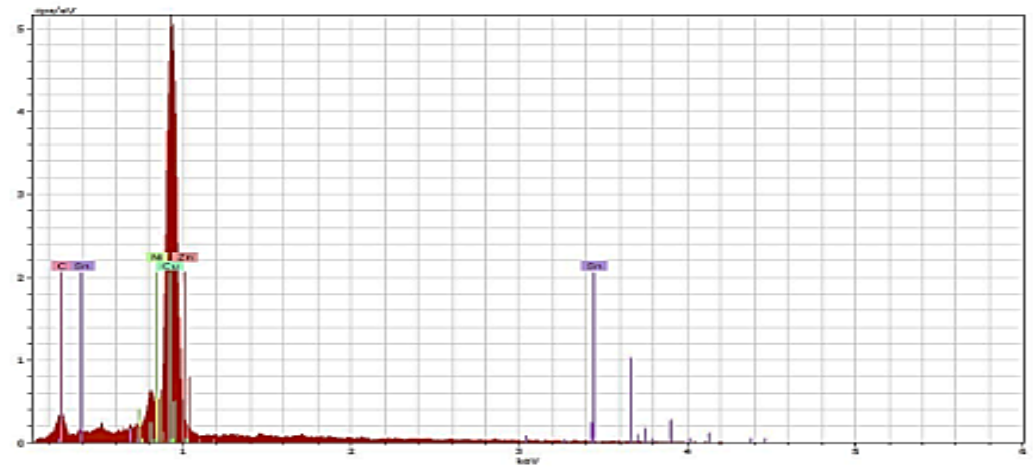

Spectrum: Acquisition 4186

El	AN	Series	unn. C [wt.%]	norm. C [wt.%]	Atom. C [at.%]	Error (1 Sigma) [wt.%]
Cu	29	L-series	93.73	93.73	87.87	14.69
Sn	50	M-series	3.95	3.95	1.98	2.36
C	6	K-series	1.97	1.97	9.79	0.94
Ni	28	L-series	0.35	0.35	0.36	0.33
Zn	30	L-series	0.00	0.00	0.00	0.00
		Total:	100.00	100.00	100.00	

B3

Application Note

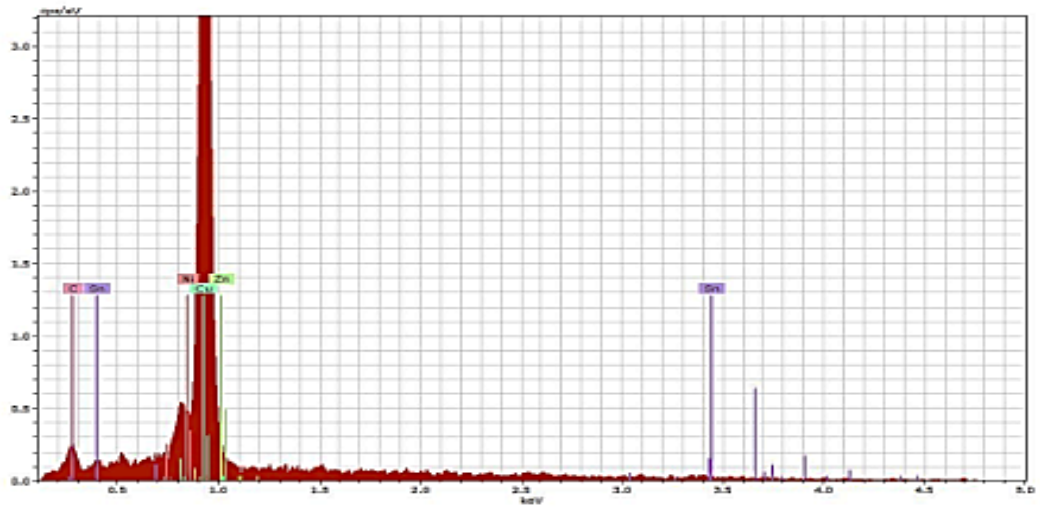

Spectrum: Acquisition 4186

El	AN	Series	unn. C [wt.%]	norm. C [wt.%]	Atom. C [at.%]	Error (1 Sigma) [wt.%]
Cu	29	L-series	91.47	91.47	82.67	14.90
Sn	50	M-series	5.45	5.45	2.64	3.19
C	6	K-series	3.07	3.07	14.69	1.40
Zn	30	L-series	0.00	0.00	0.00	0.00
Ni	28	L-series	0.00	0.00	0.00	0.00
		Total:	100.00	100.00	100.00	

B3,6T

Application Note

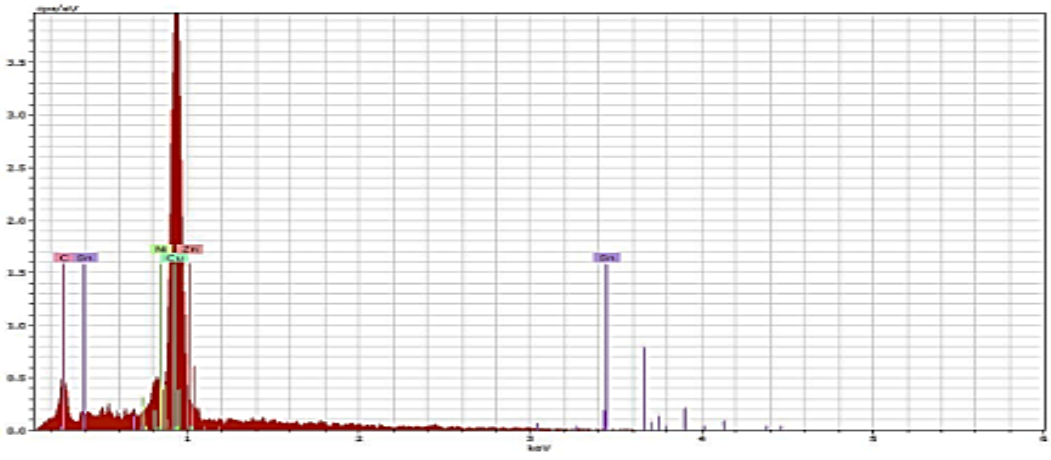

Spectrum: Acquisition 4200

El	AN	Series	unn. C [wt.%]	norm. C [wt.%]	Atom. C [at.%]	Error (1 Sigma) [wt.%]
Cu	29	L-series	90.71	90.71	81.48	17.69
Sn	50	M-series	4.50	4.50	2.16	3.69
C	6	K-series	3.13	3.13	14.90	1.63
Zn	30	L-series	1.54	1.54	1.35	0.33
Ni	28	L-series	0.12	0.12	0.12	0.30
		Total:	100.00	100.00	100.00	

B3,7.5T

Application Note

BRUKER

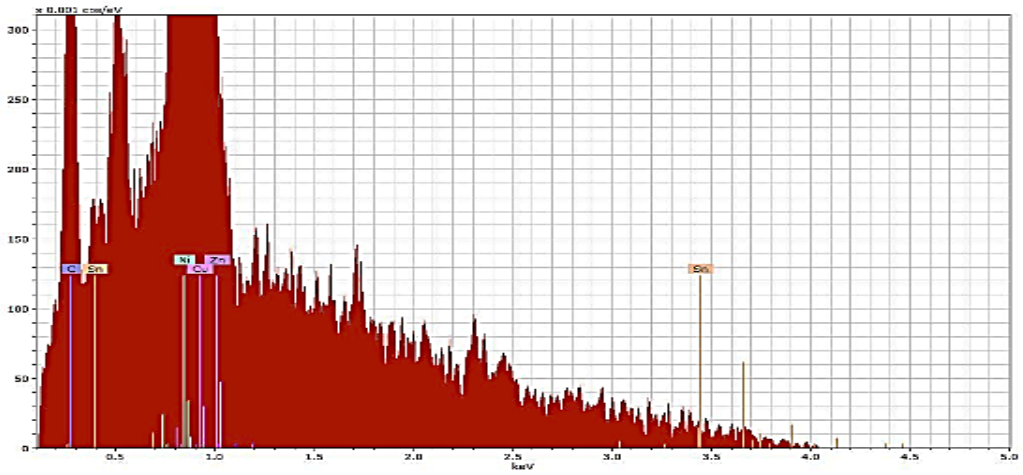

Spectrum: Acquisition 4225

El	AN	Series	unn. C [wt.%]	norm. C [wt.%]	Atom. C [at.%]	Error (1 Sigma) [wt.%]
Cu	29	L-series	94.55	94.55	84.45	13.71
C	6	K-series	3.03	3.03	14.33	0.97
Sn	50	M-series	2.27	2.27	1.08	1.38
Zn	30	L-series	0.15	0.15	0.13	0.07
Ni	28	L-series	0.00	0.00	0.00	0.00
Total:			100.00	100.00	100.00	

B5

Application Note

BRUKER

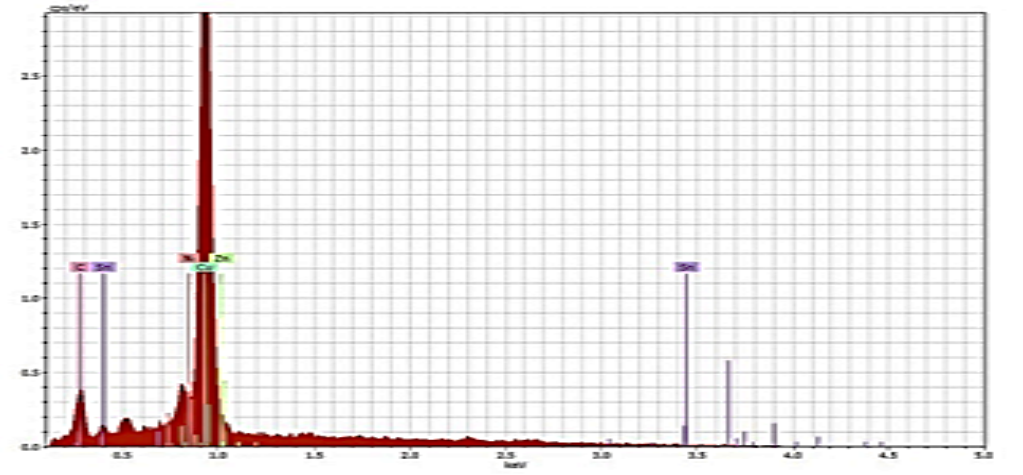

Spectrum: Acquisition 4202

El	AN	Series	unn. C [wt.%]	norm. C [wt.%]	Atom. C [at.%]	Error (1 Sigma) [wt.%]
Cu	29	L-series	88.33	88.33	73.38	13.27
Sn	50	M-series	5.53	5.53	2.46	2.79
C	6	K-series	5.35	5.35	23.52	1.76
Zn	30	L-series	0.80	0.80	0.64	0.16
Ni	28	L-series	0.00	0.00	0.00	0.00
Total:			100.00	100.00	100.00	

B5,6T

Application Note

BRUKER

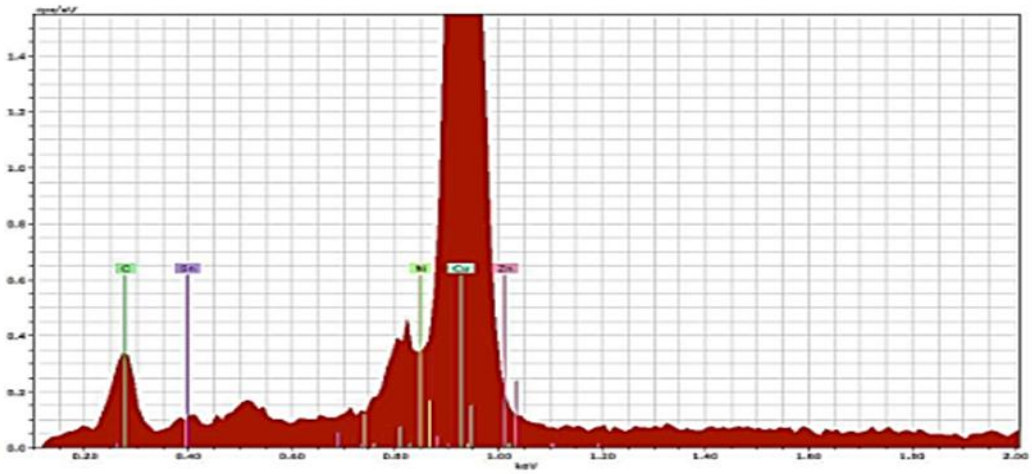

Spectrum: Acquisition 4203

El	AN	Series	unn. C [wt.%]	norm. C [wt.%]	Atom. C [at.%]	Error (1 Sigma) [wt.%]
Cu	29	L-series	91.10	91.10	76.38	11.53
C	6	K-series	4.92	4.92	21.84	1.10
Sn	50	M-series	3.97	3.97	1.78	1.39
Zn	30	L-series	0.00	0.00	0.00	0.00
Ni	28	L-series	0.00	0.00	0.00	0.00
		Total:	100.00	100.00	100.00	

B5,7.5T

Application Note

BRUKER

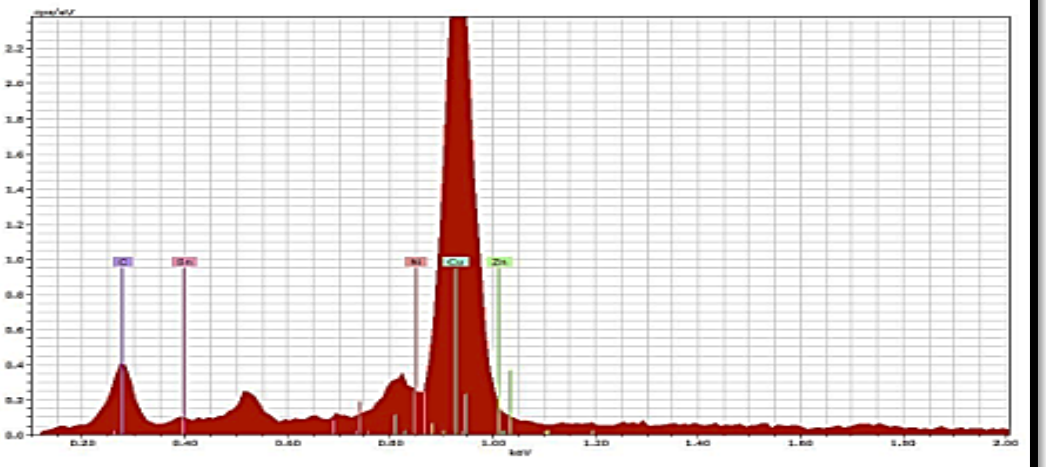

Spectrum: Acquisition 4193

El	AN	Series	unn. C [wt.%]	norm. C [wt.%]	Atom. C [at.%]	Error (1 Sigma) [wt.%]
Cu	29	L-series	91.51	91.51	76.35	11.88
C	6	K-series	5.00	5.00	22.07	1.03
Sn	50	M-series	3.43	3.43	1.53	1.25
Zn	30	L-series	0.06	0.06	0.05	0.04
Ni	28	L-series	0.00	0.00	0.00	0.00
		Total:	100.00	100.00	100.00	

Grain size measurement:

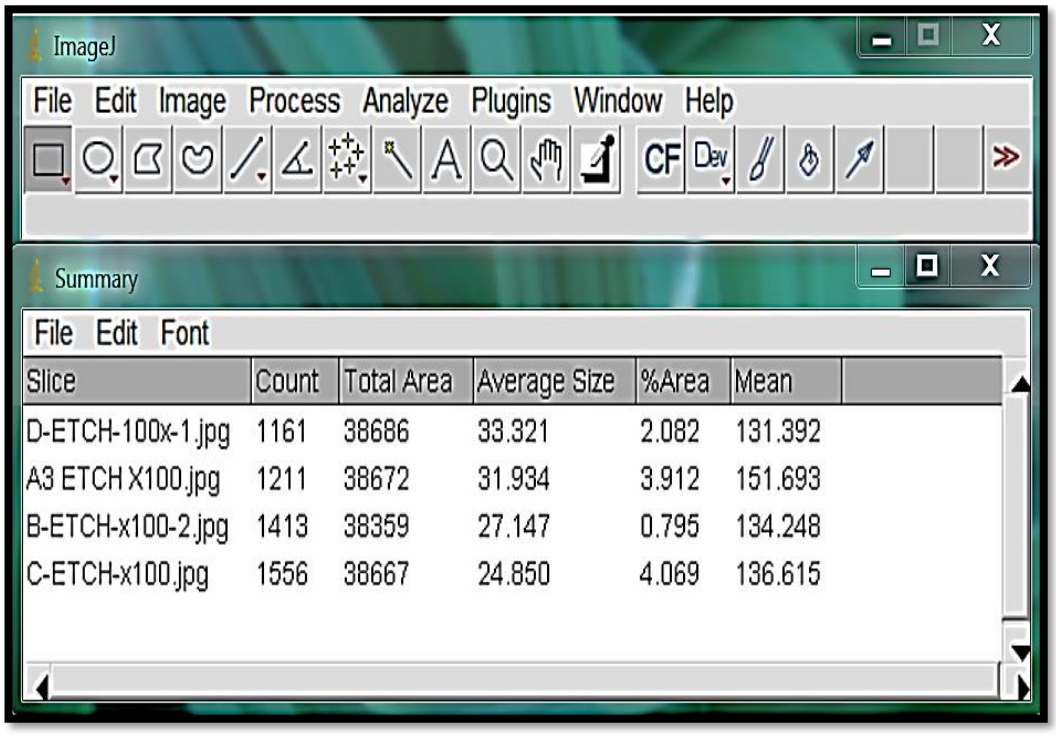

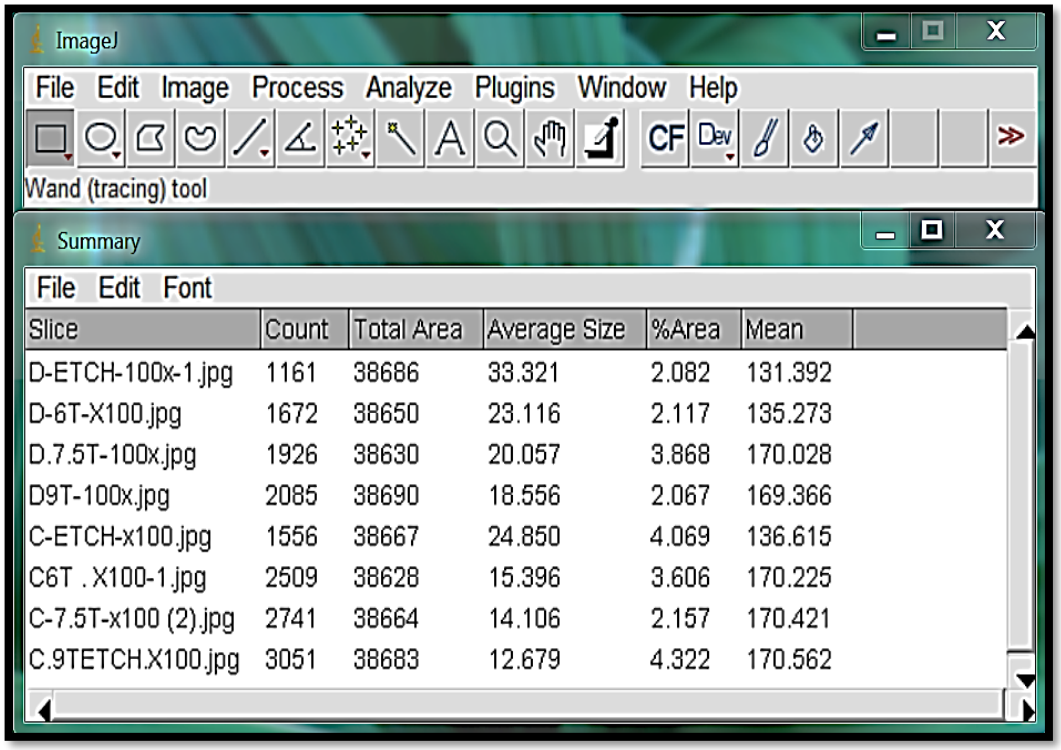

Wear Result:

Table (3): The results of the wear tests of the samples B0 and B5 before hot pressing

Sample	Time (min)	w_2 (g)	Δw (g)	Distance=$2\pi rnt/1000$ (m)	$R.W = \Delta w/2\pi rnt$ (g/m)	Friction coefficient
B5,10N w1=18.2076g	5	18.2015	0.0071	50.24 m	1.4142×10^{-4}	0.34
	10	18.1955	0.0121	100.48 m	1.2043×10^{-4}	0.32
	15	18.1895	0.0179	150,72 m	1.1852×10^{-4}	0.36
	20	18.1844	0.0232	200.96 m	1.1545×10^{-4}	0.44
B5,20N w1=18.0973g	5	18.0843	0.0130	50.24 m	2.4780×10^{-4}	0.39
	10	18.0737	0.0236	100.48 m	2.3492×10^{-4}	0.43
	15	18.0620	0.0353	150,72 m	2.3437×10^{-4}	0.48
	20	18.0560	0.0413	200.96 m	2.0571×10^{-4}	0.58
B,10N, w1=14.3524g	5	14.3437	0.0087	50.24 m	1.7408×10^{-4}	0.60
	10	14.3318	0.0206	100.48 m	1.9817×10^{-4}	0.65
	15	14.3045	0.0479	150,72 m	2.3410×10^{-4}	0.68
	20	14.2735	0.0789	200.96 m	2.5072×10^{-4}	0.72
B,20N, w1=14.3200g,	5	14.3026	0.0174	50.24 m	3.4710×10^{-4}	0.64
	10	14.2817	0.0383	100.48 m	3.8115×10^{-4}	0.69
	15	14.2623	0.0577	150,72 m	3.8314×10^{-4}	0.72
	20	14.2408	0.0792	200.96 m	3.9420×10^{-4}	0.74

Table (4): The results of the wear tests of the samples B0 and B5 after hot pressing

Sample	Time (min)	w_2 (g)	Δw (g)	Distance=$2\pi rnt/1000$ (m)	$R.W = \Delta w/2\pi rnt$ (g/m)	Friction coefficient
B5(9T),10N w1=12.2473g	5	12.2417	0.0056	50.24 m	1.1198×10^{-4}	0.36
	10	12.2362	0.0111	100.48 m	1.1089×10^{-4}	0.38
	15	12.2308	0.0165	150,72 m	1.0165×10^{-4}	0.40
	20	12.2270	0.0203	200.96 m	1.0114×10^{-4}	0.48
B5(9T),20N w1=11.1711g	5	11.1604	0.0107	50.24 m	2.1325×10^{-4}	0.40
	10	11.1500	0.0211	100.48 m	2.0966×10^{-4}	0.43
	15	11.1398	0.0313	150,72 m	2.0751×10^{-4}	0.55
	20	11.1303	0.0408	200.96 m	2.0305×10^{-4}	0.60
B0(9T),10N, w1=12.0097g	5	12.0029	0.0068	50.24 m	1.3594×10^{-4}	0.62
	10	11.9898	0.0199	100.48 m	1.9817×10^{-4}	0.66
	15	11.9862	0.0235	150,72 m	2.3410×10^{-4}	0.71
	20	11.9719	0.0378	200.96 m	2.5072×10^{-4}	0.76
B0(9T),20N, w1=10.8003,	5	10.7877	0.0126	50.24 m	2.5089×10^{-4}	0.65
	10	10.7728	0.0275	100.48 m	2.7341×10^{-4}	0.69
	15	10.7567	0.0436	150,72 m	2.8910×10^{-4}	0.79
	20	10.7363	0.0640	200.96 m	3.1823×10^{-4}	0.85

Table (5): demonstrated the friction coefficient for each sample in (20 min) of sliding time.

Time of Sliding (min)	Base alloy (B0)		Sample with 5wt.% coated graphite (B5)	
	Before hot press	After hot press	Before hot press	After hot press
	10N Load	10N load	10N load	10N Load
5	0.60	0.62	0.34	0.36
10	0.65	0.66	0.32	0.38
15	0.68	0.71	0.36	0.40
20	0.72	0.76	0.44	0.48

Table (6): The results of Machining Experiments of the samples before and after the hot pressing: (B0) and (B5)

Spindle Speed (rpm)	Feed Rate (min/rev.)	Specimens alloy	Sample code	Width of flank wear VB(micron)				Surface roughness (micron)	Tool Life (sec)
				1min	2min	3min	4min	1min	
90	0.05	Cu-10Sn	B	75	80	150	310	0.479	235
			B6T	85	100	160	315	0.456	230
			B7.5T	100	120	210	330	0,419	215
			B9T	150	170	240	360	0,385	210
	0.05	Cu-10Sn With 5wt.%	B5	60	70	110	290	0.363	250
			B5,6T	70	90	150	300	0.348	240
			B5,7.5T	95	115	170	315	0.315	235
			B5,9T	100	150	190	335	0.293	230
250	0.05	Cu-10Sn	B	80	100	180	320	0.463	230
			B6T	100	110	190	330	0.436	225
			B7.5T	120	155	250	350	0.395	210
			B9T	170	185	280	370	0.368	195
	0.05	Cu-10Sn With 5wt.%	B5	70	80	130	300	0.358	240
			B5,6T	80	100	175	315	0.343	235
			B5,7.5T	100	130	190	330	0.311	230
			B5,9T	110	165	220	355	0.289	220
			B	100	140	200	340	0.455	225

355	0.05	Cu-10Sn	B6T	110	130	220	355	0.425	215
			B7.5T	130	175	265	360	0.378	200
			B9T	180	210	290	380	0.356	190
	0.05	Cu-10Sn With 5wt.%	B5	80	110	165	315	0.349	230
			B5,6T	90	130	190	325	0.333	225
			B5,7.5T	115	160	215	345	0.305	220
			B5,9T	120	180	240	360	0.281	210
500	0.05	Cu-10Sn	B	110	155	220	355	0.432	218
			B6T	130	170	230	360	0.413	210
			B7.5T	145	180	275	370	0.367	196
			B9T	190	215	300	390	0.339	180
	0.05	Cu-10Sn With 5wt.%	B5	100	120	180	340	0.315	225
			B5,6T	120	140	230	350	0.295	215
			B5,7.5T	130	175	250	360	0.261	210
			B5,9T	150	190	270	375	0.227	200

Table (7): Porosity and density results before and after hot press for all specimens

Before Hot Press			
Sample	**ρ1 g/cm3**	***Porosity %***	
B	**8.8552**	**3.45**	
B1	**8.8645**	**3.32**	
B3	**8.8670**	**3.28**	
B5	**8.8695**	**3.11**	
At 6T			
Sample	**ρ1 g/cm3**	**ρ2 g/cm3**	**Porosity%**
B	**8.8557**	**8. 8615**	**3.3**
B1	**8.8643**	**8.8738**	**3.15**

B3	**8.8676**	**8.8770**	**3.08**
B5	**8.8684**	**8. 8795**	**2.87**
At 7.5T			
Sample	**ρ1 g/cm3**	**ρ2 g/cm3**	***Porosity***
B	**8. 8561**	**8.8663**	**3.23**
B1	**8.8 644**	**8.8828**	**2.94**
B3	**8. 8679**	**8.8865**	**2.78**
B5	**8. 8695**	**8.8849**	**2.61**
At 9T			
Sample	**ρ1 g/cm3**	**ρ2 g/cm3**	
B	**8. 8609**	**8.8784**	**2.93**
B1	**8. 8643**	**8.9940**	**2.75**
B3	**8. 8675**	**8.9971**	**2.64**
B5	**8. 8690**	**8.9997**	**2.5**

Table (8) Brinell hardness test value

Samples	Before Hot press	At 6T	At 7.5T	At 9T
B	75	107	111	137
B1	91	119	132	139
B3	93	122	125	142
B5	95	124	128	145